CHALMERS

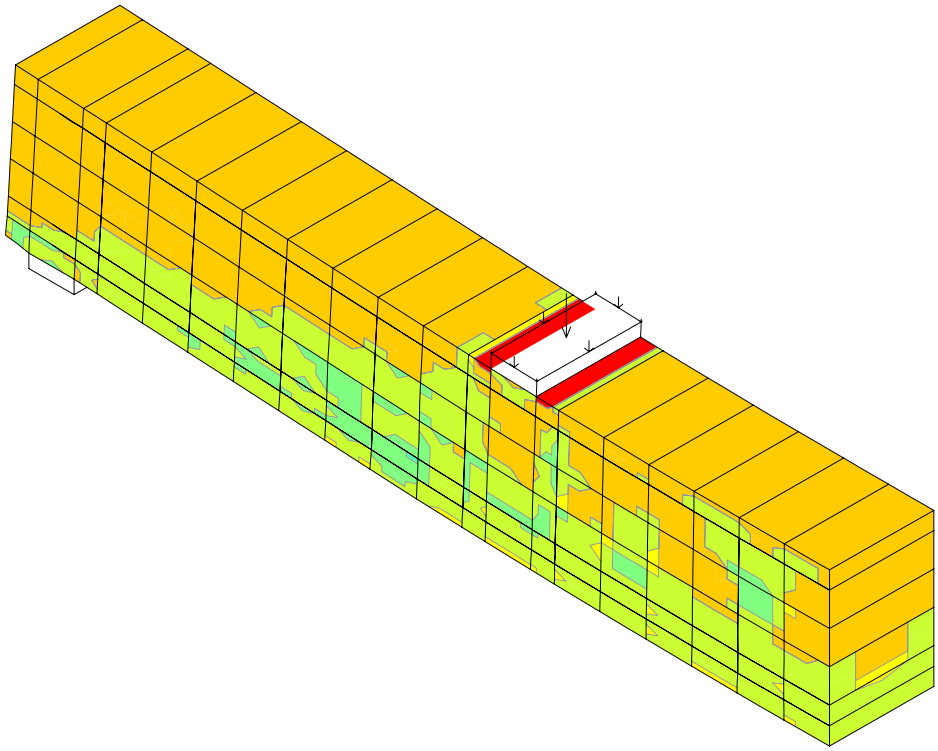

Finite element analyses for limit state design of concrete structures

Posibilities and limitations with SOLVIA

Masther's Thesis in the International Master's programme Structural Engineering

FERNANDO LOPEZ

FEJSAL AL-HAZAM

Department of Civil and Environmental Engineering
Division of Structural Engineering
Concrete Structures
CHALMERS UNIVERSITY OF TECHNOLOGY
Göteborg, Sweden 2005

Master's Thesis 2005:17

MASTER'S THESIS 2005:17

Finite element analyses for limit state design of concrete structures

Posibilities and limitations with SOLVIA

Master's Thesis in the International Master's programme Structural Engineering

FERNANDO LOPEZ

FEJSAL AL-HAZAM

Department of Civil and Environmental Engineering
Division of Structural Engineering
Concrete Structures
CHALMERS UNIVERSITY OF TECHNOLOGY
Göteborg, Sweden 2005

Finite element analyses for limit state design of concrete structures

Posibilities and limitations with SOLVIA

Master's Thesis in the International Master's programme Structural Engineering

FERNANDO LOPEZ
FEJSAL AL-HAZAM

Master's Thesis 2005:17
Department of Civil and Environmental Engineering Concrete structures
Division of Structural Engineering
Concrete Structures
Chalmers University of Technology
SE-412 96 Göteborg
Sweden
Telephone: + 46 (0)31-772 1000

Cover:
The cracking and crushing behaviour of a simply supported reinforced concrete beam, where a half of the beam were modelled, using symmetrical boundary conditions.

Name of the printers / Department of Civil and Environmental Engineering
Göteborg, Sweden 2005

Finite element analyses for limit state design of concrete structures

FERNANDO LOPEZ
FEJSAL AL-HAZAM
Master's Thesis in the International Master's programme Structural Engineering
Division of Structural Engineering
Concrete Structures
Chalmers University of Technology

ABSTRACT

During the last decades there have been many attempts at defining robust and efficient models that can represent the cracking and crushing behavior of concrete structures. Among the most popular ones are the models based on the so-called "smeared crack approach". The advantage here is that a crack solid is modeled as a continuum and cracked material can be described with stress-strain relationship. The crack pattern doesn't need to be known in advance. All these features make the smeared crack approach particularly well suited for implementation in finite element context.

The present study considers non-linear finite element analyses performed on five different FE-models implemented in SOLVIA FE-system, using plane stress, solid and truss elements. The models were created for three types of simply supported reinforced concrete beams in order to examine shear failure. The focus was on the following concrete parameters: the shear retention factor, β and the parameter which defines the ultimate crack strain κ.

The FE-results for each model were compared with the experimental results in order to evaluate the accuracy of the FE-analysis. From the comparison, it was found that, all the models gave reasonably good numerical predictions and similar results (within a reasonable range) to the results according to experimental and theoretical investigations. A parametric investigation was also performed. The reason for the parametric investigation was to examine how the ultimate loads, displacements and stresses in stirrups vary with the different combinations of β and κ.

In order to get stable analysis and a good numerical prediction of the FE-results, certain combination of concrete parameters β and κ was selected for each model. It was concluded that the parameter β had to be chosen between 0.85 and 0.9, while κ could be calculated from the fracture energy of concrete and increased with respect to the tension stiffening effect. It was found that this parameter had to be multiplied with factors within range 1.5-4.2, depending on the FE-model, in order to get stable analysis with good prediction of the results.

In general, it was concluded that non-linear analysis performed in SOLVIA can be used for limit state analysis of simply supported reinforced concrete beams, analyzed for shear type of failure.

Key words: shear retention factor, ultimate crack strain, stress, finite element method, non-linear FE-analysis, ultimate load, displacement, crack pattern, ultimate failure capacity, fixed orthogonal cracks, smeared crack approach.

Contents

Preface

This master thesis was carried out at Vägverket Konsult as a final project of the Master program in Structural Engineering at Chalmers University of Technology, Gothenburg, Sweden.

The examiner and supervisor was Mario Plos from the Department of Structural Engineering at Chalmers University of Technology who supervised and examined us. We are thankful for his guidance during the work with this project.

We would like to express our most sincere gratefulness to our supervisor at Vägverket Konsult, Costin Pacoste for his devoted guidance, support and outstanding encouragement throughout the development of this project.

We are also very thankful to Mikael Hermansson, for his constant contribution, co-operation and help in the use of the FE software.

We wish to thank Mats Carlson for allowing us to work at the company and Roland Olsson who provided the working place and all necessary equipment.

We are also very grateful to Björn Engström professor from the Department of Structural Engineering at Chalmers University of Technology for providing us with well documented experimental results needed partly as a base for the project.

Finally, we wish to thank our families, friends and people at the company who supported us during the project work period.

Gothenburg, February 2005.

Fernando López.

Fejsal Al-Hazam.

Notations

Roman upper case letters

A_{ef}	Effective tension area.
A_s	Area of longitudinal tensile reinforcing steel.
A_s'	Area of longitudinal compressive reinforcing steel.
A_{s0}	Area of the least reinforcement in the tensile zone extending not less than $l_{b,net} + d$.
A_{sv}	Cross sectional area of shear reinforcement.
C	Compressive force in the concrete cross section.
	Incremental stiffness matrix following a tensile failure.
	Constant damping matrix
E_c	Modulus of elasticity of concrete.
E_o	Tangent modulus of elasticity at zero strain of concrete.
E_s	Modulus of elasticity of tensile reinforcing steel.
E_s'	Modulus of elasticity of compressive steel reinforcement.
E_{sh}	Strain hardening modulus of reinforcing steel.
E_{sp}	Modulus of elasticity of steel plates.
E_t	Tangent modulus at which stresses normal to a crack plane cease.
F	Force.
	Nodal point force vector equivalent to the element stresses.
F_c	Force carried by the concrete.
F_s	Force carried by the tensile reinforcing steel.
F_s'	Force carried by the compressive reinforcing steel.
G	Shear modulus of elasticity of concrete.
G_f	Fracture energy.
K	Tangent stiffness matrix based on the iteration history.
L	Length.
M	Constant mass matrix.
M_n	Nominal flexural capacity.
M_u	Moment due to factored loads.
P	Unfactored concentrated load.
P^*	Calculated ultimate load.
P_a	Ultimate finite element load.
P_{cr}	Diagonal tension crack load.
P_f	Calculated ultimate load governed by flexure.
P_u	Ultimate test load.
P_v	Calculated ultimate load governed by shear.
R	External load vector.
$RMNORM$	Reference moment.
$RNORM$	Reference force.
$RTOL$	Relative force and moment tolerance used to measure equilibrium iteration convergence.
$STOL$	Tolerance used to measure line search convergence.
U	Vector of nodal point displacements.
$\dot{U}$	Nodal point velocity vector.
$\ddot{U}$	Nodal point acceleration vector.

V_a	Interface shear transfer by aggregate interlock along a diagonal crack.
V_{ay}	Vertical component of the shear transferred across a crack.
V_c	Shear resistance of concrete without stirrups.
V_{cz}	Shear transfer in the concrete compression zone.
V_d	Shear transfer by dowel action of the longitudinal tensile reinforcement.
V_R	Shear capacity of a section with shear reinforcement.
V_s	Nominal shear force carried by shear reinforcement.
V_u	Shear force due to factored loads.

Roman lower case letters

a	Shear span, distance between concentrated load and face support.
a_{tp}	Level of tensile steel centroid.
b_w	Width of the cross section.
c	Concrete cover.
d	Distance from the extreme top fiber to the centroid of tension reinforcement.
d'	Distance from the extreme top fiber to the centroid of compression reinforcement.
d_{ef}	Coefficient which takes into account the concrete cover and the bar size on the effective concrete area.
d_{max}	Maximum aggregate size of concrete.
$f(\ )$	Function of.
f_c	Compressive strength of concrete.
f_{cu}	Ultimate compressive strength of concrete.
f_{cy}	Yield strength of concrete.
$f_{t,sp}$	Splitting tensile strength of concrete.
f_t	Tensile strength of concrete.
$f_{t,fl}$	Modulus of rupture of concrete.
f_u	Ultimate strength of reinforcing steel.
f_v	Basic shear strength of members without shear reinforcement.
f_y	Yield strength of tensile steel reinforcement.
f_y'	Yield strength of compressive steel reinforcement.
f_{yv}	Yield strength of shear reinforcement.
h	Height.
i	Iteration.
l	Length.
$l_{b,net}$	Required anchorage length.
l_c	Clear beam span.
s	Spacing of stirrups measured along the longitudinal reinforcement.
s_{rm}	Average crack spacing
t	Time.
w	Crack displacement.
w_u	Ultimate crack displacement.
x	Depth of the neutral axis.

x_1	Coefficient which takes into account the bond properties of bars on the crack spacing.
x_2	Coefficient which takes into account the form of the strain distribution on the crack spacing.

Greek upper case letters

β	Shear retention factor. Principal stress ratio.
Δ	Incremental, Increment of
Υ_{xy}'	Shear crack strain with respect to the *xy* plane.
Υ_{xz}'	Shear crack strain with respect to the *xz* plane.
Υ_{yz}'	Shear crack strain with respect to the *yz* plane.
τ_{xy}'	Shear stress with respect to the cracked *xy* plane.
τ_{xz}'	Shear stress with respect to the cracked *xz* plane.
τ_{yz}'	Shear stress with respect to the cracked *yz* plane.
U	Displacement vector.

Greek lower case letters

α	Angle of the shear reinforcement to the longitudinal axis of the member.
δ_a	Maximum deflection obtained in finite element analysis.
δ_{max}	Maximum test deflection.
ε	Strain.
ε_c	Uniaxial compressive strain of concrete at f_c.
ε_{c1}	Uniaxial elastic strain of concrete at $0.6 \cdot f_c$.
ε_{cu}	Uniaxial ultimate compressive strain of concrete.
ε_s	Tensile steel strain.
ε_s'	Compressive steel strain.
ε_x', $\varepsilon_y'\varepsilon_z'$	Normal crack strains with respect to the cracked plane in the local coordinates *x',y',z'*.
ε_{su}	Ultimate strain of steel reinforcement.
ε_t	Tensile failure strain of concrete.
ε_{tu}	Ultimate crack strain.
ε_u	Ultimate compressive strain of concrete.
ε_y	Yield strain of tensile steel reinforcement.
ε_y'	Yield strain of compressive steel reinforcement.
ℓ_r	Effective reinforcement ratio.
ν	Poisson's ratio.
ρ	Density of the concrete.
ρ_w	Ratio of ordinary tension reinforcement.
σ	Stress.
σ_s	Tensile reinforcement stress.
σ_s'	Compressive reinforcement stress.
σ_{p1}, σ_{p2}, σ_{p3}	Principal stresses in *x,y,z* direction in the biaxial o triaxial failure envelopes.

σ_x', σ_y' σ_z'	Normal stresses with respect to the cracked plane in the local coordinates x',y',$z.'$
κ	Parameter which defines the ultimate crack strain.
μ	Normal retention factor.
ξ	Constant relating to section depth and curtailment of reinforcement.
η_η	Normal stiffness reduction factor.
θ	Acceleration factor obtained from a line search.
$\emptyset$	Bar diameter.

1 Introduction

1.1 Background

For analyzing the collapse behavior of concrete structures, proper constitutive and failure criteria even for the case of relative standard structural members are required. For more complex elements, the need for a realistic description of material behavior becomes more evident still, especially due to the fact that such elements need to be modeled as continua.

During the last decades there have been many attempts at defining robust and efficient models that can represent the cracking and crushing behavior of concrete. Among the most popular ones are the models based on the so-called "smeared crack" approach. The advantage here is that a cracked solid is modeled as a continuum allowing the cracked material to be described with a stress-strain relationship. Moreover, the crack pattern need not be known in advance. These features make the smeared crack approach particularly well suited for implementation in a finite element context.

This study considers a concrete material model with fixed orthogonal cracks, implemented in the SOLVIA finite element system. According to the definition of this type of models, the cracks, once they initiate, they are fixed in their original direction, and a second crack may develop in an orthogonal plane to the already existing ones. The cracks also continue to influence the cracking process, even if they at later stages become closed. The SOLVIA model uses a shear retention factor β and the ultimate crack strain κ, which together may alleviate the possible effects of locking, but, at the same time they tend to increase the convergence problems during the computation process. In addition, the type of elements used in the discretization plays also a significant role.

1.2 Purpose

The main purpose of the master thesis project is to examine the capability and limitations of the SOLVIA FE system for limit state analysis of reinforced concrete structures. The study will primary concentrate on the shear collapse mechanism of beam type members. A parametric investigation of the concrete material model implemented in SOLVIA will be performed in order to examine the behavior of concrete elements in the cracked stage. The investigation will focus on the following parameters:

1. The shear retention factor β.

2. The parameter κ which defines the ultimate crack strain.

3. The type of element used.

The parameters β and κ can be determined from the material response for plain concrete. However, for reinforced concrete modeled with complete interaction between the reinforcement and concrete, these parameters can often be varied within

certain limits without any substantial influence on the overall structure behavior.

Certain choices of the values of the parameters β and κ will reduce the risk of shear locking in concrete elements, while other combinations instead will reduce the numerical analysis problems.

2 Limit state design of reinforced concrete structures

According to Mosley and Bungey, *et al* (1999), the purpose of design is to ensure that under the worst loading conditions the structure be safe; and during normal working conditions, adequate for its intended use. The two principal types of limit states are the ultimate limit state and the serviceability limit state.

In the ultimate limit state, the structure must resist the loads for which it is designed with an adequate factor of safety against collapse. According to Allen, D.E (1982), this factor considers the probability of deviations of the load from the value specified in codes. When a load is combined with other loads, its factor is decreased by a combination that considers the reduced possibility of different loads acting simultaneously.

Once the loads are factored, the designer computes deformations or sectional forces in the structure. As the limit state is approached, the computations are based on a theory of structural behavior which suitably represents the real response of the structure.

In the case of the ultimate limit states, the component forces obtained are then compared with calculated component resistances. These resistances are calculated by means of a strength analysis of the component as a function of the specified dimensions and material properties made in the design.

A component can be a connection, member, or a material component in a composite structure, or it may be a mode of failure such as shear or compression. Resistance factors are applied to the component resistances and consider the variations of material properties and dimensions, workmanship, type of failure, etc.

According to Mosley and Bungey, *et al* (1999), the most important features in the serviceability limit state are: deflection, cracking and durability. Accordingly, other limit states that may be reached are excessive vibration, fatigue and fire resistance. The relative importance of each state may vary depending on the nature of the structure. The normal procedure is to decide the most important limit state for a particular structure and base the design on this. Also, it is required to ensure that all other relevant limit states are satisfied by the results produced.

In assessing a particular limit state for a structure it is necessary to consider all the possible variations from loads, material properties and constructional tolerances.

2.1 Non-linear behavior of concrete structures

According to Reda Taha (2003), the mechanical behavior of concrete and its components can be expressed by a stress strain diagram as shown in Figure 2.1. The concrete itself has an inelastic non linear response when the stress reaches 40 – 50% of its ultimate strength while the aggregates and the cement paste have a linear elastic behavior for up to 80% of their ultimate capacity.

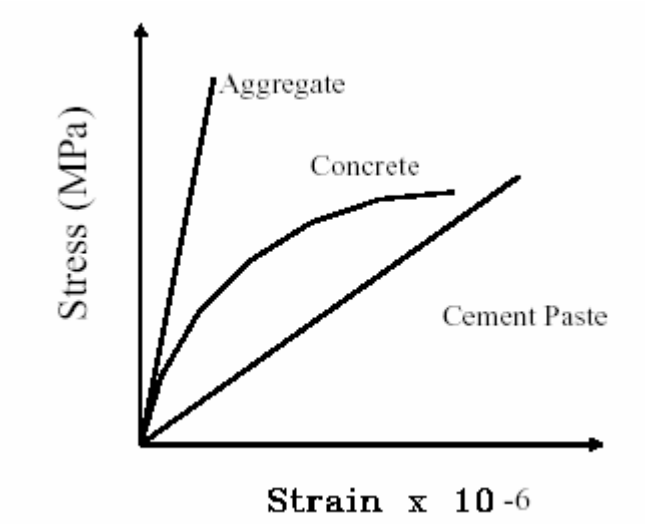

Figure 2.1 Stress strain relationship of concrete and its components, from Reda Taha and N. G. Shrive.

The non linear behavior of concrete can be explained by defining it as a three stage heterogeneous material: the aggregates, the cement paste and the transition zone. The transition zone represents the interfacial region between the aggregates and the cement paste. Because of the high porosity and low strength of the transition zone, micro cracks can easily propagate in the transition zone whereas the other two phases do not crack, which results in the non linear behavior of the concrete material.

Hsu *et al* (1963), studied crack propagation in concrete and reported that the micro cracks development and propagation determine the form of the stress strain diagram of concrete under uniaxial compression. Additionally, he reported that in all stages of loading the total amount of mortar cracks were significantly less than the cracks in the transition zone (known as bond cracking). Whereas the ascending branch of the concrete stress strain relationship depends only on cracking extent in concrete, the descending branch is highly influenced by the stiffness of the testing machine end conditions. It is well known that micro cracks already exist in the transition zone before the application of external loads, as a result of thermal stresses and shrinkage forces. The number and width of these cracks in the transition zone depend primarily on wall effect, bleeding characteristics, thermal and carbonation shrinkage and curing history. In concrete under uniaxial compression, four stages of cracking can be identified as shown in Figure 2.2:

Stage I: Stress levels up to 30% of the ultimate stress; the micro cracks in the transition zone remain stable and hence the stress strain relationship is linear.

Stage II: Stress levels between 30% and 50% of the ultimate stress; the micro cracks in the transition zone start to extend and develop. The stress strain diagram begins to deviate from the linear behavior at an intermediate stress.

Stage III: Stress levels between 50% and 75% of the ultimate stress; cracks in the cement paste zone form about 60% of the ultimate stress. When the stress is reaching a value of 75% of the ultimate load, the micro cracks in the transition become more

stable and cracks of the cement paste develop rapidly. The stress strain curve in this region is strongly non linear.

Stage IV: Stress levels between 75% and 100% of the ultimate stress; mortar cracks become continuous and propagate quickly. High strains develop and cracks develop under sustained loads. The stress strain curve reaches a maximum value and a descending branch means that a failure starts.

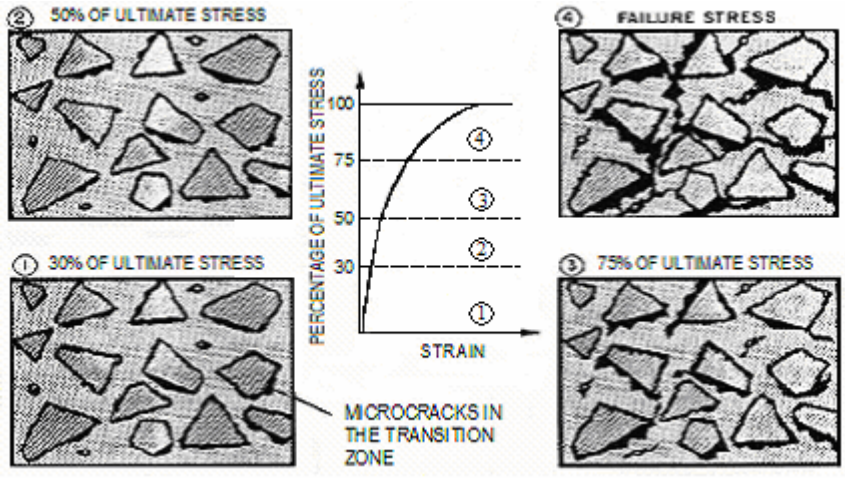

Figure 2.2 Relationship between concrete behavior and the range of cracking, from Mehta and Montrerio (1993).

The performance of concrete can be described at two levels, according to the cracking stages: first, micro cracks are formed or enlarged under low stress levels and are distributed randomly. When the stress level reaches a specific value, the micro cracks grow together into a macro crack. This macro crack will propagate until the stress reaches its critical stage. Stabilized propagation of this macro crack results in a strain softening mechanism observed for concrete.

2.1.1 Tension

According to Heidkamp (2000), the response of concrete in tension is well treated with the introduction of fracture mechanics. This is because it seems justifiable to deal with cracks in a smeared sense. One relevant aspect in concrete in tension is that it is a heterogeneous material which exhibits a strain softening behavior, due to its continuous deformation localization and failure of its components, (see Hirschhausen (1999)). One example to illustrate this theory is to consider the fracture development of a plain concrete specimen of length L subjected to uniaxial tension under displacement control, shown in Figure 2.3.

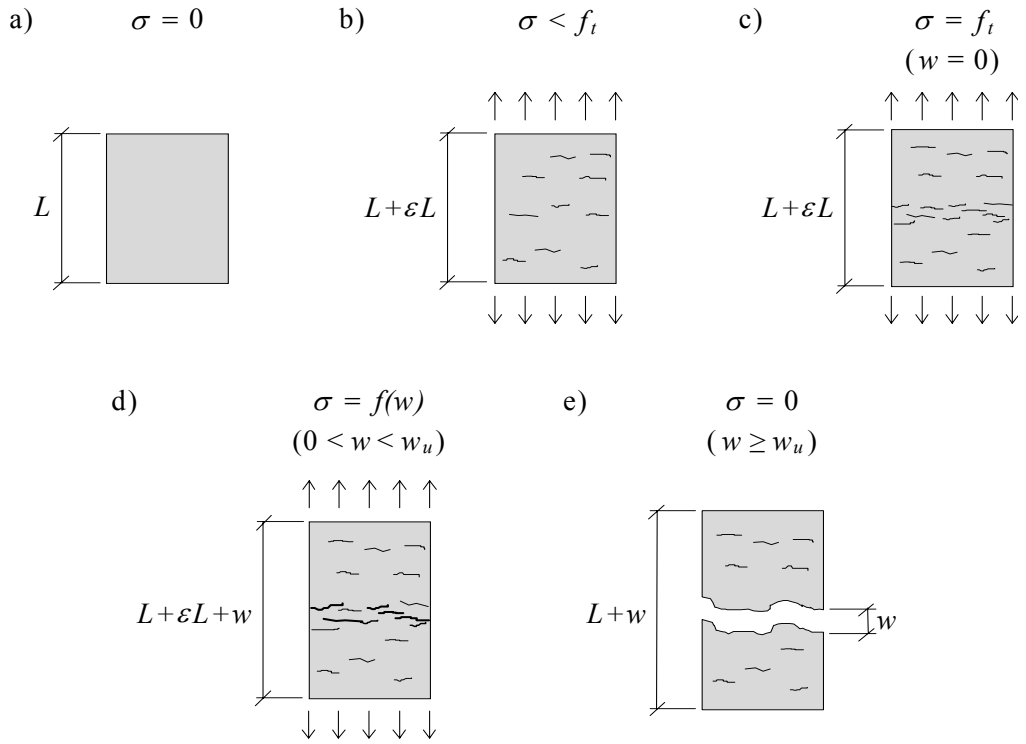

Figure 2.3 Fracture process in a plain concrete specimen, loaded uniaxially under displacement control, from Plos (1995).

According to Plos (1995), in the loading stage before the maximum stress is reached, local micro-cracks start to form at weak zones through the specimen. After further loading, the micro-cracks from the former stage start to connect each to other and to localize into a zone of deformations at the weakest section of the specimen. In this stage, the final crack is formed but not open yet ($w = 0$) and the behavior of the specimen can be described by means of a stress strain relationship with increasing load. Furthermore, as the crack opens, the stresses that can be transferred, decrease and the total deformation is governed by the material outside the damaged zone and the crack width w. Finally, no further stress can be transferred across the crack, when the micro-cracks lead to separation of the specimen $w \geq w_u$.

A widely accepted model to describe the fracture behavior of concrete is the "Fictitious Crack Model", Hillerborg (1976). In this scheme, the fracture zone is modeled as a fictitious crack with zero width before real cracking is initiated. After crack initiation, a stress crack opening relation represents the softening behavior provided by the damaged process zone, as it seen in Figure 2.4.

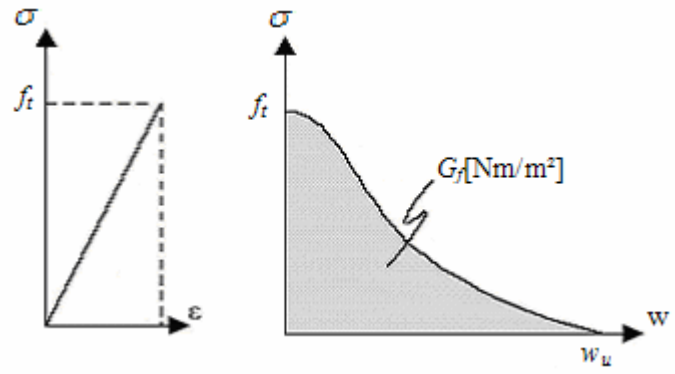

Figure 2.4 *Stress-strain relation prior to initiation of cracking and stress-crack opening relation for the post cracked state for plain concrete, from Hillerborg (1976).*

The area under the stress crack opening is called fracture energy, G_f and represents the dissipated energy during the fracture process, which can be deemed as constant for a certain concrete strength class and maximum aggregate size, (CEB-FIB, 1990). Moreover, the shape of the stress crack opening curve and the concrete tensile strength, f_t, are necessary parameters to describe the crack formation besides the fracture energy, which in turn is the most relevant of fracture mechanics for concrete.

The term "Tension stiffening" is often used to represent the tension contribution of concrete after cracking. Tension stiffening accounts for the fact that even when cracked, concrete will still contribute in the tension carrying capacity of the section by transferring the tensile stresses between cracks, see Figure 2.5. This adds to the complexity of the problem of predicting the deformations of concrete structures accurately, from Reda Taha (2003).

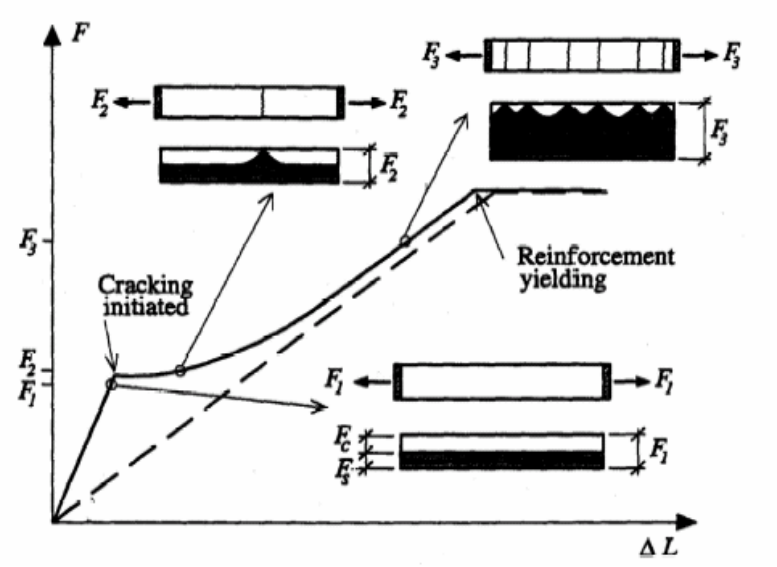

Figure 2.5 *Effect of cracked concrete in the load displacement response of a tensioned reinforced concrete prism, the tension stiffening effect, Plos (1995).*

According to Plos (1995), the tension stiffening effect can be reasonably determined by modifying the strain values of the stress strain tensile relation for concrete. Moreover, it is reflected in the structural response if the reinforcement is modeled with separate elements. The reason is that the stresses in a bar embedded in cracked concrete sections are partly transferred to the concrete elements in between the cracks. This leads to a reduction in convergence problems when using finite element techniques.

There are some important parameters that affect the tension stiffening of concrete for instance: the type of loading (monotonic, cyclic or sustained), quality of bond of the reinforcing steel and the level of tensile stress applied.

The effect of the density of reinforcement on tension stiffening should also be incorporated when tension stiffening is used for modelling reinforced concrete elements using the finite element method (Belarbi *et al*. 1994; ABAQUS 2000).

Other comprehensive models to account for concrete tension stiffening in reinforced concrete structures include those reported by Favre *et al*. (1985), CEB-FIP (1990), Eurocode (1991), Favre *et al*., (1994), Ghali *et al*. (1994), Ghali *et al*. (1999) and Gilbert (2001).

A number of variations between these models exist, but they all are based on interpolation between the uncracked and the cracked analyses.

2.1.2 Compression

According to Heidkamp (2000), structural concrete in compression exhibits localization of deformations after its maximum strength. This means that the strain softening branch can be represented by a continuous stress strain relationship, as the fictitious crack model from Hillerborg shown in Figure 2.4. The curve can then be divided into three parts, the linear elastic domain in the range of about 40% to 45% approximately with a modulus of elasticity E_c and stresses below the yield strength f_{cy},; the strain hardening domain, for stresses between the yield strength and the compressive strength f_c; and a descending branch which represents the strain softening domain for stresses up to the ultimate compressive strength f_{cu}.as it is shown in Figure 2.6.

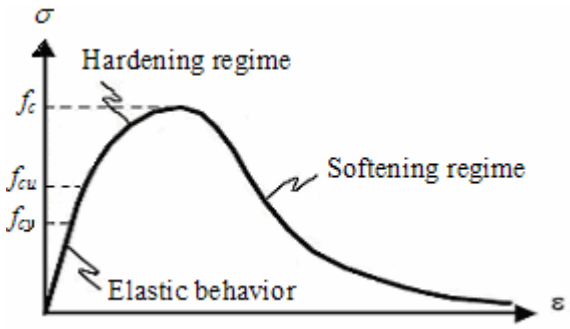

Figure 2.6 Uniaxial stress strain diagram of concrete under compression, adopted from Heidkamp (2000)

2.1.3 Bending

According to Nadim Hassoun (2002), when the maximum tensile stress in concrete reaches its tensile strength at a certain loading stage, cracks occur. To increase the flexural capacity of a concrete beam for instance, longitudinal reinforcement is used; under these conditions, the steel bars and concrete resist tension and compression forces respectively.

The flexural behavior of a reinforced concrete beam can be illustrated by means of a simple laboratory test, in which two simply supported beams are loaded to failure. One of the beams has longitudinal reinforcement in the tensile zone, whereas the other has both compressive and tensile steel reinforcement and stirrups as well. During the different loading stages the following observations can be made:

Stage 1. As the load is applied gradually from zero, the beams resist the current bending moment and shear forces at any section. The maximum bending moment occurs at the mid-span of the beam. In that section, both the tensile stresses at the bottom fibers and the compressive stresses at the top fibers are less than the allowable strength values of concrete. This results in linear elastic behavior with no cracking.

Stage 2. At a certain load level, say P_1, the tensile stresses in concrete at the bottom fibers are equal to its tensile strength.

Stage 3. At a load level beyond P_1, cracks form at the bottom fibers for values of the tensile stresses in the concrete greater than its tensile strength. The neutral axis moves upwards and the flexural cracks reach the neutral axis. The concrete still carries minimum tensile stresses but the steel reinforcement is effective in resisting these forces. A noticeable deflection of the beam can be observed at this stage. The first cracks develop first at mid-span and, as the load increases, the crack width increases and additional cracks form near the supports.

Stage 4. At this stage in the beam without stirrups, the combined action of shear forces and bending moment causes a diagonal crack. This type of cracking is initiated at a distance of approximately 1.5 times the height of the beam from the support, in the top fibers; it propagates at an angle of 45°, parallel to the direction of principal compressive stresses and continues horizontally until the support. A sudden collapse of the beam occurs by splitting of the concrete in the tensile zone, see Figure 2.7.

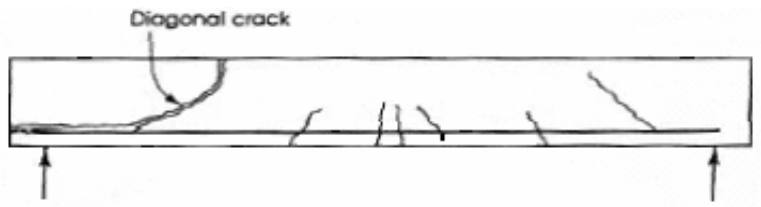

Figure 2.7 Shape of the beam 1 at shear failure, from Nadim Hassoun (2002).

In the beam with vertical reinforcement, similar diagonal parallel cracks appear in regions with high shear stresses and the stirrups are effective in resisting principal

stresses, see Figure 2.8. No longitudinal splitting along the tensile reinforcement can be developed. The stirrups prevent at this load level, the collapse of the beam.

Figure 2.8 Shape of the beam 2 at bending moment failure, from Nadim Hassoun (2002).

Stage 5. At this stage, the deformations in the steel reach the yielding strains, but still the concrete strains are still lower than the allowable value. For small load increments, the steel strains develop abruptly, and cracks widen sharply. The compressive strains in the concrete as well as the deflections increase. The collapse of the beam occurs for a small load increment, with the steel reinforcement developing strain hardening and the concrete crushing at the top compressive fibers.

2.1.4 Shear

The factors influencing inclined cracks and shear strength are so complex and numerous that it is difficult to establish a definitive conclusion regarding the mechanisms that govern such failures. The behavior of reinforced concrete beams under shear failure is different from their behavior at flexure, because the shear failure is normally sudden and brittle and the inclined cracks that form are significantly larger than flexural cracks. Regarding the design of members for shear, and due to the brittle manner in which cracks occur, the engineer has to consider sections that are strong enough to resist the external factored loads without reaching their shear strength capacity, adopted from Nawy (2003).

Types of failure of concrete beams without shear reinforcement.

Principally three types of failures occur in concrete beams without shear reinforcement: flexural failure, diagonal tension failure and shear compression failure.

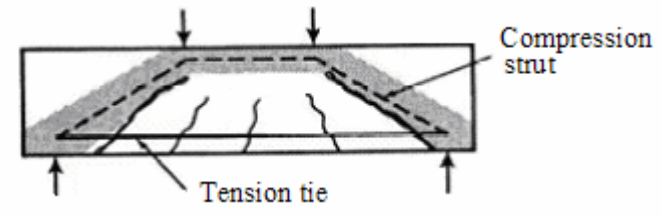

Figure 2.9 Anchorage failure and arch action behavior of a simply supported beam, from MacGregor (1997).

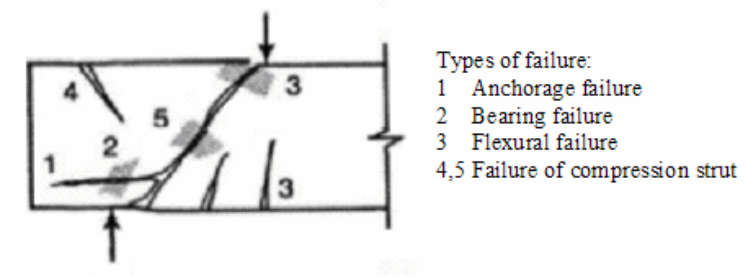

Figure 2.10 Modes of failure of short shear span beams, $0.5 \le \frac{a}{d} \le 2.0$*, from MacGregor (1997).*

In regions of large bending moments, cracks are mainly vertical. These cracks result from very small shear stresses and a dominant flexural stresses. As the external load increases, additional cracks develop in the same region of the beam. The initial cracks widen and extend deeper towards the compressed fibers causing a marked deflection of the beam. This is called **flexural failure**. If the beam is under-reinforced, failure occurs in a ductile manner and it is initiated by the yielding of the tensile reinforcement, see Figure 2.11. However, if the beam is over-reinforced, the steel does not yield nor give failure warning prior to collapse, Nawy (2003).

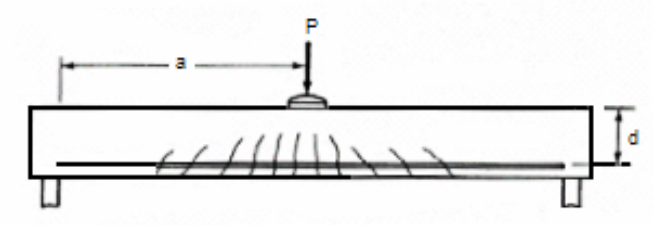

Figure 2.11 Flexural failure pattern as a function of beam slenderness, from Nawy (2003).

The **diagonal tension failure** starts with the formation of few vertical flexural cracks at the mid-span. Thereafter, the bond between the reinforcing steel and the surrounding concrete is destroyed at the support by longitudinal splitting. Few inclined cracks form at about 1.5 to 2d distance from the face of the support, weakening the anchorage of the reinforcement. As the inclined cracks stabilize, they become wider and form a principal diagonal extending to the top compression fibers, see Figure 2.12.

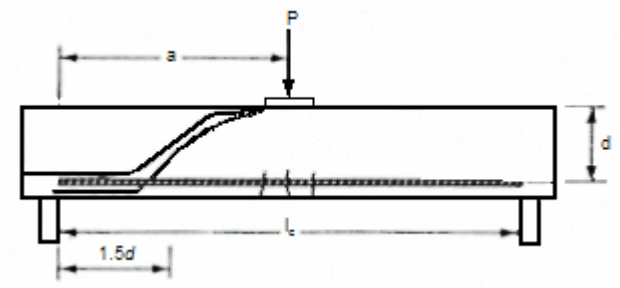

Figure 2.12 Diagonal tension failure pattern as a function of beam slenderness, from Nawy (2003) .

In the **shear compression failure** few flexural cracks start to develop at the mid-span and stop propagating as destruction of the bond occurs between the longitudinal bars and the surrounding concrete at the support region. Thereafter, an inclined steep crack suddenly occurs and continues to propagate towards the neutral axis. The rate of its progress is reduced with crushing of the concrete and redistribution of stresses in the top compression fibers. The final failure occurs suddenly when the inclined crack joins the crushed concrete zone, see Figure 2.13.

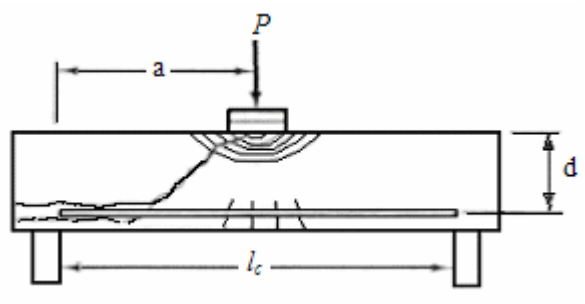

Figure 2.13 Shear compression failure pattern as a function of beam slenderness, from Nawy (2003).

Internal forces in a beam without stirrups in shear failure.

The internal forces transferring shear across an inclined crack are shown in Figure 2.14.

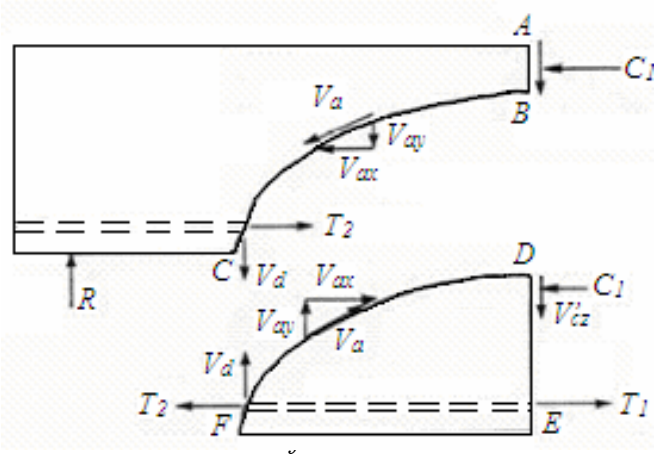

Figure 2.14 Internal forces in a cracked beam without stirrups, from MacGregor (1997).

According to MacGregor (1997), the shear is transferred across the crack trajectory ABC by V_{cz}, the shear in the compression zone; V_{ay}, the vertical component of the shear transferred across the crack on both of its faces by interlock of the aggregate particles; and V_d, the dowel action of the longitudinal reinforcement. Right after crack initiation, about 40% to 60% of the total shear is carried by V_d and V_{ay}. As the crack opens with increasing the shear force V_{cz} and the dowel force V_d, the transferred shear V_a decreases. This causes a splitting crack in the concrete along the reinforcement and V_d and V_a to drop to zero. When this two shear forces disappear, all the shear and compression are transmitted through the portion AB above the crack causing crushing of this section.

Factors affecting the shear strength of reinforced concrete beams without stirrups.

A reinforced concrete beam without web reinforcement fails when inclined shear cracking occurs and hence its shear capacity is equal to the inclined cracking shear, from MacGregor (1997).

Tensile concrete strength. The cracking load is frequently related to the split cylinder test in biaxial state of stresses. Inclined cracking occurs at a principal tensile stress of one third of the tensile strength on uncracked sections; when flexural cracks which appear before diagonal failures delay the elastic stress field developed at such stage.

Longitudinal reinforcement ratio. The following Equation expresses the shear strength of reinforced concrete beams without vertical reinforcement, when the steel ratio $\rho_w = A_s / b_w d$ varies between $0.0075 \le \rho_w \le 0.025$.

$$V_c = 2\sqrt{f_c} b_w d \qquad (2.1)$$

When the steel ratio ρ_w is small, flexural cracks extend higher into the beam and open wider than would be the case for large values of ρ_w. As a result, inclined cracking occurs earlier.

Shear span to depth ratio. This quotient is the relation between the shear span and the depth of the tensile reinforcement. It is represented as *a/d*, and has a certain effect on the shear resistance. Moments and shears at diagonal cracking in a rectangular beam without web reinforcement can be represented as a function of this factor as shown in Figure 2.15.

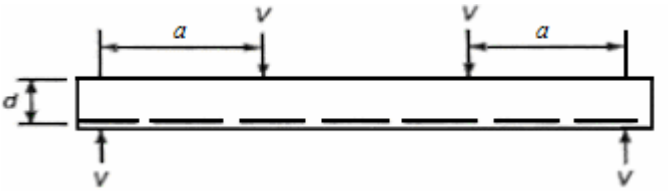

Figure 2.15 Geometry and loading of a simply supported beam with symmetric loads, from MacGregor (1997).

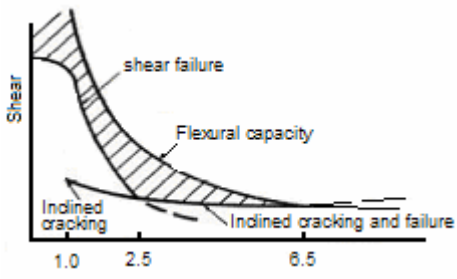

Figure 2.16 Shear at cracking and failure as a function of a/d ratio, from MacGregor (1997).

The maximum moment that occurs correspond to the moment capacity M_n of the cross section. According to Figure 2.16, very short shear spans $0 > a/d > 1$, develop inclined cracks as links between the loads and supports, destroying the transfer of shear flow from the longitudinal steel to the compression zone due to arch action (see Figure 2.17).

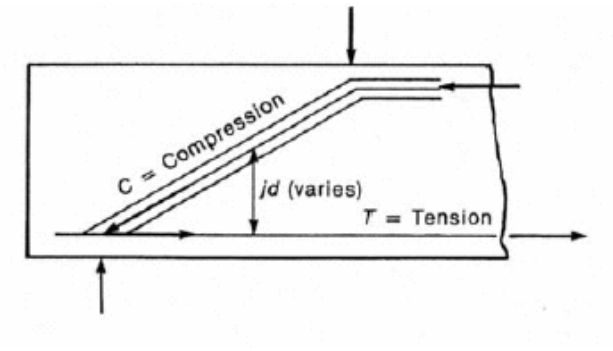

Figure 2.17 Arch action in a beam, from MacGregor (1997).

Subsequently, the steel acts as a tension tie of a tie arch with uniform tensile force. The most common type of failure in a beam with this shear to span ratio is anchorage failure at the ends of the tension tie.

Short shear spans $1 > a/d > 2.5$, develop inclined cracks and after a redistribution of internal forces, are able to carry additional load partly by arch action. The final failure for this beam is a bond failure, splitting failure, or dowel failure along the tensile reinforcement, as is shown in Figure 2.18.

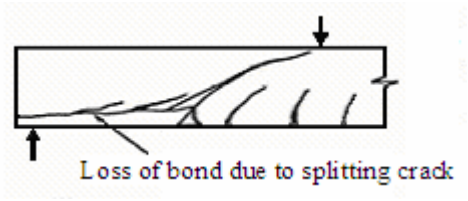

Figure 2.18 Shear tension failure, from MacGregor (1997).

Splitting crack or by crushing of the compressive fibers over the crack, see Figure 2.19

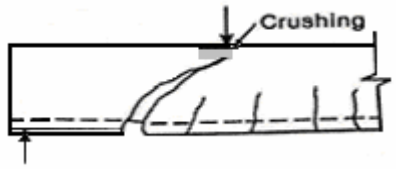

Figure 2.19 Shear compression failure, from MacGregor (1997).

For beams with slender shear spans $2.5 > a/d > 6$, the beam fails at the inclined cracking load shown in Figure 2.20, when the equilibrium is disrupted by such discontinuities.

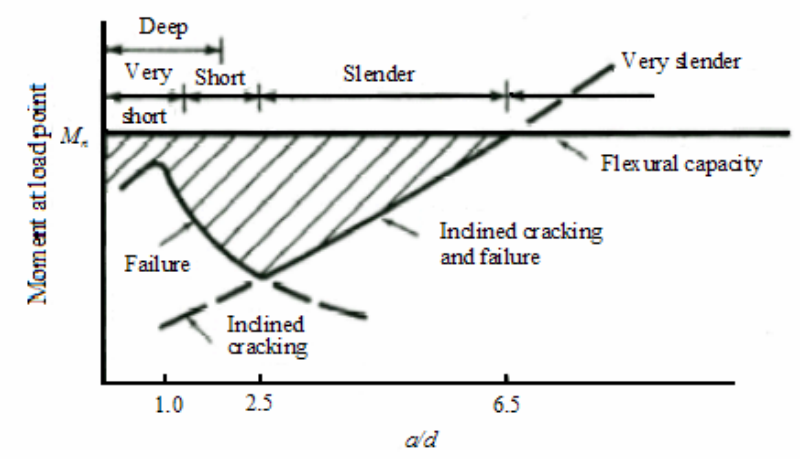

Figure 2.20 Moments at cracking and failure, from MacGregor (1997).

For beams with very slender shear spans $a/d < 6$, the shear required to form an inclined crack exceeds the flexural failure load and therefore the beam fails in flexure before prior the formation of inclined cracks, see Figures 2.16 and Figure 2.20.

Size of the beam. The shear stress at diagonal cracking tends to decrease for given values of a/d, f_c *and* ρ_w as the overall depth of the section increases. Also, crack widths in the tensile zone increase with increasing overall depth, leading to a reduction of the aggregate interlock across the crack and hence earlier splitting.

Behavior of beams with web reinforcement.

According to Bresler and Scordelis (1961), the shear capacity of a reinforced concrete beam is increased by using vertical reinforcement. Prior the development of diagonal cracks, the shear reinforcement contributes very little to the shear resistance. The vertical reinforcement increases the shear capacity of the beam after diagonal cracking and a redistribution of internal stresses develop in the cross section. When the amount of shear reinforcement is too small, failure due to yielding of the stirrups may be expected, but if the amount is too high a shear compression failure can occur.

The internal forces transferring shear across an inclined crack are shown in Figure 2.21 below. The notations are the same as in Figure 2.14.

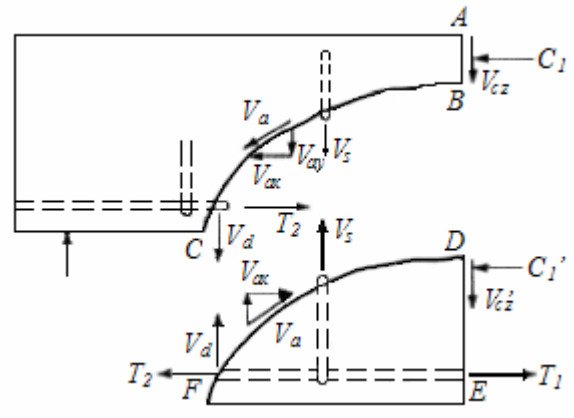

Figure 2.21 Internal forces in a cracked beam with stirrups, from Macgregor (1997).

The shear transferred by tension in the stirrups is V_s. When the diagonal crack opens, the compressive force C_1' and the shear force V_{cz}', act always on the part of the beam below the crack. As a consequence T_2 becomes less than T_1 and this difference depends on the amount of shear reinforcement. Before flexural cracks all the shear is carried by the concrete. Between the flexural and inclined cracking stages, the external shear is carried by V_d, V_{ay} and V_{cz}. Eventually, the stirrups crossing the inclined crack yield and V_s remain constant for higher shear forces. When the stirrups yield, the inclined crack opens more rapidly causing V_{ay} to decrease and V_{cz} and V_d to increase rapidly as well; this action continues until either a splitting failure or crushing in the top fibers occurs due to a combination of shear and compression forces (from MacGregor (1997)).

3 Crack modeling of concrete structures

According to Plos (1995), to analyze properly the behavior of concrete structures in the ultimate limit state, the use of non-linear finite element methods is necessary. This is the case when the concrete crushes in the compressive zone and the reinforcement yields in the cracked tensile zones. Choosing a linear method can lead to incorrect results due to the strongly non linear material behavior caused by cracking.

Structural engineers must have basic knowledge in the use of finite element programs and methods due to the constant and rapid development of such techniques. The quality of the analysis depends on one hand on the choice regarding the level of detailing on which the analyst models the problem; but also on a number of other options such as material models, iteration method and convergence criteria, type of elements, modeling of applied loads and supports and so on.

Cracking represents the key feature in modeling the nonlinear behavior of reinforced concrete, governing its failure mechanism. Therefore, reliable finite element crack models must have successful numerical treatment methods as a prerequisite, Pavlovič (1995).

3.1 Smeared crack approach

One of the fundamental features required in order to analyze reinforced concrete structures in a realistic way, lies on a suitable material model. The description of cracking and failure within finite element analysis of quasi-brittle materials such as concrete has led to two fundamentally different approaches: the discrete and the smeared one. The smeared crack approach is based on the development of appropriate continuum material models; cracks are smeared over a certain finite element area corresponding to a Gauss point of the finite element, Cervenka Consulting (2000). Traditional smeared-crack models are known to be susceptible to stress locking and possible instability at late stages of the loading process, Jirásek (1998). Smeared crack models are nowadays widely used by structural engineers for most practical analyses since these models give reasonable and accurate results at lower costs than in the discrete crack models.

A computational advantage in this technique is that no mesh modifications are required throughout the analysis of the structure. This allows the element size to be similar as that of the specimens from which the constitutive relations and fracture criteria were obtained. The main issue in this approach is the modification of the stiffness properties and equilibrium conditions at integration points of cracked areas.

The smeared crack models are usually formulated in stress strain space. In the case of softening materials, this can lead to strong mesh size dependence and no energy dissipation in the finite element calculations. Consequently, special considerations are necessary to introduce some of the energy concepts of fracture mechanics.

The smeared crack models are classified into four categories: fixed orthogonal crack models; fixed non-orthogonal crack models; rotating crack models and plasticity

models. In this project, fixed orthogonal crack models have been used. In the fixed orthogonal crack models once a crack is initiated it is locked in its original direction, i.e. perpendicular to the principle tensile stress at the initiation point. Additional cracks can form at the same point but only in a plane which is orthogonal to the existing ones. Also, once a crack is formed it is never removed and continues to influence the failure process even if at later stages during the loading history it is completely closed.

3.2 The shear retention factor

According to Buyukozturk (2004), structural members subjected to shear forces, resist also the effects of flexure, axial forces and sometimes torsion. Shear stresses in concrete members may produce inclined cracks across the section as well as a sliding type of failure along a well defined plane due to external tension, load history, shrinkage, etc. Upon the application of shear forces the problem of quantifying the shear stress transfer across the crack sections arises. The general shear transfer mechanisms are: through uncracked concrete, arch or truss analogy, dowel action and aggregate interlock. The latter is defined as the portion of aggregates from one side of a crack into open spaces for the transfer of compressive and shear loads through the crack trajectory with parallel directions between the crack surfaces.

Consider the beam in Figure 3.1 which has a flexural shear failure that propagates from the extreme compression fiber to the tensile reinforcement. The shear is transferred across the crack by a combination of the following three actions: direct shear transfer by the uncracked concrete in the compression zone V_{cz}, aggregate interlock, V_a and dowel action of the longitudinal tension steel, V_d.

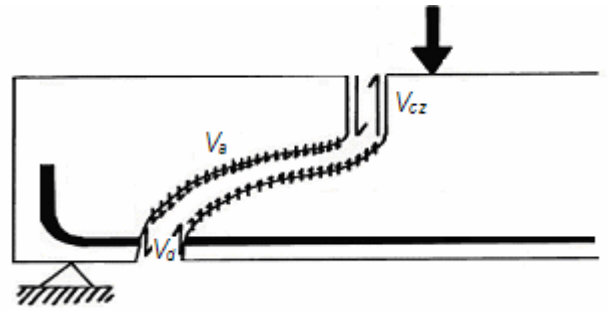

Figure 3.1 Shear transfer mechanism in a simply supported reinforced concrete beam, from Basu (2003).

Now, when the concept of aggregate interlock has been clearly outlined, it is important to point out the parameter called Shear Retention Factor (β) in numerical analysis.

According to Pavlovič (1995), in finite element analyses, the cracking response of concrete structures can be described by continuum constitutive models that account for the strain softening normal to the cracked plane. In addition, finite element models consider the reduction in shear stiffness along the cracked plane at integration points

in an element. These points can be defined as the points in an element used for the numerical integration of stiffness matrices and internal force vector. Consequently, material properties of finite element meshes need to be evaluated at these points.

Before cracking, the constitutive relations at each integration point can be expressed in the form:

$$\begin{bmatrix} \Delta\sigma_x \\ \Delta\sigma_y \\ \Delta\sigma_z \\ \Delta\tau_{xy} \\ \Delta\tau_{xz} \\ \Delta\tau_{yz} \end{bmatrix} = \begin{bmatrix} 2G+\mu & \mu & \mu & 0 & 0 & 0 \\ \mu & 2G+\mu & \mu & 0 & 0 & 0 \\ \mu & \mu & 2G+\mu & 0 & 0 & 0 \\ 0 & 0 & 0 & G & 0 & 0 \\ 0 & 0 & 0 & 0 & G & 0 \\ 0 & 0 & 0 & 0 & 0 & G \end{bmatrix} \begin{bmatrix} \Delta\varepsilon_x \\ \Delta\varepsilon_y \\ \Delta\varepsilon_z \\ \Delta\gamma_{xy} \\ \Delta\gamma_{xz} \\ \Delta\gamma_{yz} \end{bmatrix} \quad (3.1)$$

Where

G is the shear modulus of concrete.

μ is a normal retention factor.

$\Delta\sigma_x$, $\Delta\sigma_y$, $\Delta\sigma_z$. are the increments of normal stresses in the global coordinates.

$\Delta\tau_{xy}, \Delta\tau_{xz}, \Delta\tau_{yz}$ are the increments of shear stresses in the global coordinates.

$\Delta\varepsilon_x, \Delta\varepsilon_y, \Delta\varepsilon_z$ are the increments of normal crack strains in the global coordinates.

$\Delta\gamma_{xy}, \Delta\gamma_{xz}, \Delta\gamma_{yz}$ are the increments of shear crack strains in the global coordinates.

When cracking occurs, strains develop orthogonally to the direction of the maximum principal tensile stresses. As a consequence, the stress state changes from biaxial to uniaxial. Therefore, a constitutive C-matrix becomes anisotropic and the material coordinate system rotates. This means that the axes coincide with the principal stress directions with reference to a local coordinate system (*x',y'*) across and along the crack. A constitutive relation at each integration point may be expressed in the form:

$$\begin{bmatrix} \Delta\sigma_x' \\ \Delta\sigma_y' \\ \Delta\sigma_z' \\ \Delta\tau_{xy}' \\ \Delta\tau_{xz}' \\ \Delta\tau_{yz}' \end{bmatrix} = \begin{bmatrix} 2G+\mu & \mu & 0 & 0 & 0 & 0 \\ \mu & 2G+\mu & 0 & 0 & 0 & 0 \\ 0 & 0 & 0 & 0 & 0 & 0 \\ 0 & 0 & 0 & G & 0 & 0 \\ 0 & 0 & 0 & 0 & \beta G & 0 \\ 0 & 0 & 0 & 0 & 0 & \beta G \end{bmatrix} \begin{bmatrix} \Delta\varepsilon_x' \\ \Delta\varepsilon_y' \\ \Delta\varepsilon_z' \\ \Delta\gamma_{xy}' \\ \Delta\gamma_{xz}' \\ \Delta\gamma_{yz}' \end{bmatrix} \quad (3.2)$$

Where the notations in Equation (3.2) are the same as in Equation (3.1), but within the local coordinate system. Parameter β represents the shear retention factor.

This parameter quantifies the decrease in the incremental shear stiffness that occurs due to cracking.

What is the value that should be assigned to β?

The absence of a shear retention factor and for an element with all the integration points cracked in parallel planes, the stiffness matrix C in Equation (3.2) leads to either zero values in the diagonal elements or to ill conditioning.

In practical situations, it is common to have the whole concrete finite elements in tensile zones so that all their integration points may crack. The number of mechanisms increases when the structure goes from the uncracked to the cracked stage (β = 0.1) and even more when β is reduced from 0.1 to 0. Therefore, the modeling of brittle materials requires minimizing this possibility by the assignment of a non zero value to β.

It should be pointed out that the shear retention factor is a parameter associated with the concept of aggregate interlock. A widely held assumption states that aggregate interlock plays an important role in transferring shear across cracked areas. However, experimental evidences point out contrary conclusions.

This is the case of a simply supported reinforced concrete beam subjected to two symmetrical point loads with cracks preformed in the region below the neutral axis. By performing a finite element analysis to determine the ultimate load it is noticed that these conditions cause a drop of about 30% in the load carrying capacity of the beam in comparison to the analysis of the same beam without preformed cracks. This is because aggregate interlock does not have any effect on the shear resistance, which means that when cracking occurs the remaining stiffness in the post cracking concrete is negligible.

Aggregate interlock is not in agreement with the fundamental failure mechanisms of concrete, since a crack propagates in the direction of the maximum principal compressive stresses and opens in the orthogonal direction.

4 The SOLVIA FE-System

4.1 General

SOLVIA is a powerful finite element system for linear and nonlinear analysis of displacements, stresses and temperatures under static or dynamic conditions, SOLVIA Engineering AB (2000). It consists of three processors SOLVIA-PRE, SOLVIA and SOLVIA-POST, see Figure 4.1.

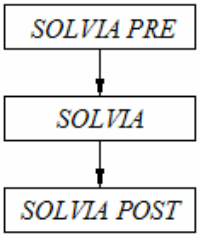

Figure 4.1 The three stages of SOLVIA, from SOLVIA Engineering AB (1999).

A general overview of the process in generating models and obtaining different results is presented.

The analyses models are defined by SOLVIA-PRE which is free format and is given as commands, parameters and data lines. This is where all input data is generated and stored as well as built up in a logical sequence.

In the SOLVIA stage, incremental equilibrium equations are used to solve nonlinear static displacement and stress analyses with different iteration methods based on time dependent variables.

In the SOLVIA-POST database the results from the analyses are stored. The nodal and element results can be displayed, listed and scanned with components referenced to a user selected coordinate system.

4.2 The concrete material model in SOLVIA

To consider non linear deformations in reinforced concrete structures, it is necessary to define suitable material models to represent this behavior. These models should be able to predict the non linear load deformation characteristics of the fracture process, von Hirschhausen (1999).

For the analysis of a reinforced concrete beam, the modeling should consider apart from a concrete model, a material model able to describe the behavior of the reinforcing steel.

In the SOLVIA finite element analyses three different material models were used i.e. concrete, plastic and elastic to simulate the collapse behavior of the different beams.

4.2.1 Stress strain relationship

The concrete material model in SOLVIA is considered as plastic based on a non linear uniaxial stress strain relation including strain softening. These features allow the analyst to model tensile failures (cracking) using the smeared crack approach and compression failures (crushing) by failure envelopes.

A common uniaxial stress strain curve relation for the concrete material model in SOLVIA is shown in Figure 4.2, which shows three phases: $\varepsilon \geq 0,\ 0 > \varepsilon \geq \varepsilon_c$, and $\varepsilon_c > \varepsilon \geq \varepsilon_u$.

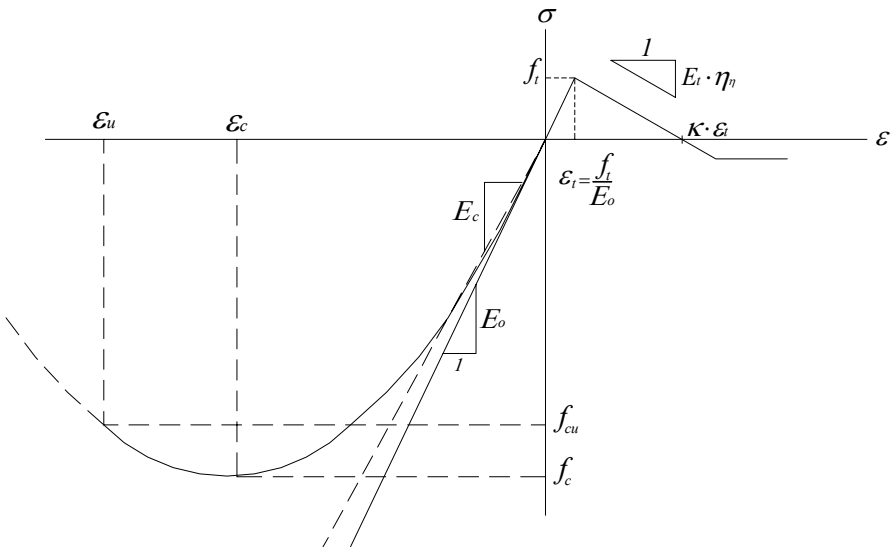

Figure 4.2 Uniaxial stress strain relationship for concrete

The material is in tension when $\varepsilon > 0$ and the stress strain curve is linear with an elastic Young's modulus E_o until the maximum tensile strength is reached.

$$\sigma = E_o \cdot \varepsilon \tag{4.1}$$

When the material is in compression $\varepsilon < 0$ the following relations are employed

$$\sigma / f_c = \frac{(E_o / E_c)(\varepsilon / \varepsilon_c)}{1 + A(\varepsilon / \varepsilon_c) + B(\varepsilon / \varepsilon_c)^2 + C(\varepsilon / \varepsilon_c)^3} \tag{4.2}$$

$$E = \frac{E_o[1 - B(\varepsilon / \varepsilon_c)^2 - 2C(\varepsilon / \varepsilon_c)^3]}{[1 + A(\varepsilon / \varepsilon_c) + B(\varepsilon / \varepsilon_c)^2 + C(\varepsilon / \varepsilon_c)^3]^2} \tag{4.3}$$

$$A = \frac{(E_o / E_u) + (p^3 - 2p^2)(E_o / E_c) - (2p^3 - 3p^2 + 1)}{p(p^2 - 2p + 1)} \quad (4.4)$$

$$B = \frac{2E_o}{E_c} - 3 - 2A \quad (4.5)$$

$$C = 2 - \frac{E_o}{E_c} + A \quad (4.6)$$

The stress strain relationship in the above equations assumes monotonic loading conditions. The parameters E_o, f_c, ε_c, E_c, f_{cu}, ε_u, $p = \varepsilon_u / \varepsilon_c$, and $E_u = f_{cu} / \varepsilon_u$ can be obtained from uniaxial tests, because sometimes is difficult to determine accurate values. However, they can be assumed reasonably by the analyst within a base range.

In order to define the mentioned parameters of concrete, a comparison among different stress strain curves for concrete is presented by means of several plots, see Figure 4.3.

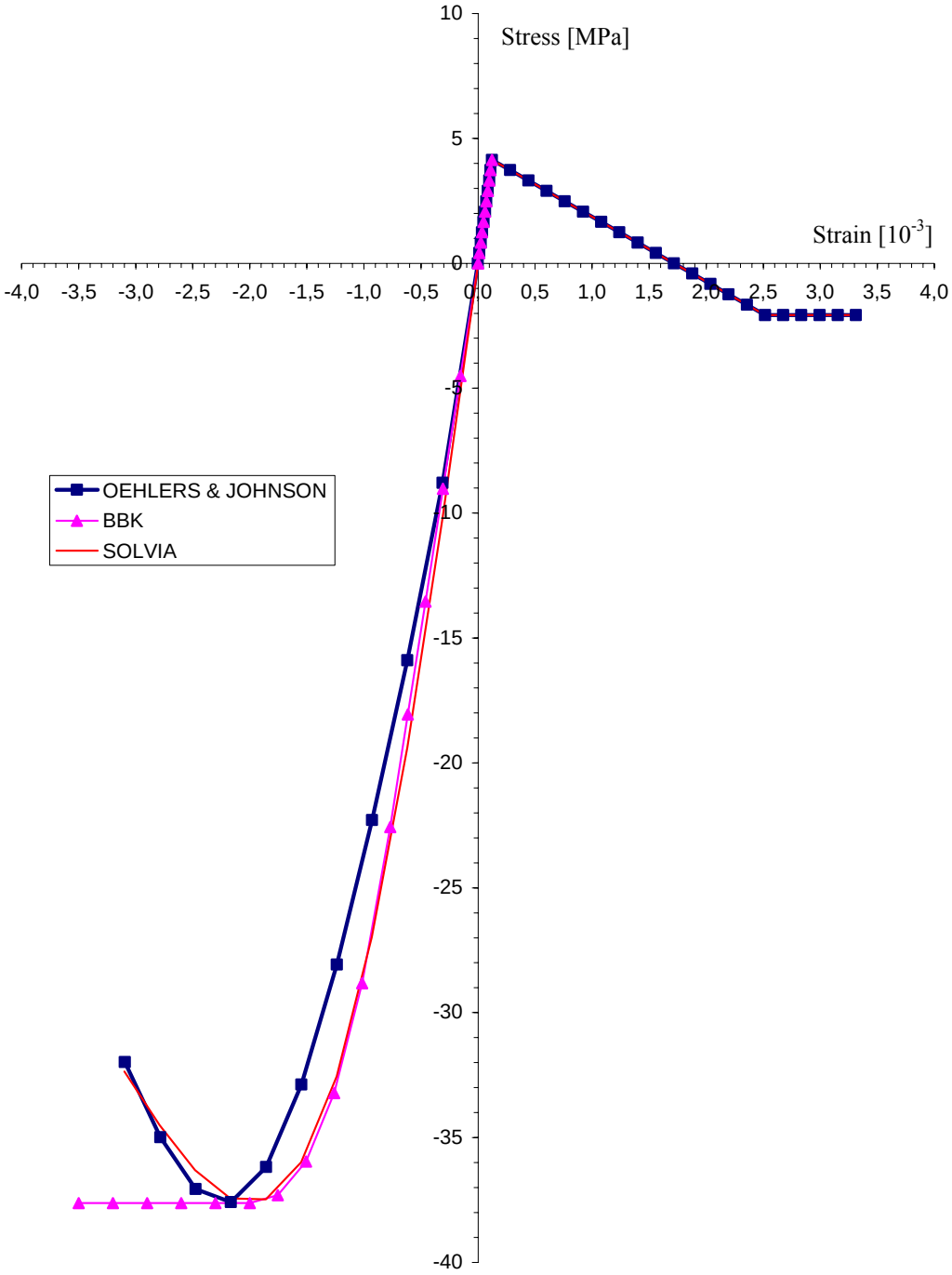

Figure 4.3 Uniaxial concrete stress strain relations based on different approaches.

The principal parameters in the curve with rectangular symbols in Figure 4.3 are calculated according to Oehlers (1995) and Johnson (2004).

From the CSA Code (Ref 3-7) the initial tangent modulus E_o is assumed to be about 10 percent greater than the secant modulus:

$$E_o = 5500\sqrt{f_c} \quad \textit{(MPa units)} \qquad (4.7)$$

The compressive strain ε_c at f_c is found from the parabolic stress strain curve by the following relation:

$$\varepsilon_c = 2\frac{f_c}{E_o} \tag{4.8}$$

The ultimate compressive stress f_{cu} can be determined by

$$f_{cu} = 0.85 \cdot f_c \tag{4.9}$$

The ultimate compressive strain ε_u can be calculated with Equation 4.10 which represents the unloading portion of the curve in Figure 4.2, giving the post-peak region of the stress strain diagram.

$$\varepsilon_u = \varepsilon_c\left(1+\sqrt{\frac{f'_c}{f_c}}\right) \tag{4.10}$$

Where $f'_c = f_{cu}$

The curve with triangular symbols was calculated using the equations given in BBK.

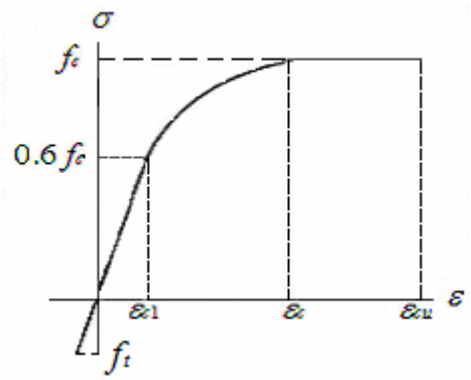

Figure 4.4 Uniaxial stress strain relationship for concrete, adopted from BBK (1994).

The linear portion of the curve is defined as

$$\varepsilon_{c1} = \frac{0.6 f_c}{E_c} \tag{4.11}$$

The non linear branch $\varepsilon_{c1} < \varepsilon < \varepsilon_c$ is approximated by

$$\frac{\sigma}{f_c} = 1 - 0.4\left(\frac{\varepsilon_c - \varepsilon}{\varepsilon_c - \varepsilon_{c1}}\right)^k \tag{4.12}$$

$$\varepsilon_c = 0.0020 \tag{4.13}$$

$$k = 1.5\left(\frac{\varepsilon_c}{\varepsilon_{c1}} - 1\right) \tag{4.14}$$

$$\varepsilon_{cu} = \left(0.3 + 0.7\frac{\rho}{2400}\right) \cdot 0.0035 \qquad (4.15)$$

Where ρ is the density of the concrete in (kg/m³) assumed to be 2400 for this case, which gives $\varepsilon_{cu} = 0.0035$.

Finally, the principal parameters in the last curve without symbols can be defined with the ranges: $0.8 f_c \le f_{cu} \le 0.95 f_c$, $0.0031 \le \varepsilon_{cu} \le 0.0035$ and $0.0020 \le \varepsilon_c \le 0.0022$, from the SOLVIA concrete model.

4.2.2 Failure envelopes

According to SOLVIA Engineering (1995), material failures envelopes are employed to model the material failures of concrete in tension and compression in two and three dimensional analyses as well as to account for multiaxial conditions in the stress strain diagram. A biaxial failure envelope in two directions is shown in Figure 4.5.

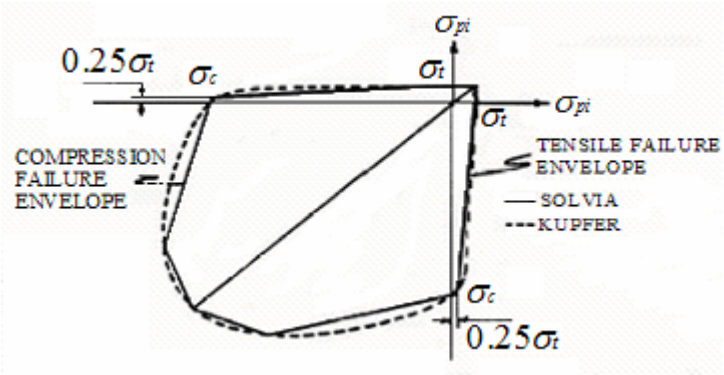

Figure 4.5 Biaxial failure envelope, from SOLVIA Engineering (1995).

As it is seen the material tensile strength decreases with the introduction of compressive stresses in any of the two principal directions, but not with tensile stresses. The biaxial failure envelope is a special case of the triaxial failure envelope for crushing and splitting failures for two dimensional analyses.

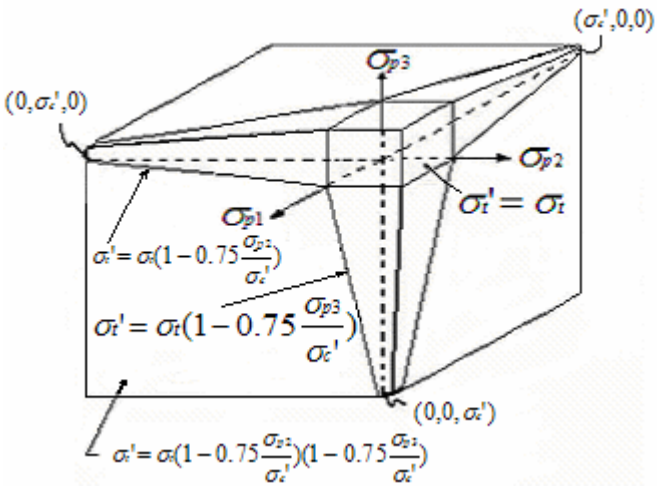

Figure 4.6 *Triaxial failure envelope for concrete in tension, from SOLVIA Engineering (1995).*

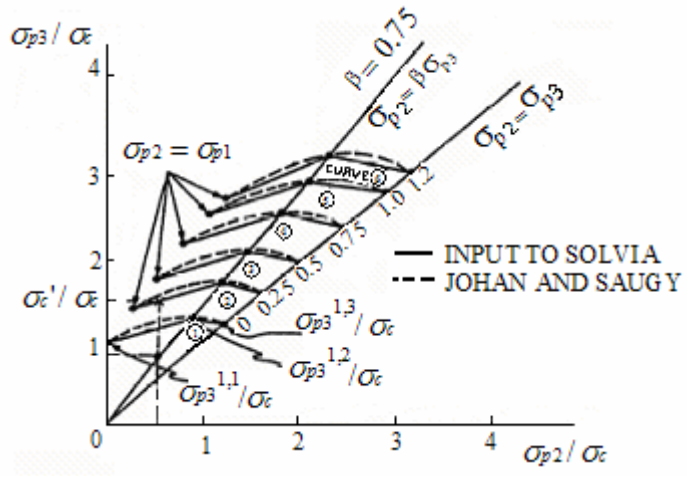

Figure 4.7 *Triaxial failure envelope for concrete in compression, from SOLVIA Engineering (1995).*

The triaxial tensile failure envelope is a general case of the biaxial envelope in two dimensional analyses (see Figure 4.6). However, the compressive failure envelope is defined by 24 points in terms of discrete ratios as shown in Figure 4.7 These input points should cover all the expected principal stress values ($\sigma_{p1} \geq \sigma_{p2}, \sigma_{p3}$, where σ_{p3} is the minimum principal stress). For six different input values of σ_{p1}, sections parallel to the plane σ_{p2} - σ_{p3} are input as well. In this plane, only one section is required. This is defined by $\sigma_{p1} = \sigma_{p2} > \sigma_{p3}$ *to* $\sigma_{p1} > \sigma_{p2} = \sigma_{p3}$. For values of σ_{p1} in between the input points, linear interpolation is used to define a biaxial failure surface for the σ_{p2} - σ_{p3} stresses. In this region, a bilinear failure envelope is obtained from the input values of σ_{p3} *at* $\sigma_{p1} > \sigma_{p3} = \sigma_{p2}$, $\sigma_{p1} > \sigma_{p2} = \beta\,\sigma_{p3}$ (with $0 < \beta < 1$), and $\sigma_{p1} > \sigma_{p2} = \sigma_{p3}$, where $\beta = \sigma_{p2}/\sigma_{p3}$ and represents the principal stress ratio in Figure 4.7. Biaxial and triaxial compression loads delay the formation of bond and mortar cracks because the period of stable crack propagation is longer and concrete becomes more ductile.

Tensile failure

A tension failure is assumed to occur if the tensile stress in a principal stress direction exceeds the tensile strength. This leads to crack formation orthogonal to the principal stress directions, with an increase in strains and decrease of stiffness and stress across the crack plane respectively. The normal and shear stiffness in a crack plane are reduced by two factors denoted as η_n and β respectively. The factor β is also referred to as the shear retention factor.

The incremental stress strain matrix, following a tensile failure is as follows:

$$C = \frac{1}{1-\nu^2}\begin{bmatrix} E_t & E_t\eta_\eta & E_t\eta_\eta & 0 & 0 & 0 \\ & E_c & \nu E_c & 0 & 0 & 0 \\ S & & E_c & 0 & 0 & 0 \\ & y & & G\beta & 0 & 0 \\ & & m & & G\beta & 0 \\ & & & m & & G \end{bmatrix} \qquad (4.16)$$

Where

E_t is the stiffness across a crack plane.

$G = E_c/2\cdot(1+\nu)$ is the shear modulus of elasticity.

E_c is the modulus of elasticity of concrete.

η_n is the normal stiffness reduction factor.

β is the shear stiffness reduction factor.

The shear stress in an active crack plane is limited by

$$\sigma \leq \beta \cdot f_t \qquad (4.17)$$

The concrete tensile behavior at a given section is determined using a bilinear stress strain relationship that allows the concrete to retain certain amount of tensile stress beyond the cracking strain. In the smeared crack approach, the concrete tensile stresses are averaged over a representative length to span cracks.

As it is seen in Figure 4.2, the parameter κ governs the gradient of the descending branch beyond the cracking strain of concrete, by specifying the strain value at which the concrete tensile stress is assumed to be zero. This gradient E_t can also be realistically estimated by $E_t = -70E_c/(57+f_t)$, which gives a value of $\kappa = 7.7$, Bazant (1984).

Compression failure

Crushing failure occurs when the stresses σ_{p2} and σ_{p3} obtained by interpolation from σ_{p1} in the triaxial compressive failure envelope lie outside the biaxial failure envelope, resulting in isotropic material properties with strain softening in all directions.

4.3 Numerical iteration methods and convergence criteria

In SOLVIA, two basic methods are implemented: Full Newton, Modified Newton and the BFGS method. All these iteration methods can be used with or without a line search procedure. The suitable choice of an iteration method depends directly on the treated problem. In this project the BFGS method was used.

4.3.1 The BFGS method with line searches

This method belongs to the family of Quasi Newton schemes developed for iteration on nonlinear system of equations, from Hirschhausen (1999). The method is suited for softening materials. According to Klaus-Jürgen Bathe (1996), the method consists in the establishment of a secant stiffness matrix from a previous solution. This secant matrix is then continuously updated. This type of methods can predict the softening behavior more effectively than the Modified Newton method, and with smaller errors than the Full Newton, (Hirschhausen (1999)) . The following equations are established in iteration (i) to define the algorithm of the method:

$$ {}^{t+\Delta t}K^{(i-1)}\Delta U^{(i)} = {}^{t+\Delta t}R^{(i)} - {}^{t+\Delta t}F^{(i-1)} \quad (4.18)$$

$$ \Delta U^{(i)} = {}^{t+\Delta t}U^{(i)} - {}^{t+\Delta t}U^{(i-1)} \quad (4.19)$$

$$ {}^{t+\Delta t}U^{(i)} = {}^{t+\Delta t}U^{(i-1)} + \theta^{(i)}\Delta U^{(i)} \quad (4.20)$$

Where

K is a tangent stiffness matrix based on the iteration history.

ΔU is a incremental displacement vector.

U is a vector of nodal point displacements.

R is an external load vector.

F is a nodal point force vector equivalent to the element stresses.

θ is an acceleration factor obtained from a line search in the direction of ΔU .

The procedure is as follows:

1. Define the direction of a displacement vector increment

$$\Delta U = ({}^{t+\Delta t}K^{-1})^{(i-1)}({}^{t+\Delta t}R^{(i)} - {}^{t+\Delta t}F^{(i-1)}) \quad (4.21)$$

2. Evaluate the equilibrium of the displacement vector increment ΔU with a line search

$${}^{t+\Delta t}U^{(i)} = {}^{t+\Delta t}U^{(i-1)} + \theta^{(i)}\Delta U^{(i)} \quad (4.22)$$

3. The acceleration factor $\theta^{(i)}$ is varied until the component of the out of balance loads in the direction of the displacement vector increment, i.e., $(\Delta U^T)({}^{t+\Delta t}R - {}^{t+\Delta t}F^{(i-1)})$ is satisfied for a convergence tolerance *STOL* with the following Equation:

$$(\Delta U^T)({}^{t+\Delta t}R^{(i)} - {}^{t+\Delta t}F^{(i)}) \le STOL \cdot (\Delta U^T)({}^{t+\Delta t}R^{(i)} - {}^{t+\Delta t}F^{(i-1)}) \quad (4.23)$$

4. The final value of θ that satisfies Equation 4.23 determines the solution of Equation 4.22.

5. The stiffness matrix is then updated with the following relation

$$({}^{t+\Delta t}K^{-1})^{(i)} = A^{(i)T}({}^{t+\Delta t}K^{-1})^{(i-1)}A^{(i)} \quad (4.24)$$

Under the condition that

$$c^{(i)} = \left(\frac{(\Delta U^{(i)T}) \cdot ({}^{t+\Delta t}R^{(i)} - {}^{t+\Delta t}F^{(i-1)})}{(\Delta U^{(i)T}) \cdot ({}^{t+\Delta t}K^{(i-1)}\Delta U^{(i)})} \right)^{1/2} < TOL \quad (4.25)$$

where

$A^{(i)} = I + v^{(i)}w^{(i)T}$ is an *n x n* matrix with vectors

$$v^{(i)} = -c^{(i)} \cdot {}^{t+\Delta t}K^{(i-1)}\Delta U^{(i)} - ({}^{t+\Delta t}R^{(i)} - {}^{t+\Delta t}F^{(i-1)}) \quad (4.26)$$

$$w^{(i)} = \frac{\Delta U^{(i)}}{(\Delta U^{(i)^T}) \cdot ({}^{t+\Delta t}R^{(i)} - {}^{t+\Delta t}F^{(i-1)})} \quad (4.27)$$

$${}^{t+\Delta t}K^{(i-1)}\Delta U^{(i)} = \theta \cdot ({}^{t+\Delta t}R^{(i)} - {}^{t+\Delta t}F^{(i-1)}) \quad (4.28)$$

A line search is an important feature for many iterative solution procedures. With the line search performed within iteration (*i*), the expense of the iteration increases, but less iteration may be needed for convergence. In addition, the line search may prevent divergence of the iterations. This increased robustness is the major reason why a line search can in general be effective, Klaus-Jürgen Bathe (1996).

4.3.2 Convergence criteria for the different methods

The different iterative solution methods in SOLVIA use the same convergence criteria in every iteration step to define equilibrium. In this project, the following criteria were used:

Force and Moment convergence criteria

For the translational degrees of freedom:

$$\frac{\left| {}^{t+\Delta t}R - M\,{}^{t+\Delta t}\ddot{U}^{(i-1)} - C\,{}^{t+\Delta t}\dot{U}^{(i-1)} - {}^{t+\Delta t}F^{(i-1)} \right|}{RNORM} \le RTOL \qquad (4.29)$$

For the rotational degrees of freedom:

$$\frac{\left| {}^{t+\Delta t}R - M\,{}^{t+\Delta t}\ddot{U}^{(i-1)} - C\,{}^{t+\Delta t}\dot{U}^{(i-1)} - {}^{t+\Delta t}F^{(i-1)} \right|}{RMNORM} \le RTOL \qquad (4.30)$$

Where

R and F have the same meaning as in Equation (4.18).

M is a constant mass matrix.

$\dot{U}$ is a nodal point velocity vector.

$\ddot{U}$ is a nodal point acceleration vector.

C is a constant damping matrix.

RNORM is a reference force.

RMNORM is a reference moment.

RTOL is a relative force and moment tolerance used to measure equilibrium iteration convergence.

5 Description of tested beams

5.1 Test specimen

Bresler and Scordelis investigated experimentally the shear strength of 12 simply supported reinforced concrete beams. Two of the test beams considered by Bresler and Scordelis were included in this report. These are denoted as OA-3 and A-1. In addition one beam tested at Chalmers University of Technology and denoted as B-14 was also analyzed.

Beams OA-3 and A-1 were subjected to a concentrated load acting at mid span, while beam B-14 was loaded with two symmetrical concentrated loads.

Figures 5.1-5.3 show the geometry of the tested beams with reinforcement and applied concentrated load (the dimensions of the beams are expressed in meters). The dimensions of the loading and support steel plates can be found in table 5.1. The dash lines in the figures indicate the location of the longitudinal and vertical reinforcement.

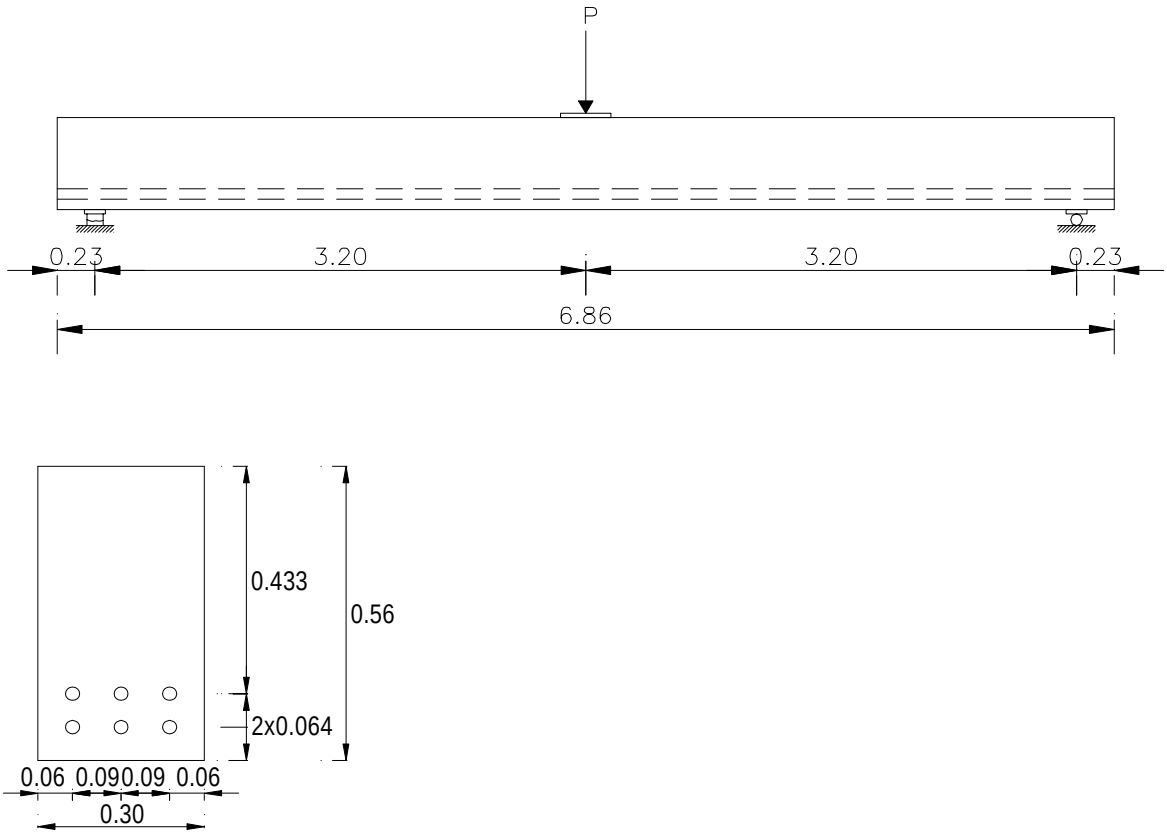

Figure 5.1 Geometry, loading and cross section for beam OA-3

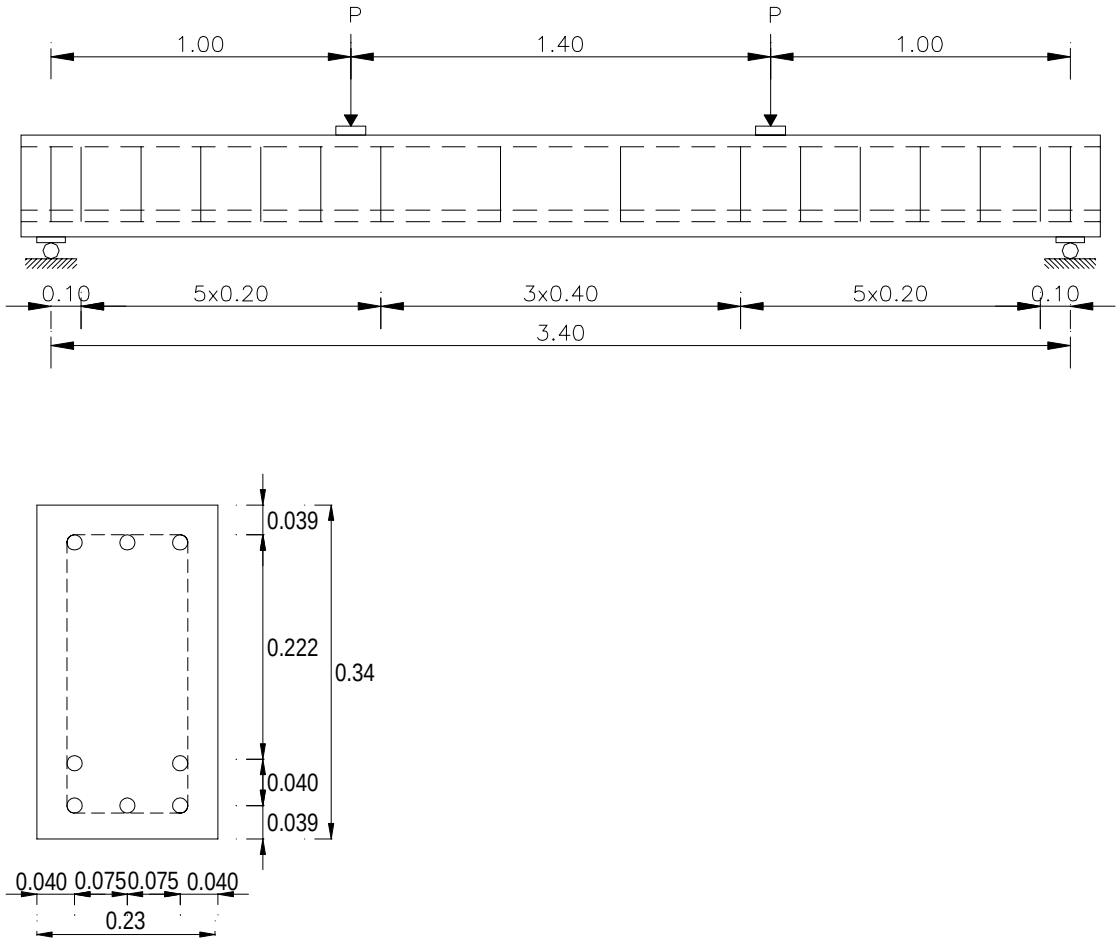

Figure 5.2 Geometry, loading and cross section for beam B-14.

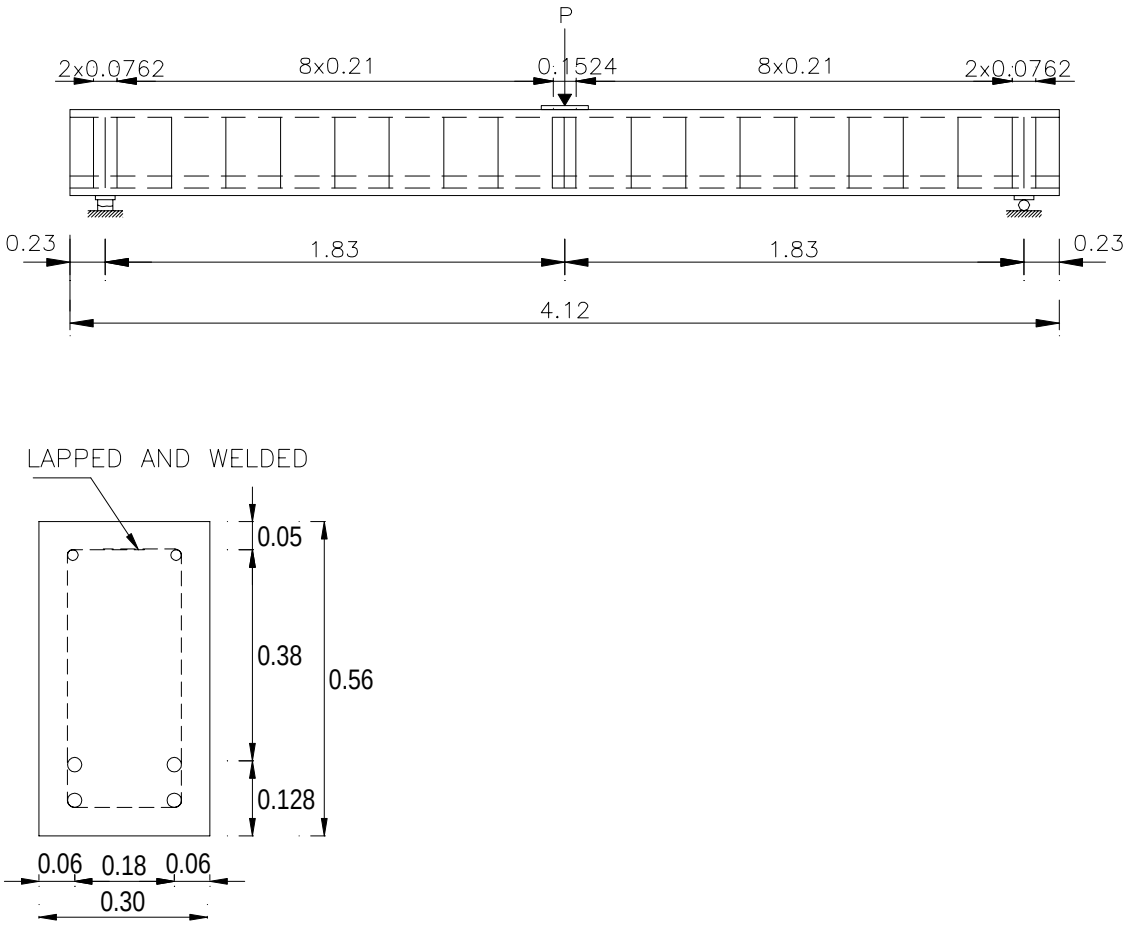

Figure 5.3 Geometry, loading and cross section for beam A-1.

Table 5.1 Dimensions of the support and loading steel plates for the tested beams.

Beam	Support plate			Loading plate		
	l [mm]	*b* [mm]	*h* [mm]	*l* [mm]	*b* [mm]	*h* [mm]
OA-3	304.8	127	25.4	304.8	304.8	25.4
B-14	230	100	30	230	100	30
A-1	304.8	127	25.4	304.8	304.8	25.4

5.2 Material properties

5.2.1 Concrete

The material properties of all the beams investigated experimentally are shown in Table 5.2 (mean values).

The values of the compressive strength f_c, were obtained from tests on 15x30-cm cylinders at an age of 28 days. The mean compressive strength for beam the B-14 was obtained from a test series which included three specimens, while ten specimens were used, to get the same parameter for beams OA-3 and A-1. Using the compressive strength f_c, for beam B-14 the values for E_c and f_t for the same beam were calculated.

The average values of modulus of rupture $f_{t,fl}$, for beam OA-3 and A-1, obtained by loading 15.24x15.24x2.54-cm beams at the third points of an 45.72-cm span, can also be found in table 5.2.

Table 5.2 Concrete material properties for tested beams(mean values)

Beam	E_c [MPa]	f_c [Mpa]	f_t [MPa]	$f_{t,fl}$ [MPa]
OA-3	-	37.62	-	4.14
B-14	30.4	29.2	2.78	-
A-1	-	24.09	-	3.86

5.2.2 Reinforcing steel

The reinforcing steel was modeled using a bilinear elastic-plastic model with isotropic strain hardening based on the Von Mises criteria and monotonic loading conditions.

In all cases, the longitudinal and vertical reinforcing steel was modeled by using truss elements. The following stress strain relationship shown in Figure 5.4 for the steel reinforcement model was considered to define the strain hardening modulus in the FE analyses.

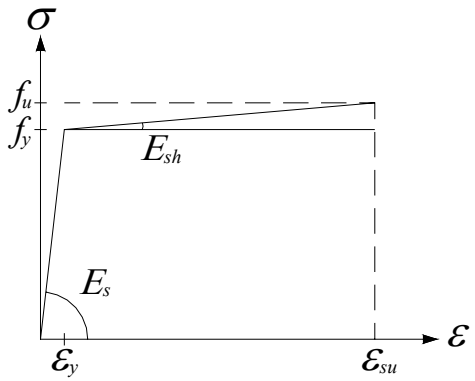

Figure 5.4 Stress strain relationship for reinforcing steel.

The steel plates were modeled using an isotropic linear elastic material model with plane stress elements and solid elements. The properties of the reinforcing steel for the beams tested experimentally and the dimensions of the support and loading steel plates can be seen in Tables 5.3 and 5.4

Table 5.3 Material properties and cross section area for the longitudinal reinforcement.

Beam	A_s [mm²]	A_s '[mm²]	E_s [MPa]	f_y [MPa]	E_s '[MPa]	f_y '[MPa]
OA-3	3847.81	-	205718.66	552.96	-	-
A-1	2565.21	253.35	218144.62	555.72	201576.68	345.86
B-14	1005.32	603	207000	628	207000	628

Table 5.4 Material properties and cross section area for the stirrups.

Beam	A_s [mm²]	E_s [MPa]	f_{yv} [MPa]
A-1	63.34	189.841	325.84
B-14	56.5	207000	325.84

5.3 Test performance

Beams OA-3 and A-1 were tested under center point load at an age of 13 days, and deformation control was performed in the tests. The beam was first loaded at about 30% of the ultimate load and in two or three increments and then the load was removed. The load was reapplied in increments of 45 *kN* to the load near failure and then it was increased in increments of 22.25 *kN* until failure occurred.

Beam B-14 was tested under two point loads using deformation control. The beam was gradually loaded to the failure stage and unloaded stepwise afterwards.

5.4 Results from the experiments

A brief summary of the overall behavior, cracking load and ultimate strength of designed series of test beams is presented below.

5.4.1 Type of failures

According to experimental results two different types of failures were obtained for the tested beams:

- Diagonal tension failure
- Shear compression failure

Diagonal tension failure occurred in the beams OA-3 and B-14. This beams failed shortly after the formation of the "critical diagonal tension crack". The reason for the failure is the longitudinal splitting in the compression zones, near the load point and horizontal splitting along the tensile reinforcement near the bottom edge of the beam.

Shear compression failure occurred in beam A-1. In this case the diagonal tension cracks were formed at approximately 60 percent of the ultimate load. Failures developed without propagation of the flexural cracks, indicating that the mechanism of failure was shear-compression. Final failures occurred due to splitting in the compression zone, but without splitting along the tension reinforcement.

The crack pattern for all tested beams can be seen in figures 7.7, 7.14 and 7.21 in sections 7.1-7.3.

5.4.2 Loads and deflections

The ultimate and cracking loads together with the maximum deflection obtained from the experiments can be found in Table 5.5. The load-deflection diagrams for all tested beams together with corresponding analysis results are shown in Figures 7.3, 7.10 and 7.17 in Sections 7.1-7.3.

Table 5.5 Summary of the experimental results.

Beam	P_{cr} [KN]	P_u [KN]	δ_{max} [mm]
OA-3	311.76	378.57	27.94
A-1	267.22	467.64	14.22
B-14	90	118.22	23.56

6 Finite element modeling

6.1 General

The finite element program SOLVIA was used for the FE-analysis. Five different models were used to examine the capabilities and limitations of the SOLVIA FE-system. The BFGS iteration method with LINE SEARCHES was employed for the FE-analysis. The AUTO-STEP method with different force norms and tolerances was used to control the load increment up to the ultimate load.

6.2 Coordinate system

The finite element models were defined in a Cartesian coordinate system with a y-z plane and an x-axis pointing outwards. The y-axis was pointing along the length of the beam in the east direction. The z-axis was point along the height of the cross section in the north direction.

6.3 Geometry

Due to symmetry only half of the beams were modeled. The following types of elements were chosen:

- 27-node solid elements for the concrete material models in three dimensions and 8-node plane stress elements for the concrete models in two dimensions.

- 3-node parabolic truss elements with an elastic-plastic material model for the steel reinforcement (stirrups and longitudinal reinforcement).

- 8-node plane stress elements for the support and loading plates in three dimensions and 8-node plane stress elements for the same plates in two dimensions.

6.4 Material models

The concrete was modeled using the SOLVIA concrete material models, based on an uniaxial stress-strain relationship, see Figure 4.2 in Section 4.2.1. A detailed explanation of the concrete material model in SOLVIA can be found in section 4.2.

The reinforcing steel was modeled using a bilinear elastic-plastic model, with isotropic strain hardening based on the Von Mises criteria and monotonic loading conditions. In all the cases, the longitudinal and vertical reinforcing steel was modeled by using truss elements. The following stress strain relationship shown in Figure 6.1

for the steel reinforcement model was considered to define the strain hardening modulus in the FE analyses.

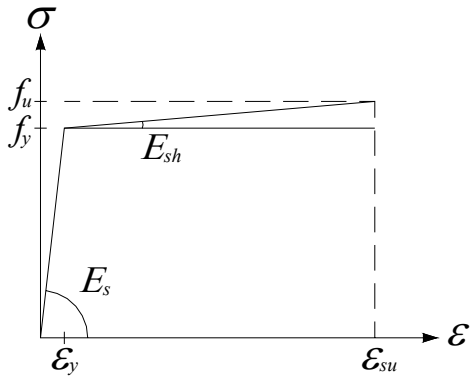

Figure 6.1 Stress strain relationship for reinforcing steel.

The steel plates were modeled using an isotropic linear elastic material model with plane stress elements or solid elements depending on the model. The properties of the reinforcing steel for the beams tested experimentally and the dimensions of the support and loading steel plates can be seen in Tables 5.3 and 5.4.

The material parameters of concrete and reinforcing steel used in the finite element analyses can be found in Tables 5.2-5.4, where the summary of the material properties is given. The parameters which are not given in the tables, such as E_0, f_{cu}, ε_u, ε_c were chosen and calculated according to Section 4.2.1. Principal stress ratio β, and stiffness reduction factor (described as 'stifac' in the SOLVIA code) were set to be 0.75 and $0.1 \cdot 10^{-3}$ respectively. The chosen and calculated values of the mentioned concrete parameters used in the FE-analysis for all the models can be found in Table 6.1. In the FE-analysis for model 1, 3 and 5 the average values of modulus of rupture, as the tensile strength of concrete were used.

Table 6.1 The concrete parameters used in FE-analysis, for the models

Model	κ	β	E_o [Mpa]	f_t [Mpa]	f_c [*Mpa*]	f_u [Mpa]	ε_c	ε_u
1	14	0.89	33734	4.14	-37.62	-32.353	-0.002	0.0031
2	13	0.887	30400	2.78	-29.2	-24.82	-0.002	0.0031
3	18	0.8	26994.9	3.86	-24.09	-22.828	-0.002	0.0031
4	14	0.89	33734	4.14	-37.62	-32.353	-0.021	0.0031
5	16	0.887	30400	2.78	-29.2	-24.82	-0.002	0.0031

The modulus of elasticity for steel plates, was chosen E_{sp} = 210 *GPa*, while the strain hardening modulus for reinforcement was calculated as $E_{sh} = 0.03 \cdot E_s$ in accordance with Figure 5.4 in section 5.2.2, where E_s, is given for each model in Table 5.3.

In the following section a detailed descriptions of the FE-models can be found. The models 1-3, were created using plane stress elements in 2D for beams OA-3, A-1 and B-14 respectively, while model 4 and model 5 were created with solid elements in 3D and represent beams OA-3 and B-14 respectively.

6.5 Boundary conditions and loads

Two different approaches were used to define the boundary conditions and the loads on the FE models based on the type of elements:

- The boundary conditions for the models created with plane stress elements in 2D were defined according to the following assumptions: the middle nodes at the bottom of the supporting plate were locked in z-direction, while the nodes along the symmetry line were fixed in y-direction. The boundary conditions for the models created with solid elements in 3D were defined as following: The surface of the cross section in the mid-span of the beam was fixed in the y-direction and the displacements of all the nodes in the surface were prevented. The horizontal surface at the bottom of the supporting plate was locked in z-direction. A disadvantage of the modeling of pinned boundary conditions using this approach is that, it generates a small moment reaction as in clamped boundaries. However, in the analysis for the 3D models, this type of boundary conditions resulted in good numerical predictions.

- The initial applied load was chosen as: concentrated for the models created with plane-stress elements in 2D (model 1-3) and pressure for the models made with solid elements in 3D (model 4 and model 5).

The initial applied load varied depending on the model. For model 1 and model 3 the initial load were set to be concentrated, equal to 500 *N*, while the same load were set to be 1000 *N* for model 2. The pressure was applied as initial load for the models 4-5, equal to 10714.668 N/m^2 and 43478.261 N/m^2 respectively. These pressure loads were obtained from the calculations, when the forces of 1000 *N* and 500 *N* were divided with the area of the plate surface, where the pressure load acts. The calculation of the pressure loads was performed in order to obtain load-deflection curves comparable to the curves from the experimental results. For all the models the location of the applied initial load, and defined boundary conditions can be seen in Figures 6.2-6.8.

6.6 Mesh for model 1

The concrete section for model 1 representing beam OA-3, was defined using 161 plane-stress elements, while the steel reinforcement consists of 46 parabolic truss elements. Steel plates were modeled with one plane-stress element.

The length of the plane-stress elements was chosen to be equal, for the elements above the supporting plate, as well as for the elements under the loading plate. The element height in the z direction was adjusted by the location of the reinforcement. Therefore, two different element heights were defined, one for inner and outer concrete covers and another for remaining plane-stress elements. The length of all truss elements was defined in the same way as the plane elements, see Figure 6.2.

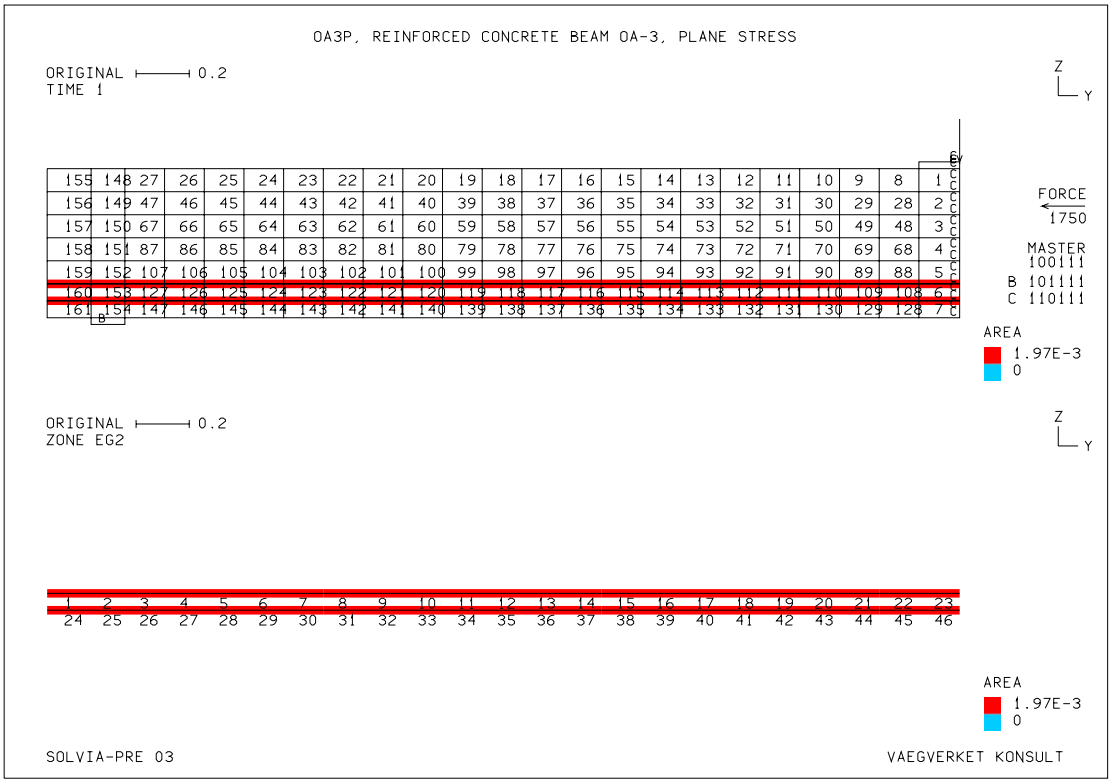

Figure 6.2 Mesh of the concrete and reinforcing steel for model 1.

6.7 Mesh for model 2

The concrete section for model 2 representing beam B-14 was modeled using 114 plane stress elements while the longitudinal steel reinforcement and the stirrups were modeled using 54 and 28 parabolic-truss elements respectively. The steel plates were modeled using one single plane stress element.

The plane-stress elements have the same length except elements 73-78 and 85-90. Similar to model 1, the element height in the z direction was determined by the location of the longitudinal reinforcement.

The mesh of the concrete and reinforcing steel, with element numbers, applied loads and defined boundary conditions are shown in Figure 6.3.

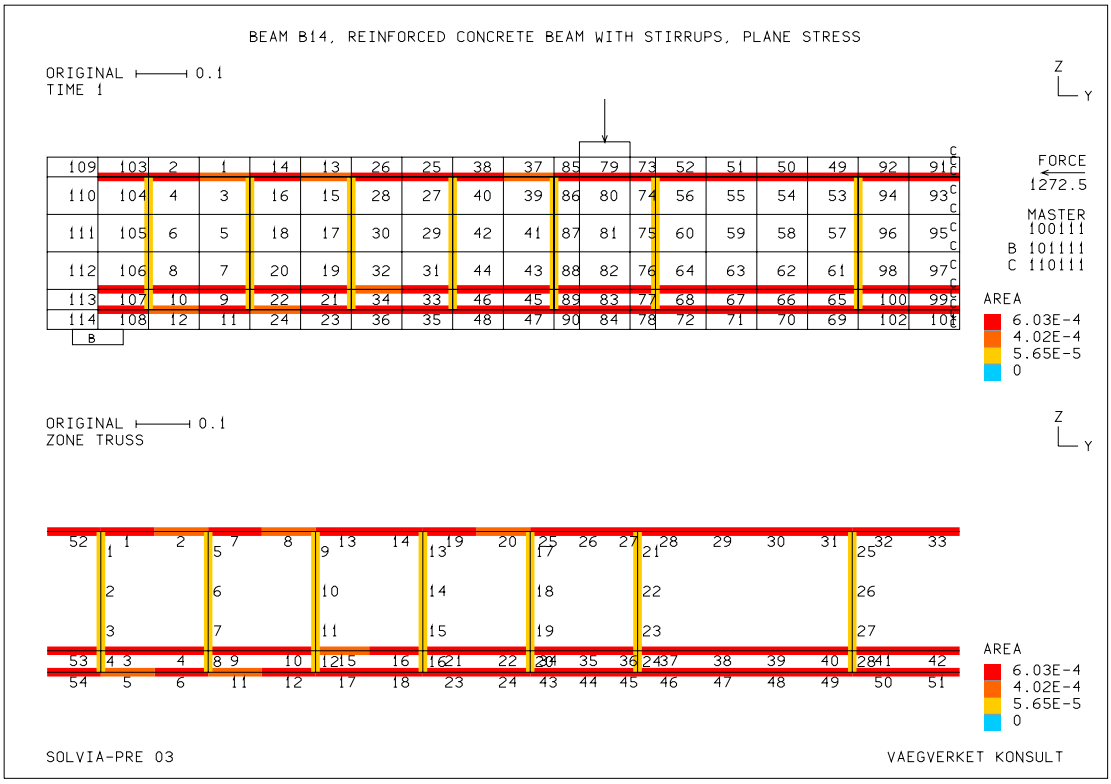

Figure 6.3 Mesh of the concrete and reinforcing steel for model 2.

6.8 Mesh for model 3

To model the concrete of beam A-1, 203 plane-stress elements were used while the longitudinal steel reinforcement and stirrups consists of 54 and 28 parabolic truss elements respectively. Steel plates were modeled with 2 equal plane-stress elements. The dimensions of the plane-stress elements and truss elements were as in the previous models, affected by the location of the longitudinal and vertical reinforcement, see Figure 6.4.

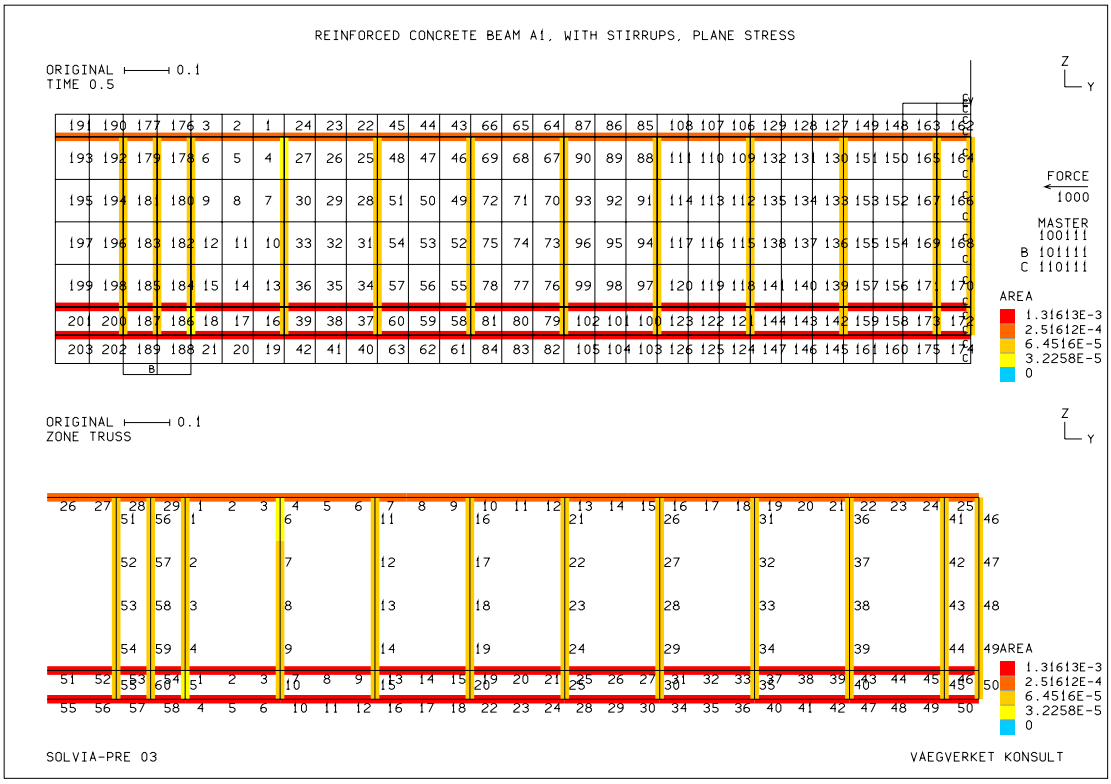

Figure 6.4 Mesh of the concrete and reinforcing steel for model 3.

6.9 Mesh for model 4

The concrete section for three dimensional model of beam OA-3, was created using 154 solid elements. One solid element was chosen to model each steel plate. The element dimensions for the longitudinal reinforcement were chosen according to the same approaches as for model 1. The mesh for model 4, together with the element numbers can be seen in Figures 6.5 and 6.6.

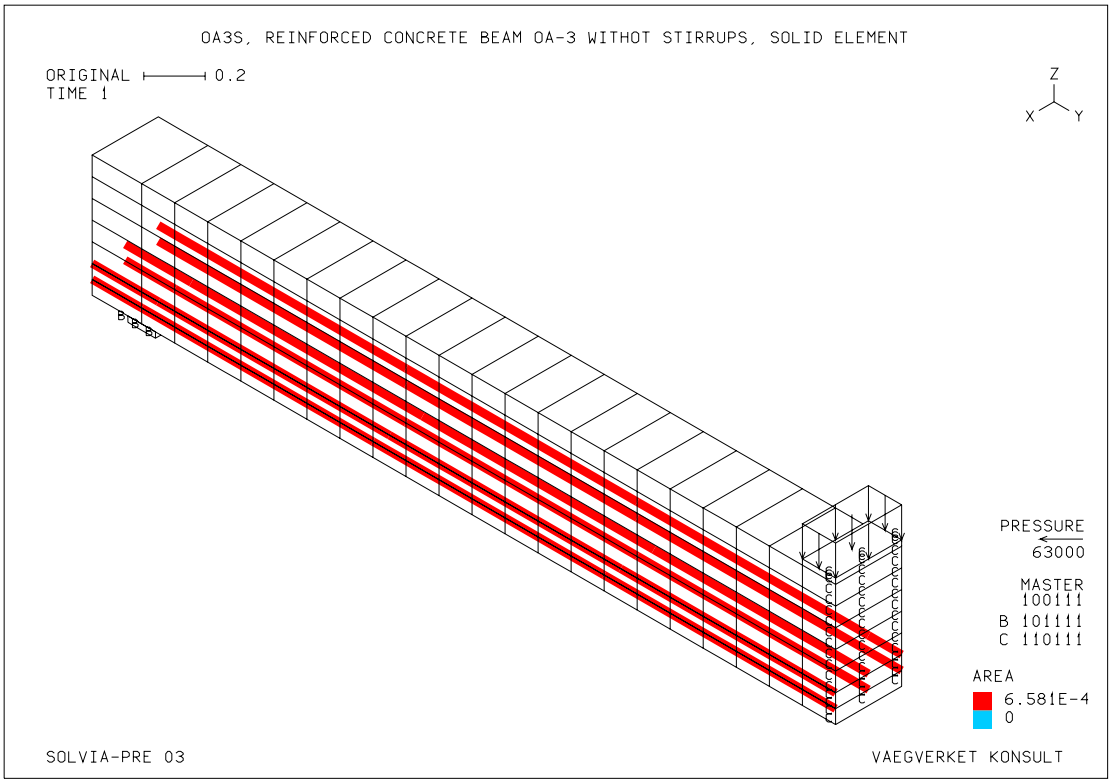

Figure 6.5 *Mesh of the concrete with shown location of the reinforcement for model 4.*

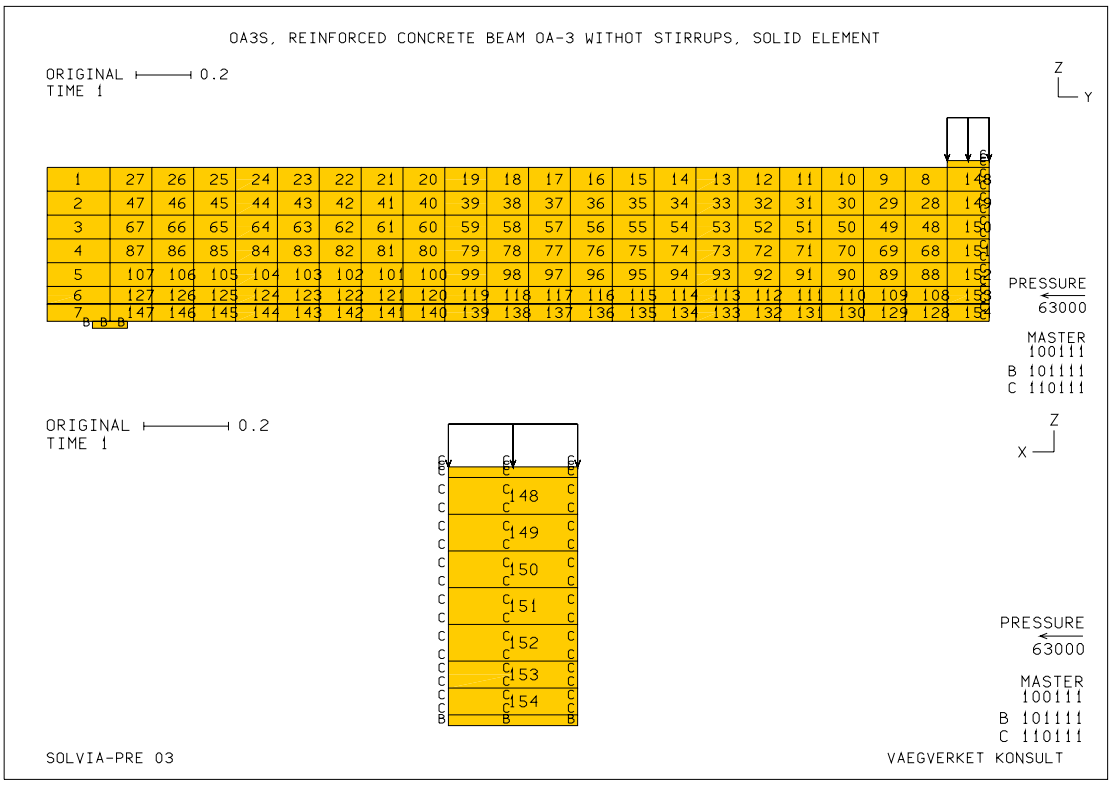

Figure 6.6 *Mesh of the concrete for model 4.*

6.10 Mesh for model 5

The mesh of the concrete section for model 5 made in 3D for beam B-14 consists of 120 solid elements. Each steel plate was modeled with one solid element, see Figures 6.7 and 6.8. The element length for the longitudinal reinforcement was chosen according to the same principle as they were done for model 2. The details for FE mesh and number of elements used to model the longitudinal reinforcement and stirrups for model 5 can be found in Appendix A.

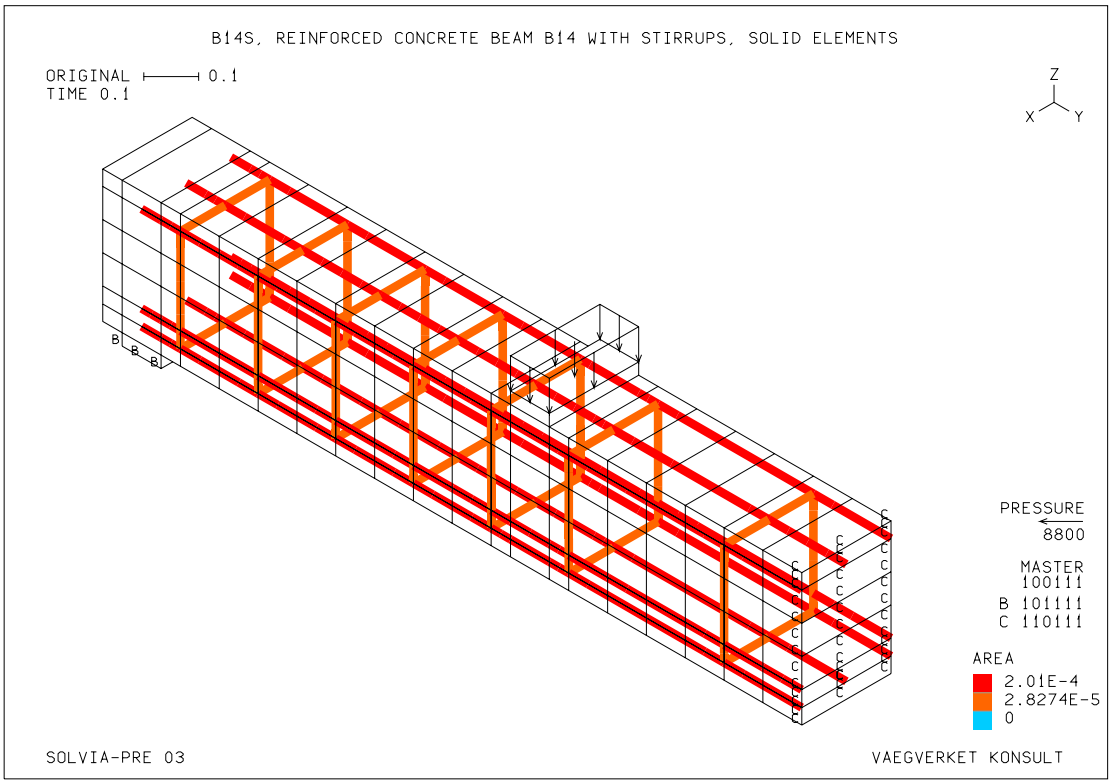

Figure 6.7 Mesh of the concrete with shown location of the reinforcement for model 5.

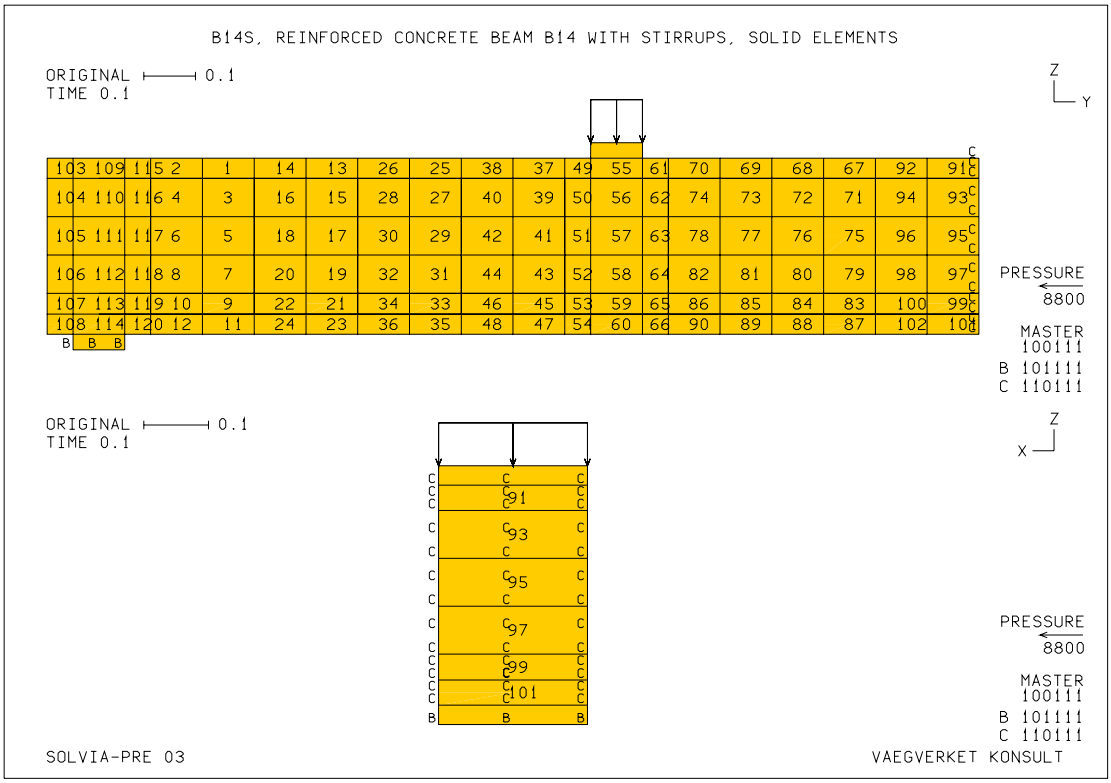

Figure 6.8 *Mesh of the concrete with shown cross-section and element numbers for model 5.*

7 FE-results

The FE-results, including plots of the predicted crack pattern for each of the models are presented in detailed in sections 7.1-7.5. For all the models the force tolerance during the iteration steps was chosen to be one percent. Five types of diagrams were obtained from the FE-analysis, these are: load-displacement relationship, stress-strain relationship and stress variation as well as strain variations over the concrete sections and reinforcing bars. Two different types of plots were also obtained according to FE-analysis and these are: contour plots of cracks and displacement and vector plots of the same items.

To plot the load-deflection diagrams and the stress-strain diagrams certain points were chosen. The chosen points represent critical points in the structure were the maximum values are expected to occur.

For load-deflection diagrams the points at mid-span were chosen as a reference points. The reference points selected to plot the stress-strain relationships for the concrete and longitudinal reinforcement are integration points for certain elements in the structures. In Figures 7.1 and 7.2 the location of the integration points for plane stress elements, solid and truss elements is shown.

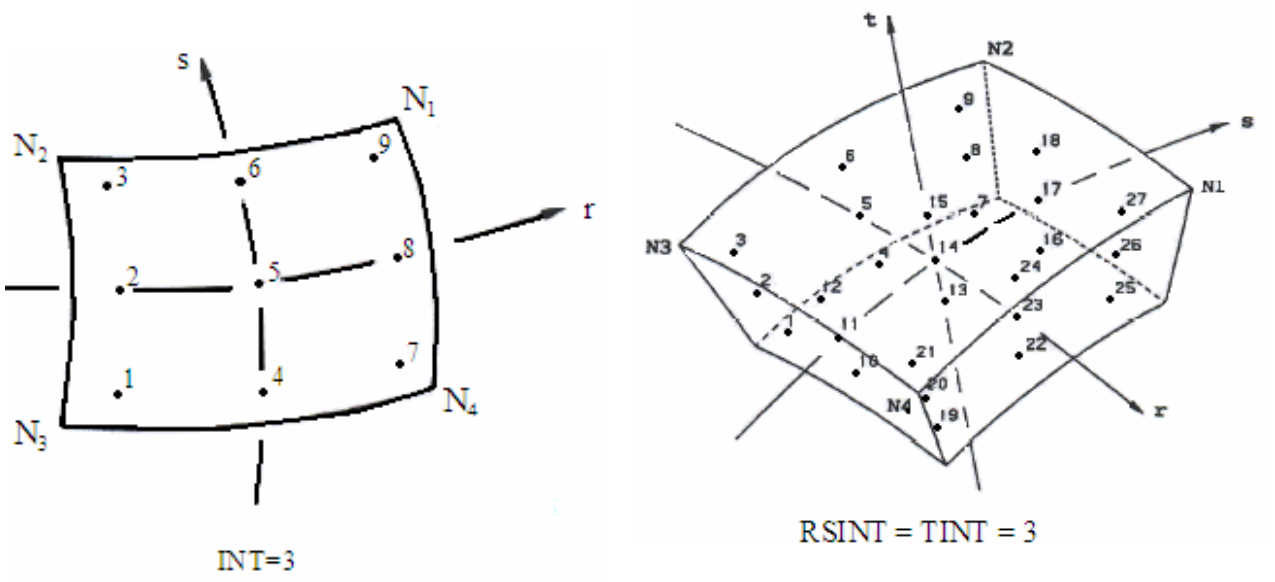

Figur 7.1 The location of integration points for plane and solid elements.

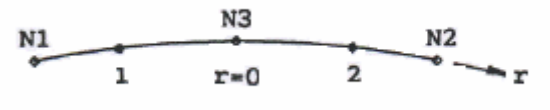

Figur 7.2 The location of integration points for truss elements.

The values in both the load-deflection and the stress-strain diagrams were calculated in each load step, while the values in contour and vector plots of cracks and displacement were calculated in the last load step. To plot the stress and strain variations over the cross-section and along reinforcing steel, certain cross-sections and bars were chosen. These sections were critical, and were obtained in the last load step.

7.1 Model 1

Model 1 is the plane stress model for beam OA-3, tested experimentally. In the FE-analysis the concrete parameters shear retention factor β, and the parameter κ, which defines the ultimate crack strain were set to be 0.89 and 14 respectively for this model. A force norm of 180 *kN* was chosen.

7.1.1 Load-displacement relationship

To examine how the deflection varies with increasing load, a plot of the load deflection curve was used. A load of 347.90 *kN* and a mid-span deflection of 22.10 *mm* were obtained from the FE-analysis in the last load step, see Figure 7.3.

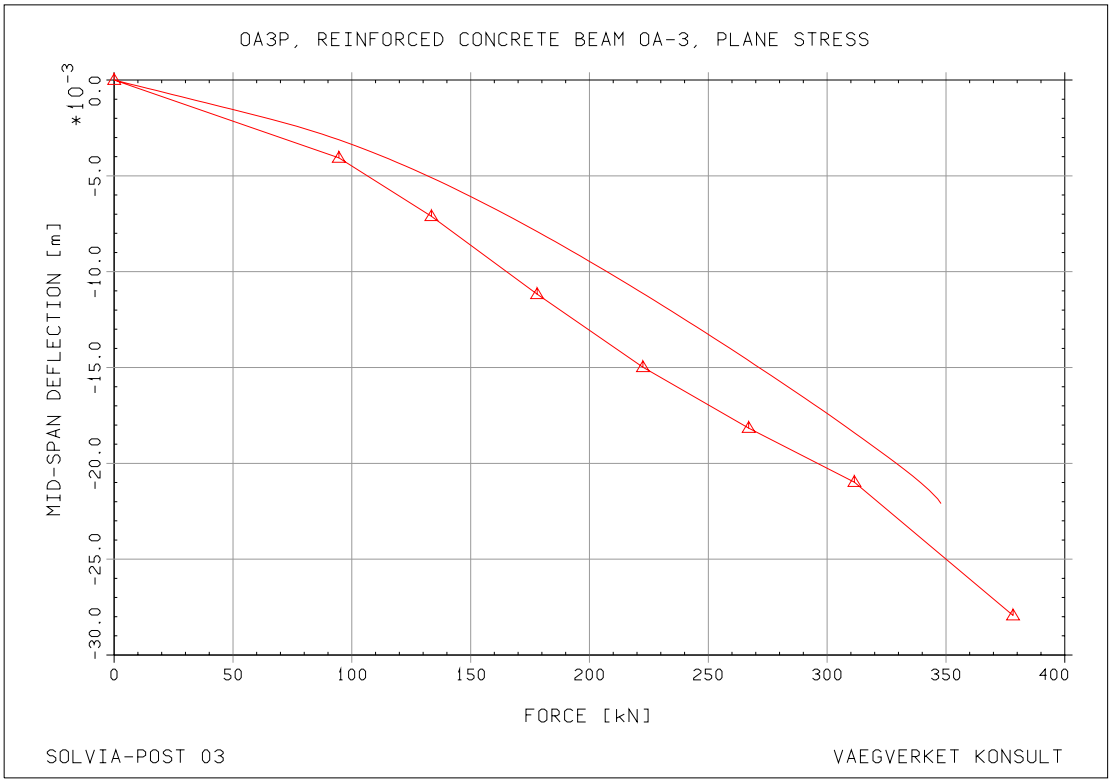

Figure 7.3 Load-deflection relationship. The lines with triangular symbols represent experimental results, while the lines without symbols are according to two-dimensional FE-analysis performed for beam OA-3.

In Figure 7.4 the vertical displacement for model 1 as a contour plot and the vertical displacement of all the nodes in the model as a vector, calculated in the last load step are presented. It can be observed that the elements close to the location where the load was applied have the largest vertical displacement, while the elements close to the support plate have very small displacement. Over the support plate displacement was prevented.

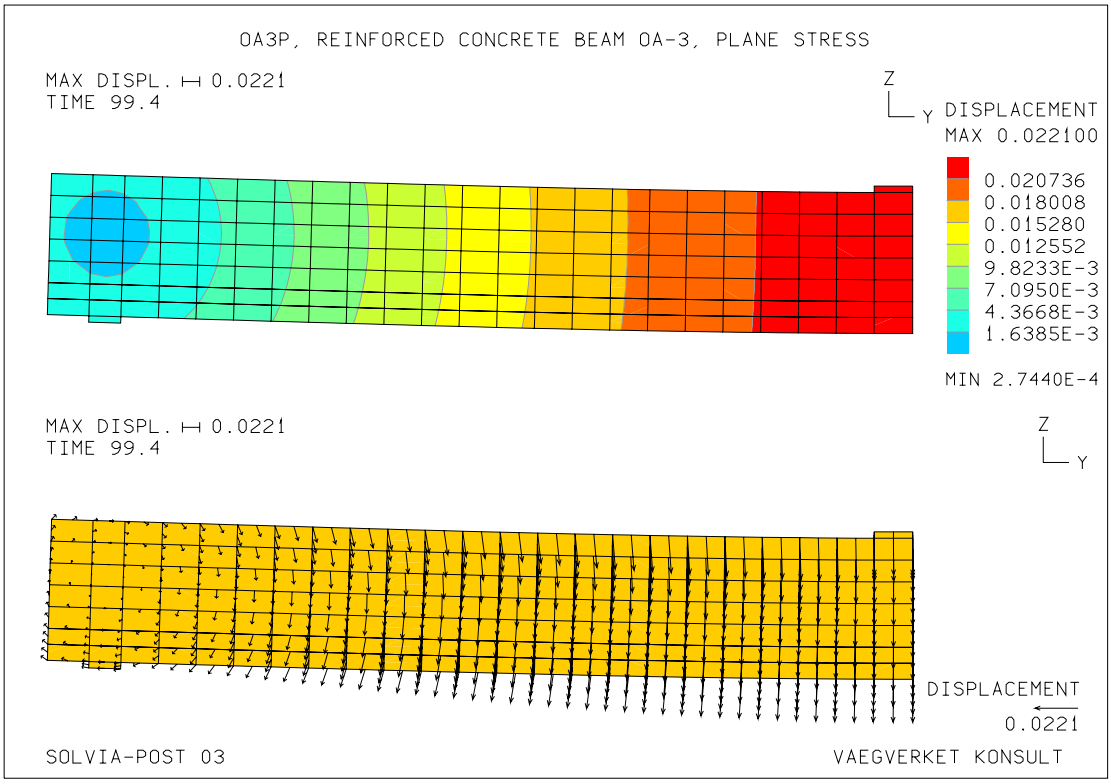

Figure 7.4 Contour and vector plots of the displacements in the last load step for model 1.

7.1.2 Crack pattern

A plot of the state of the concrete for the last load step is shown in Figure 7.5. The plot shows the crushed concrete in the compression zone and crack pattern predicted by the FE-model. The crushing of the concrete at the loading plate was a result of local high stress concentrations. In the crack pattern, obtained from the FE model, several flexural cracks can be noted, together with the splitting in the tension zone. The initiation of the critical diagonal tension crack can also be observed in the compression zone, near the load point, see Figure 7.6. The crack pattern in Figure 7.6 illustrates an interpretation of the vector crack normal, according to the FE-analysis.

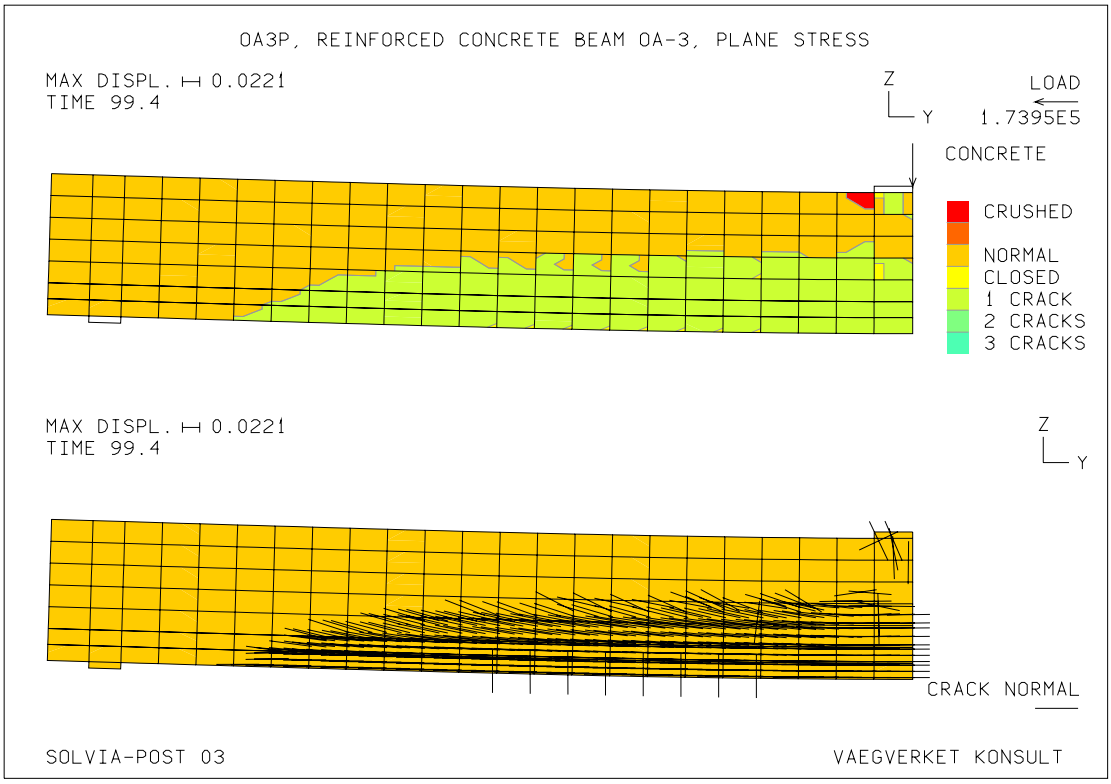

Figure 7.5 *Contour plot of the state of concrete including the values of the maximum ultimate load, (upper plot) together with the plot of vector crack- normal, for Model 1. The plots were obtained in the last load step.*

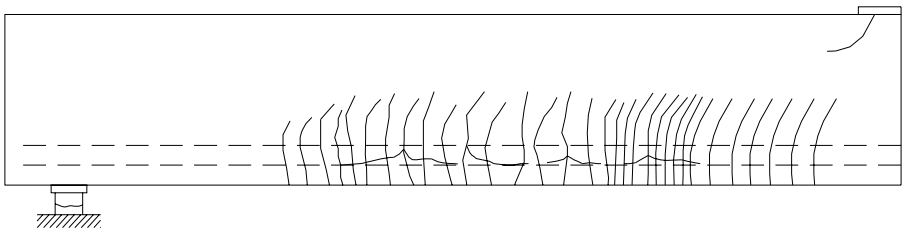

Figure 7.6 *Crack trajectories according to the vector plot of crack normal in Figure 7.5, for Model 1.*

The real crack pattern for beam OA-3, according to the performed tests can be seen in Figure 7.7.

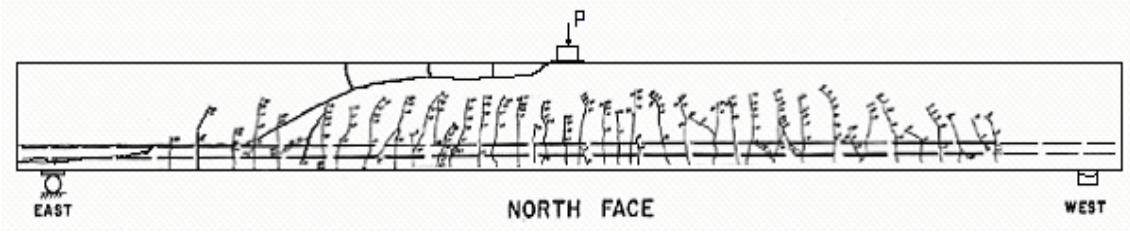

Figure 7.7 *Crack pattern for beam OA-3 according to the experimental results.*

7.1.3 Stresses and strains in the concrete and reinforcement

Figure 7.8 shows the diagrams of the stress and strain variations along the height of the selected cross section and the outer reinforcement layer. The values in these diagrams were calculated in each load step. The depth of the neutral axis is approximately 0.30 meters, according to the diagrams.

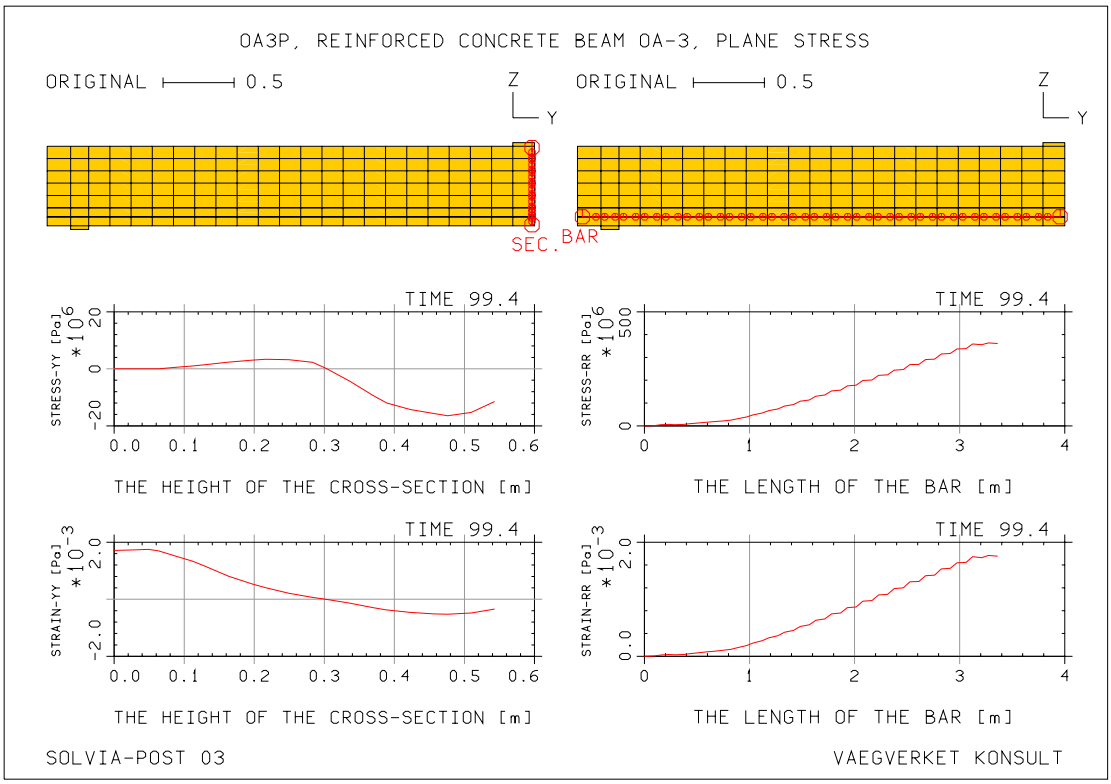

Figure 7.8 Stress and strain variations over selected cross section and along the longitudinal reinforcement for Model 1, calculated in each load step.

The stress-strain relationship for concrete and reinforcing steel obtained in each integration (load) step can be found in Figure 7.9. To plot the stress-strain relationship for concrete in tension, integration point 9 in element 7 was chosen. To obtain a diagram for the stress-strain relationship for the concrete section in compression, element 8 and integration point 9 were chosen. Point 2 in element 44 was selected to plot stress-strain relationship for reinforcing steel. All these elements with the integration points can be found in the diagrams for stress strain relationship, where 'EL' and 'P' denote elements and integration points respectively.

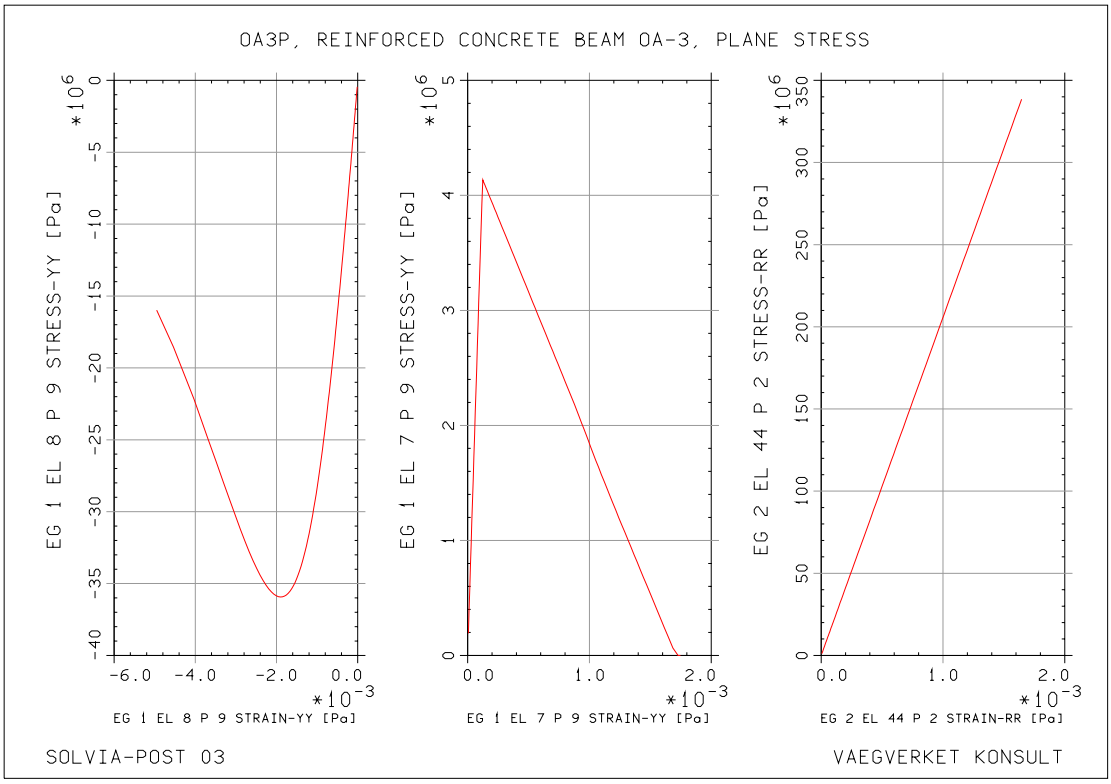

Figure 7.9 *Stress-strain relationships in the concrete and reinforcing steel calculated in each load step, for Model 1. The first and second diagrams from the left to the right represent compressive and tensile behavior of the concrete, while the diagram on the right shows the tensile behavior of reinforcing steel.*

7.2 Model 2

Model 2 is the one created for test beam B-14, using plane stress elements. The concrete parameters β and κ for this model were chosen to be 0.887 and 13 respectively. The force norm is equal to 80 *kN* in this case.

7.2.1 Load-displacement relationship

In this case, the maximum load reached according to the FE-analysis was 117.90 *kN*, while the reached mid-span deflection was 15.26 *mm*, see Figure 7.10. These items were obtained in the last load step.

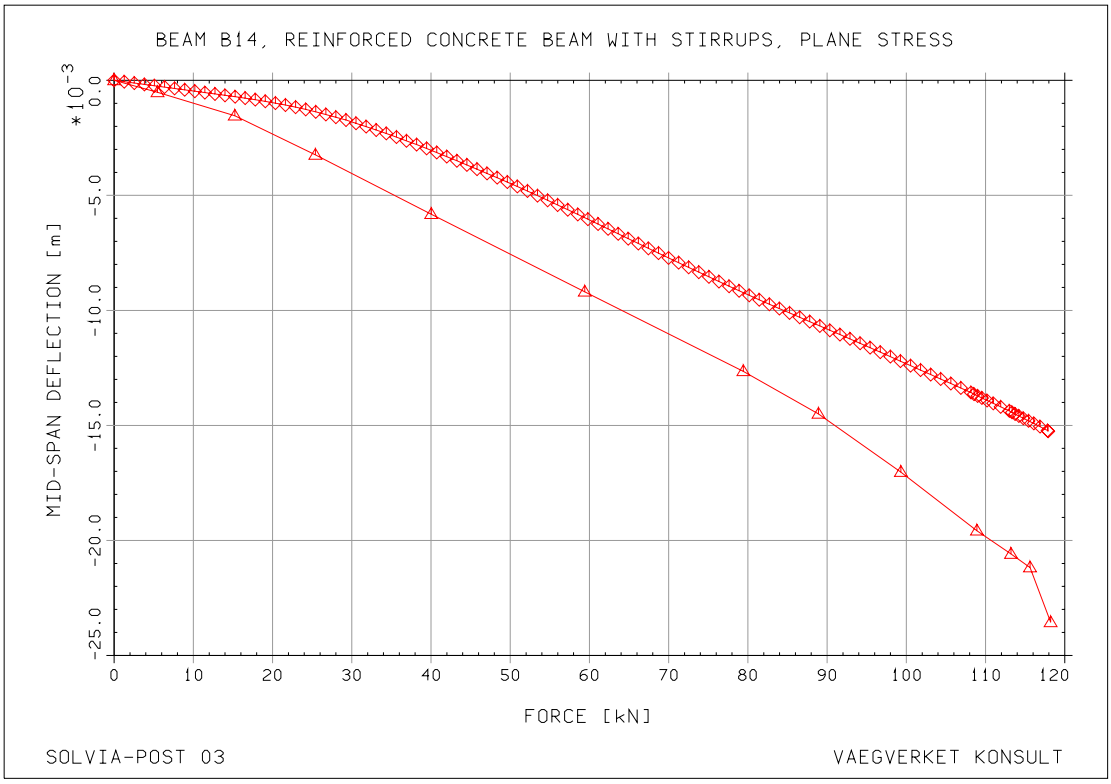

Figure 7.10 Load-deflection relationships. The lines with triangular symbols represent the experimental results, while the lines with rectangular symbols are according to two-dimensional FE-analysis for beam OA-3.

In the plot of the vertical displacements for the model, the zone on the right side of the loading plate has the largest vertical displacements. The vertical displacements decrease in the zone closer to support plate. Over the support plate the vertical displacement were locked, see Figure 7.11. The plots of the displacements as a vector and as a contour were reached in the last load step.

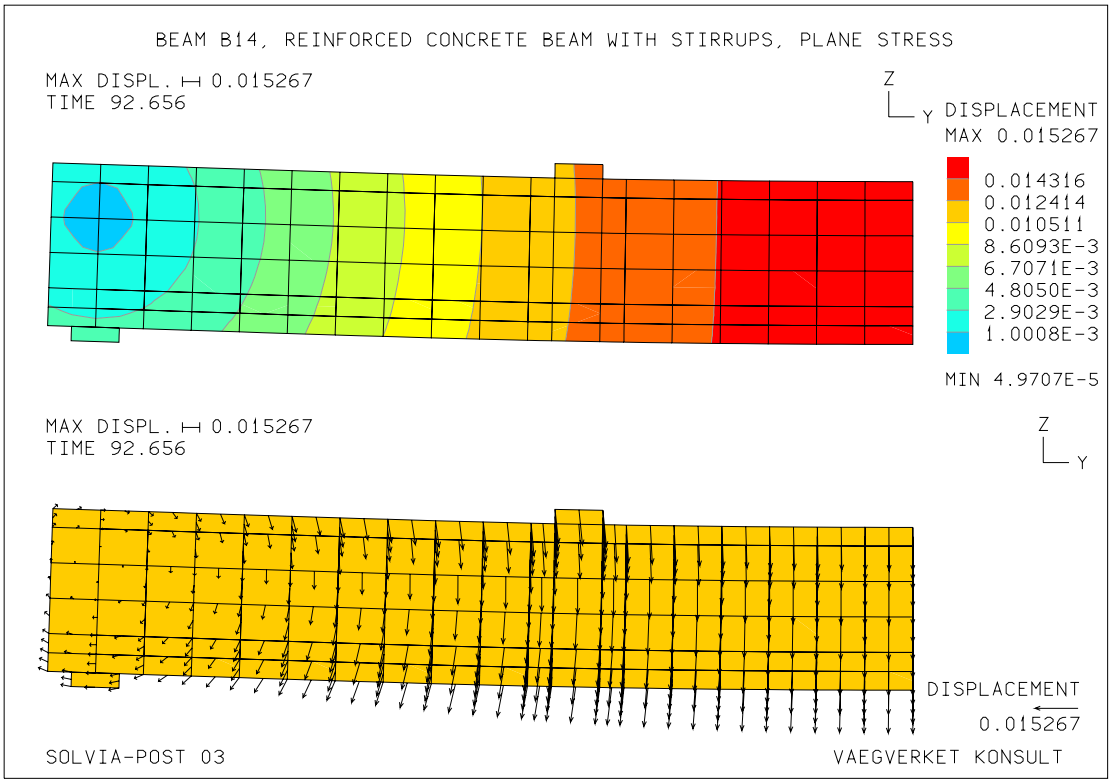

Figure 7.11 Contour and vector plots of the displacements in the last load step for model 2.

7.2.2 Crack pattern

Similarly as in Figures 7.5 and 7.6 the behavior and crack pattern of the Model 2 was illustrated. Figure 7.12 indicates crushing of concrete on both sides of the plate. This is due to high stress concentrations in the zone near the load point. The crack pattern according to FE model shows flexural cracks in the tension zone and the formation of a 'diagonal tension crack' in both the compression and tension zones. The initiation of the diagonal tension crack can be observed in both the compression zone near the loading plate and in the tension zone close to the support. These crack trajectories shown in Figure 7.13, represent the interpretation of the vector plot of crack normals, obtained in the FE-analysis.

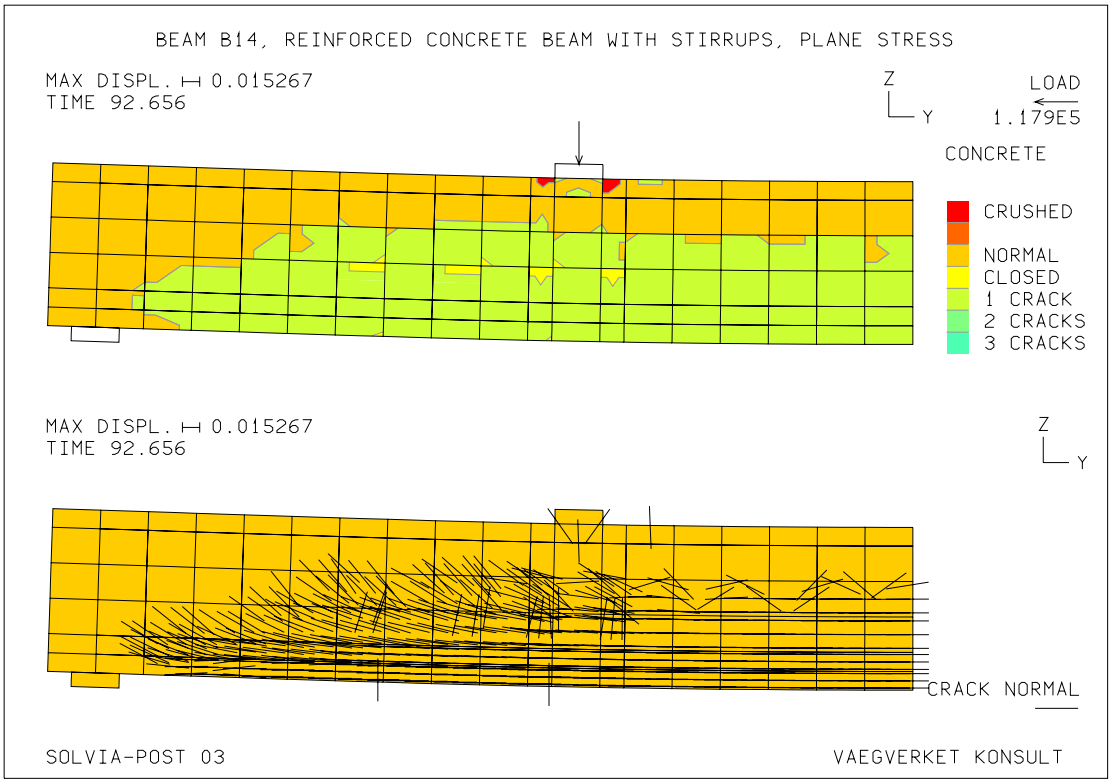

Figure 7.12 *Contour plot of the state of concrete including the values of the maximum ultimate load, (upper plot) together with the plot of vector crack- normal, for Model 2. The plots were obtained in the last load step.*

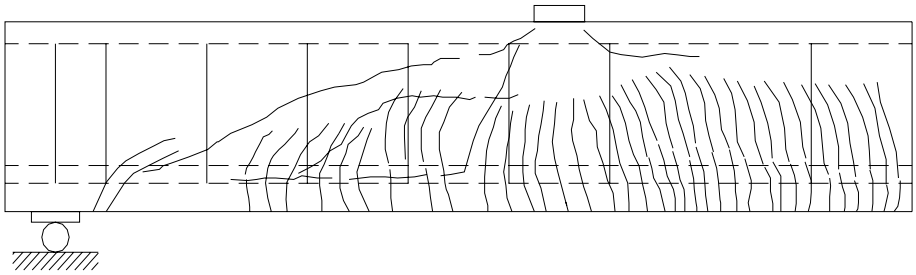

Figure 7.13 *Crack trajectories according to the vector plot of crack normal in Figure 7.12, for Model 2.*

In Figure 7.14 the crack pattern according to the tests, performed for beam B14 can be found.

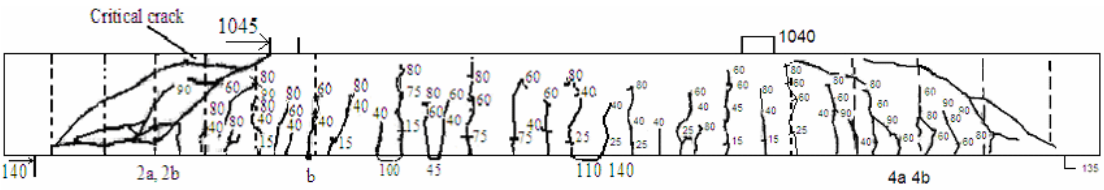

Figure 7.14 *Crack pattern for beam B-14 according to the experimental results.*

7.2.3 Stresses and strains in the concrete and reinforcement

In Figure 7.15, the diagrams of the stress and strain variations along the height of the selected cross section and the outer reinforcement layer are shown. The particular cross-section and reinforcement used to construct the diagrams are shown in the same figure. The values in the diagrams were calculated in each load step.

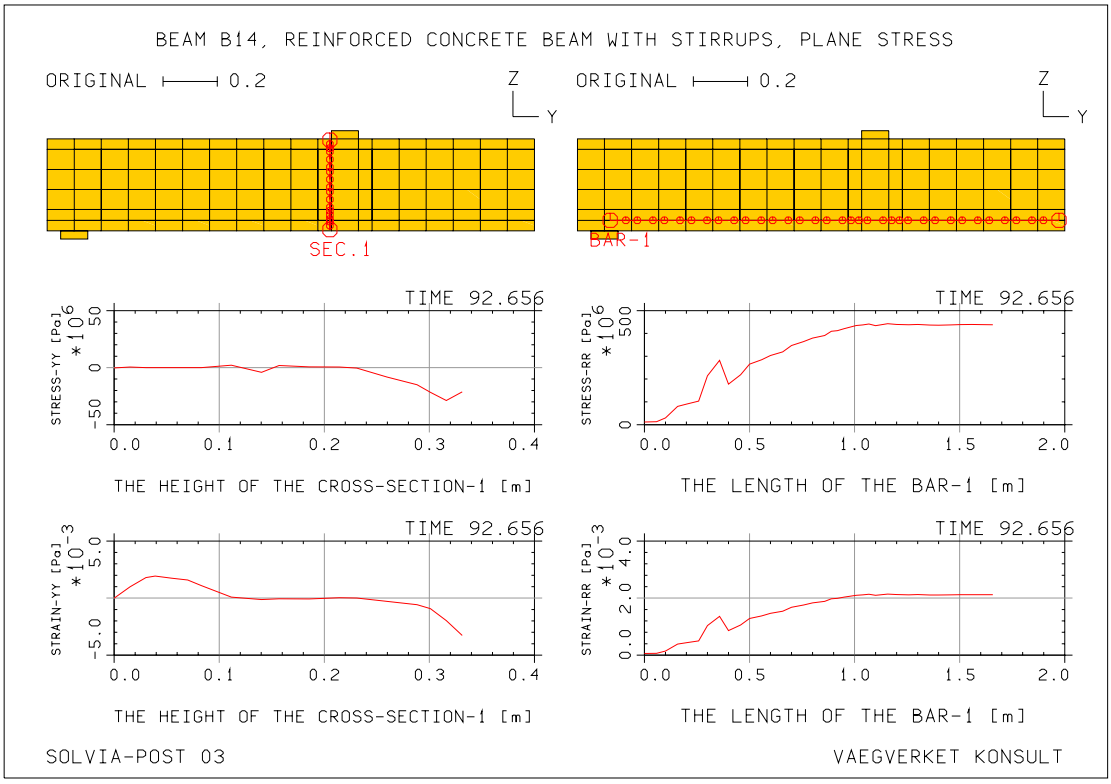

Figure 7.15 Stress and strain variations over selected cross section and along the longitudinal reinforcement for Model 2, calculated in each load step.

Figure 7.16 shows the stress-strain relationship for concrete and reinforcing steel for the critical elements and integration points. The chosen elements with the integration points can be found in the diagrams and the values in these diagrams were calculated in each load step.

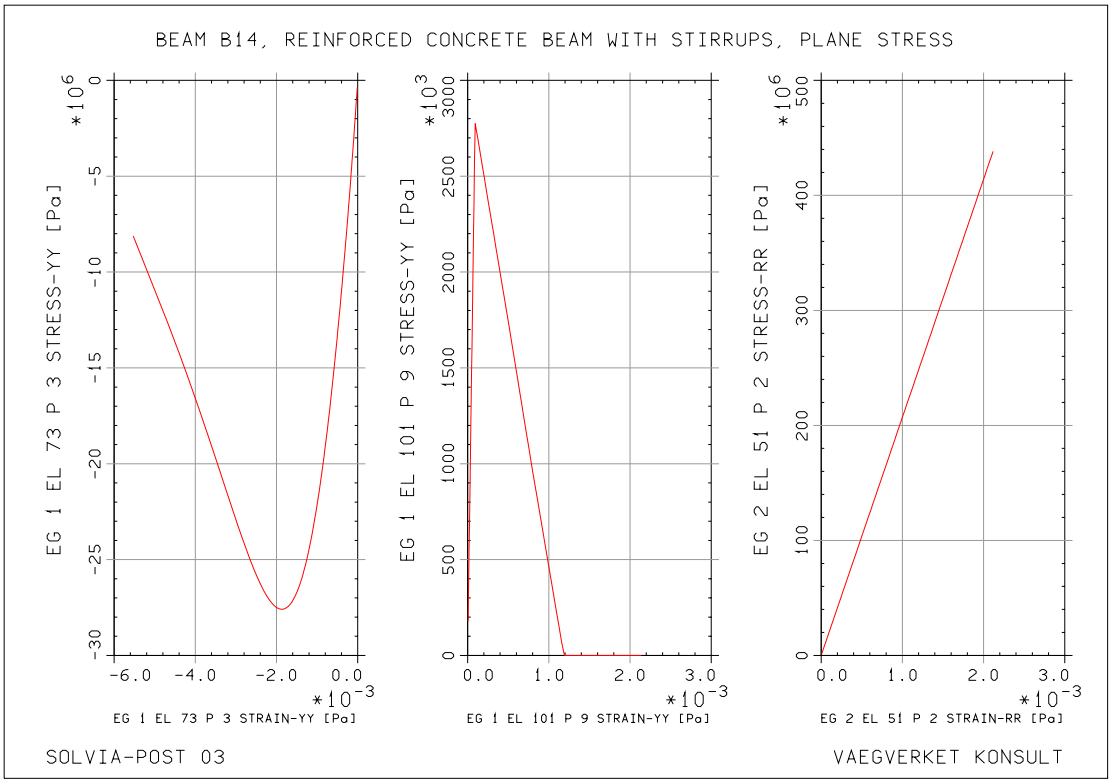

Figure 7.16 Stress-strain relationships in the concrete and reinforcing steel calculated in each load step, for Model 2. The first and second diagrams from the left to the right represent compressive and tensile behavior of the concrete, while the diagram on the right shows the tensile behavior of reinforcing steel.

7.3 Model 3

Model 3 was created for experimentally investigated beam A-1. The concrete parameters $\beta = 0.8$ and $\kappa = 18$ were used in this case. For this model, a force norm was set to be 100 *kN*.

7.3.1 Load-displacement relationship

A maximum load of 478 *kN* and a mid-span deflection of 9.053 *mm* were reached for this model in the last load step, see Figure 7.17.

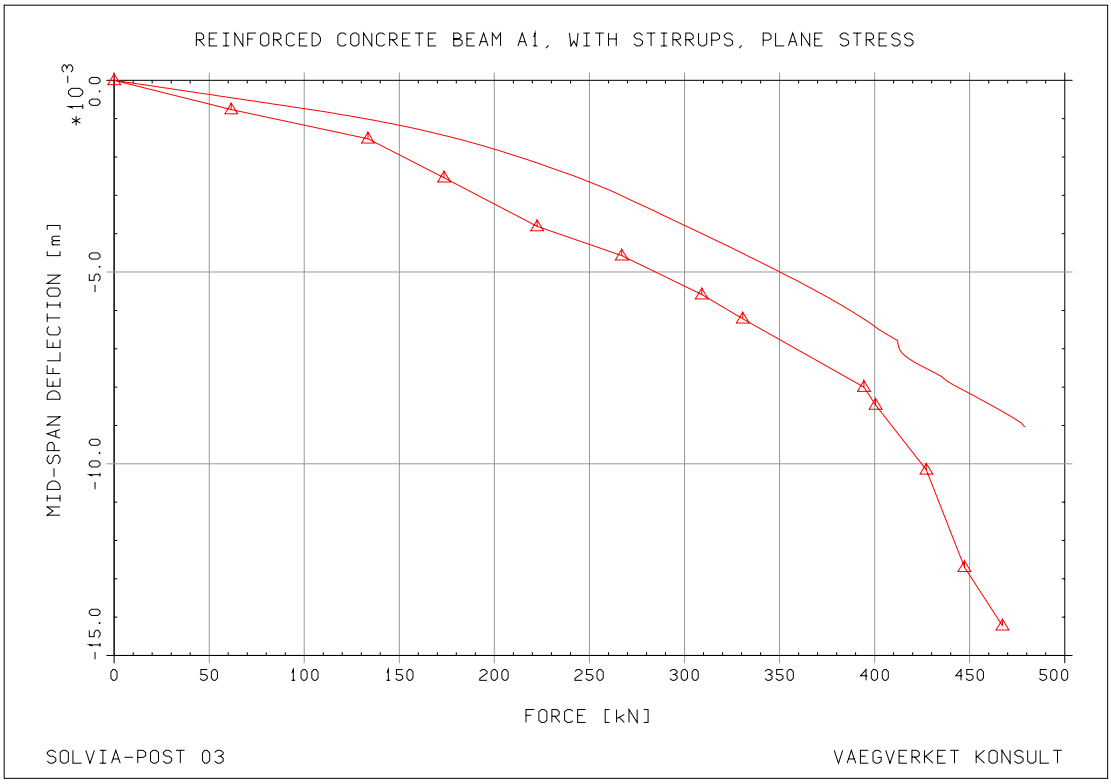

Figure 7.17 Load-deflection relationships. The lines with triangular symbols are according to the experimental results, while the lines without symbols were obtained in two-dimensional FE-analysis performed for beam A-1.

The vertical displacement for model 3, shown as a contour and as a vector, calculated in the last load step, can be found in Figure 7.18.

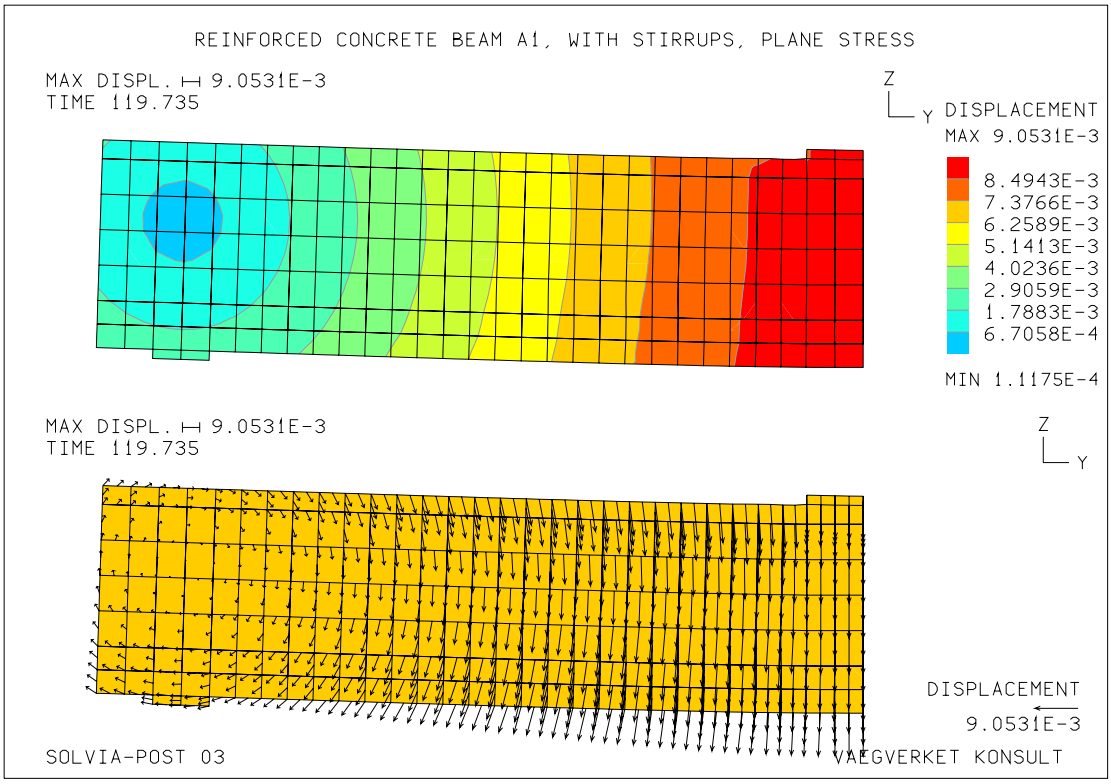

Figure 7.18 Contour and vector plots of the displacements in the last load step for model 3.

7.3.2 Crack pattern

Figure 7.19 shows the crushing of the concrete in the zone under the loading plate and the vector plot of crack normals, calculated in the last load step.

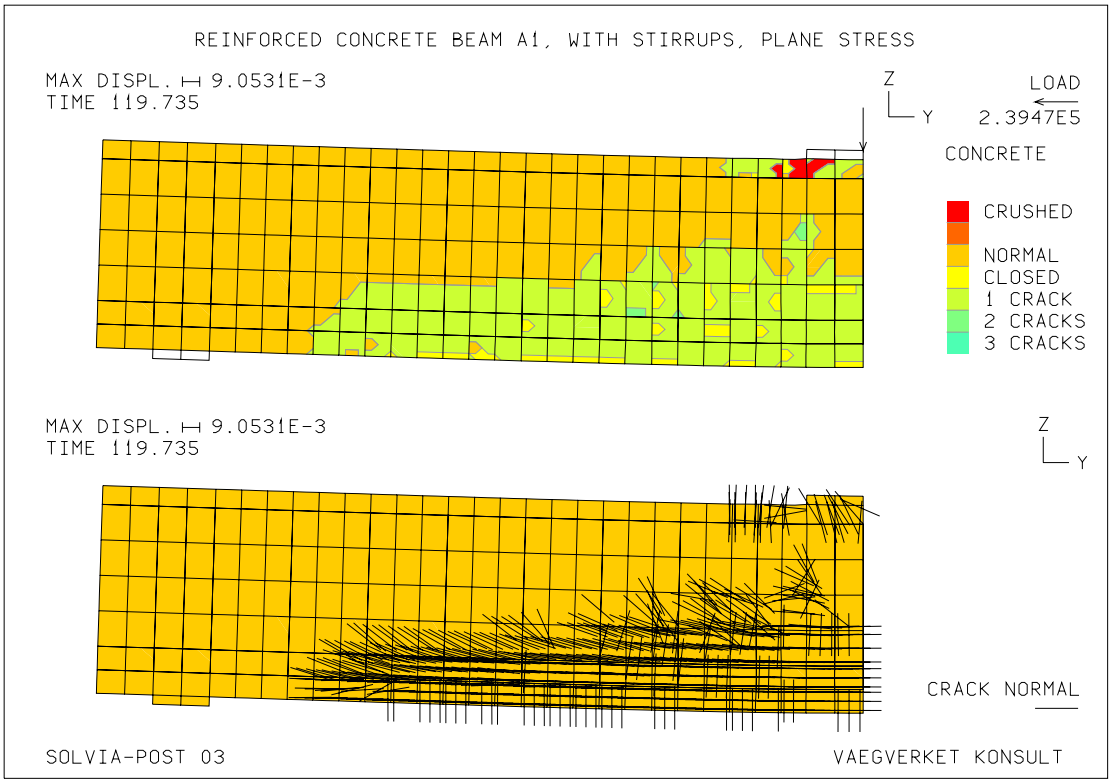

Figure 7.19 *Contour plot of the state of the concrete including the values of the maximum ultimate load, (upper plot) together with the plot of vector crack- normal, for Model 3. The plots were obtained in the last load step.*

The crack pattern for model 3 is very similar to the crack pattern for model 1. The only difference compared with model 1 is the 'critical diagonal tension crack'. A small part of the 'critical diagonal tension crack', initiated at the loading plate in the compression zone, can be observed, see Figure 7.20. The crack trajectories in this Figure illustrate the interpretation of the vector plot of crack normals, according to the FE-model.

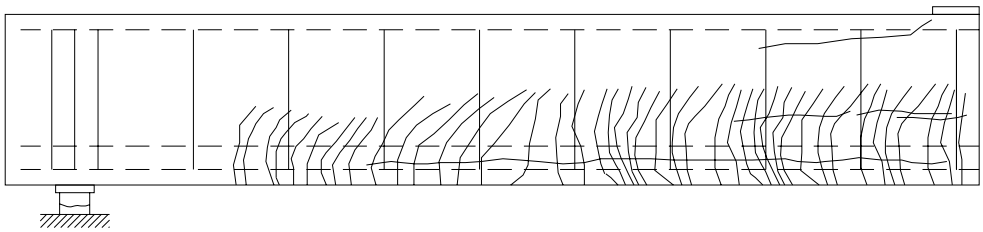

Figure 7.20 *Crack trajectories according to the vector plot of crack normal in Figure 7.19 for Model 3.*

The real crack pattern for beam A-1 obtained in the experiments is shown in Figure 7.21.

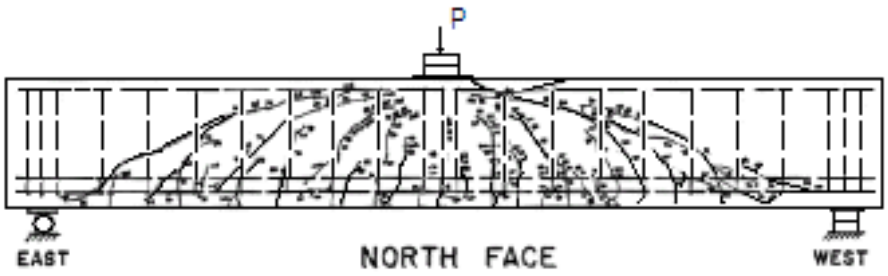

Figure 7.21 Crack pattern for beam A-1, according to the experimental results.

7.3.3 Stresses and strains in the concrete and reinforcement

In Figure 7.22, the diagrams for stress and strain variations over the selected cross-section and along the reinforcement layer are presented. The values for these diagrams were obtained in each load step.

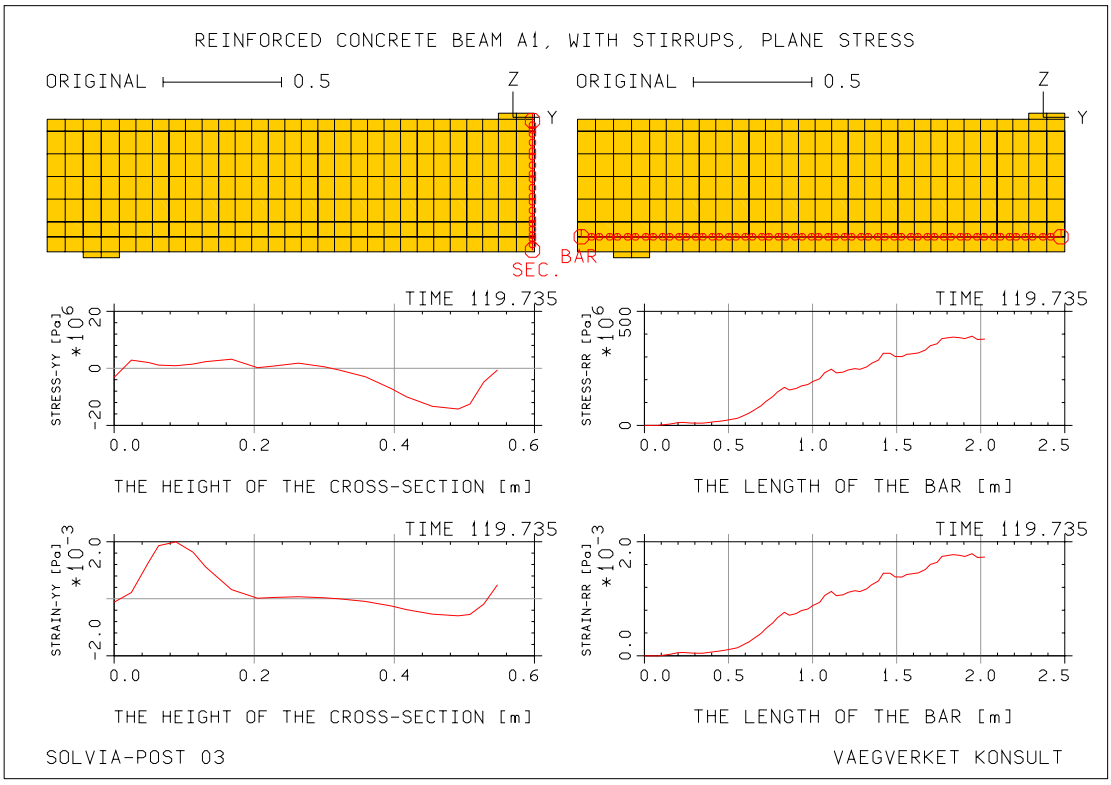

Figure 7.22 Stress and strain variations over selected cross section and along the longitudinal reinforcement for Model 3, calculated in each load step.

The stress-strain relationship for concrete and reinforcing steel in each load step can be found in the diagrams shown in Figure 7.23.

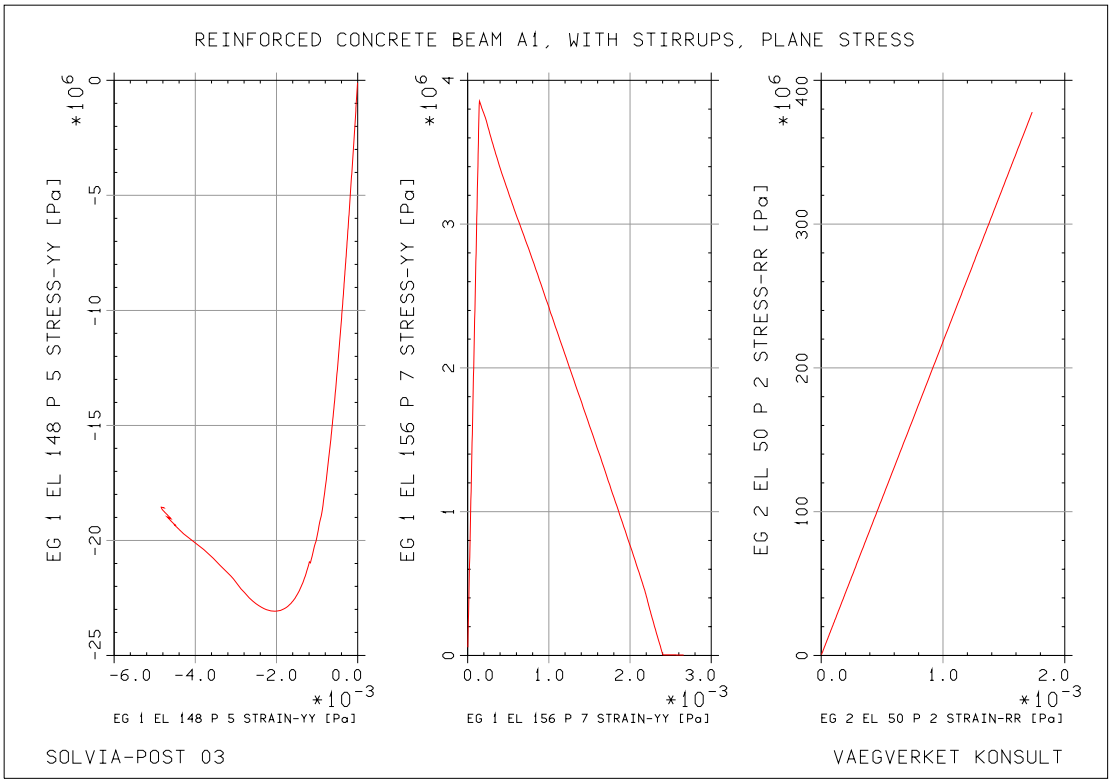

Figure 7.23 Stress-strain relationships in the concrete and reinforcing steel calculated in each load step, for Model 3. The first and second diagrams from the left to the right represent compressive and tensile behavior of the concrete, while the diagram on the right shows the tensile behavior of reinforcing steel.

7.4 Model 4

Model 4 is the solid model for tested beam OA-3. In this case parameters β and κ are equal to 0.89 and 14 respectively. A force norm of 80 *kN* and a force tolerance of one percent were chosen in the FE-analysis.

7.4.1 Load-displacement relationship

The maximum load and mid-span deflection obtained in the FE-analysis in the last load step, for model 4 were 369.84 *kN* and 24.28 *mm* respectively, see Figure 7.24.

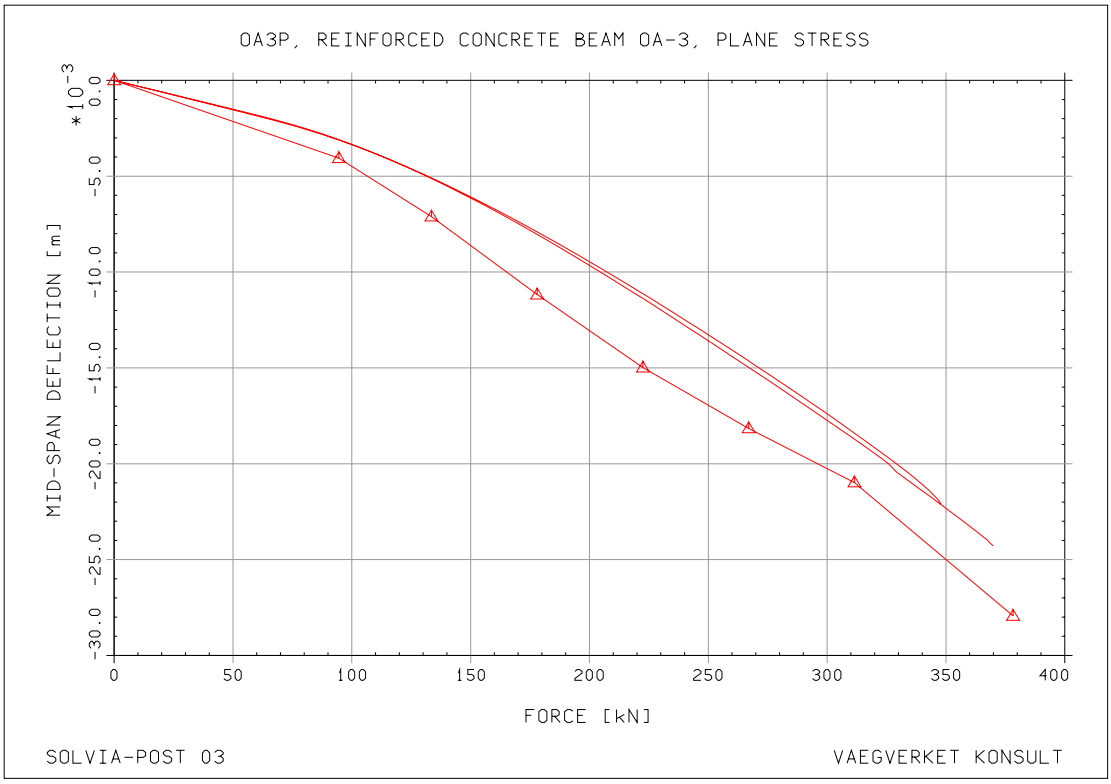

Figure 7.24 Load-deflection relationships for beam OA-3, obtained in the last load step. The lines with triangular symbols represent experimental results, while the lines without symbols are according to the FE-analysis performed in 2D and in 3D respectively. The larger load and displacement were obtained in 3D analysis.

The vertical displacement for Model 4 as a contour plot and the vertical displacement of all nodes of the model as a vector, obtained in the last load step can be found in Figure 7.25.

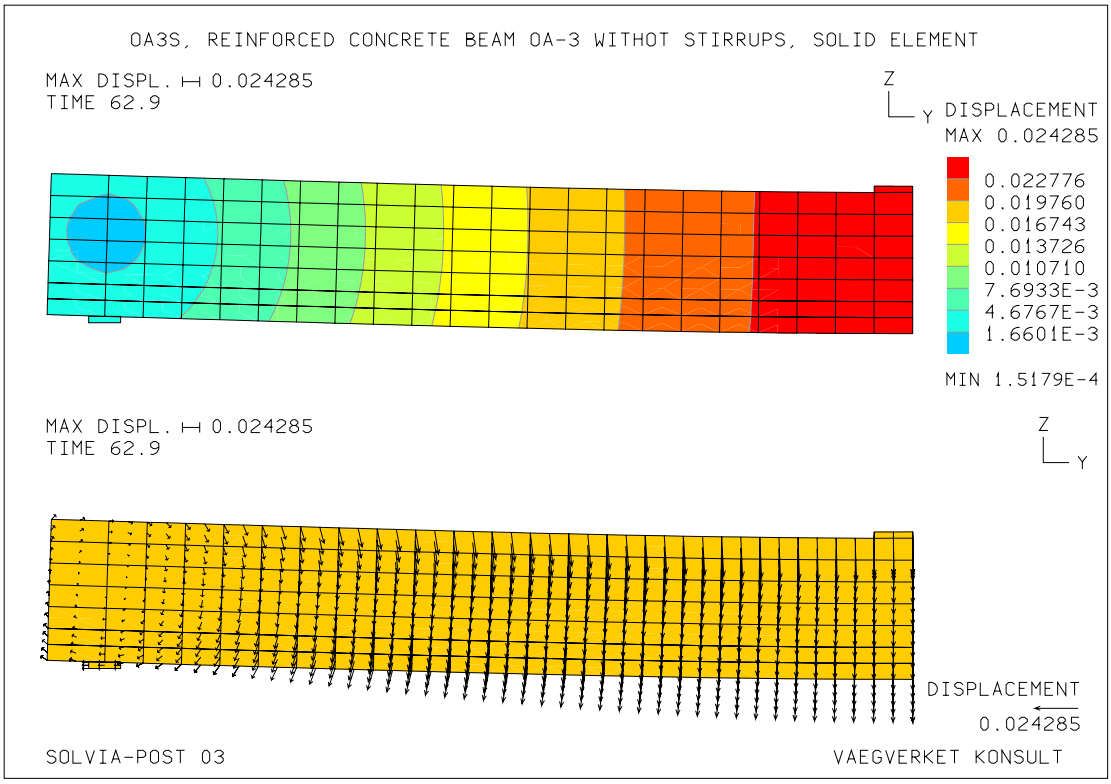

Figure 7.25 Contour and vector plots of the displacements in the last load step for Model 4.

7.4.2 Crack pattern

Figure 7.26 indicates the crushing zone at the loading plate for model 4, created with solid elements in 3D. It can be observed that the crushing zone for model 4 is much smaller than the same zone for model 1, created for the same beam, but as a 2D model. The plots of the cracking and crushing concrete zone were obtained in the last load step.

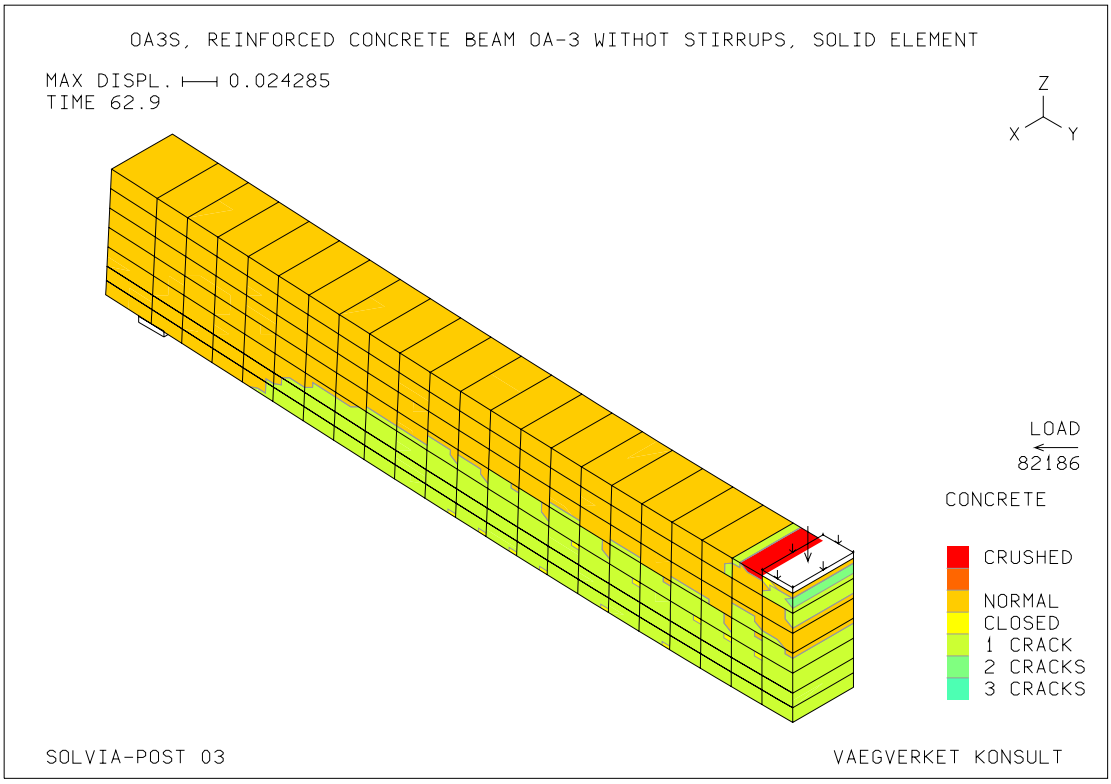

Figure 7.26 The contour plot of the crushing and cracking zone in 3D for Model 4.

The plot of the crushed zone in the concrete and vector plot of the crack-normal in y-z plane, reached in the last load step are shown in Figure 7.27.

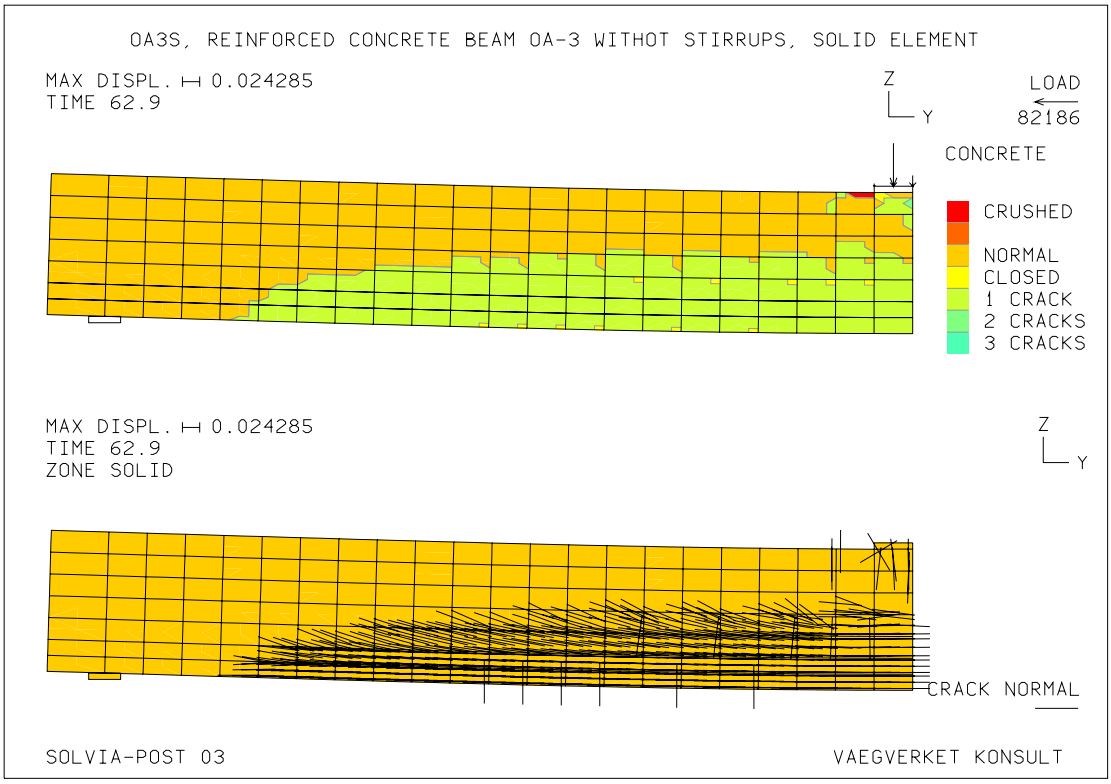

Figure 7.27 Contour plot of the state of concrete including the values of the maximum ultimate load, (upper plot) together with the plot of vector crack- normal, for Model 4. The plots were obtained in the last load step.

The crack pattern for the model is very similar to the crack pattern obtained for model 1; the crack trajectories are the interpretation of the vector plot of crack normals from the FE-analysis, see Figure 7.28.

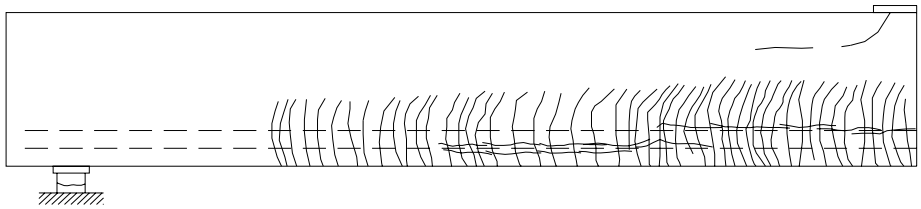

Figure 7.28 Crack trajectories according to the vector plot of crack normal in Figure 7.27 for Model 4.

The real crack pattern for beam OA-3 according to the experimental studies is shown in Figure 7.29.

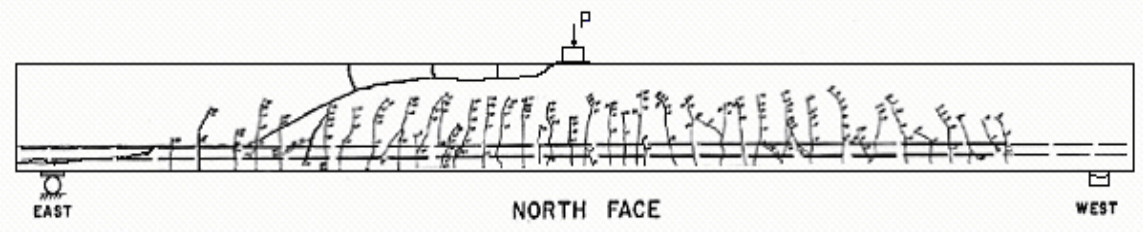

Figure 7.29 Crack pattern for beam OA-3, according to the experimental results.

7.4.3 Stresses and strains in the concrete and reinforcement

In Figure 7.30, the stress and strain variations over the cross-section in the mid-span and along the length of the outer reinforcement layer, for model 4 are presented. The values in these diagrams were obtained in each integration step.

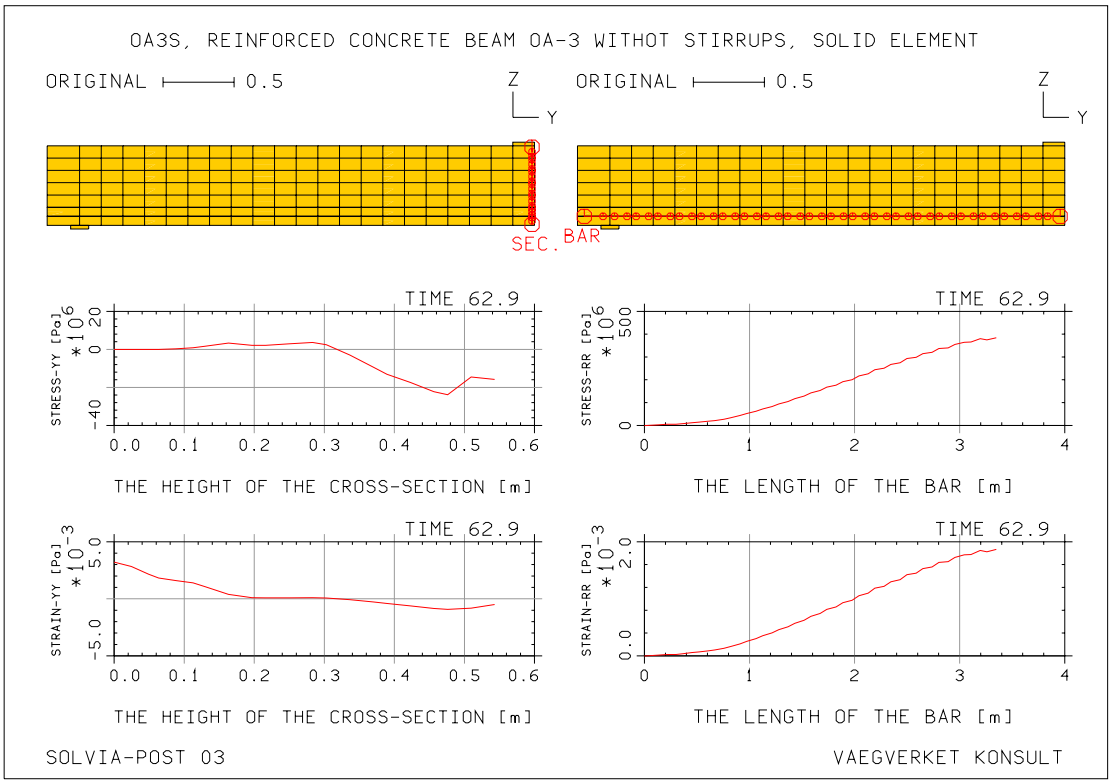

Figure 7.30 Stress and strain variations over selected cross section and along the longitudinal reinforcement for Model 4, calculated in each load step.

Stress-strain relationship in the concrete and reinforcing steel for model 4 can be found in Figure 7.31, where the values in the diagrams were obtained in each load step.

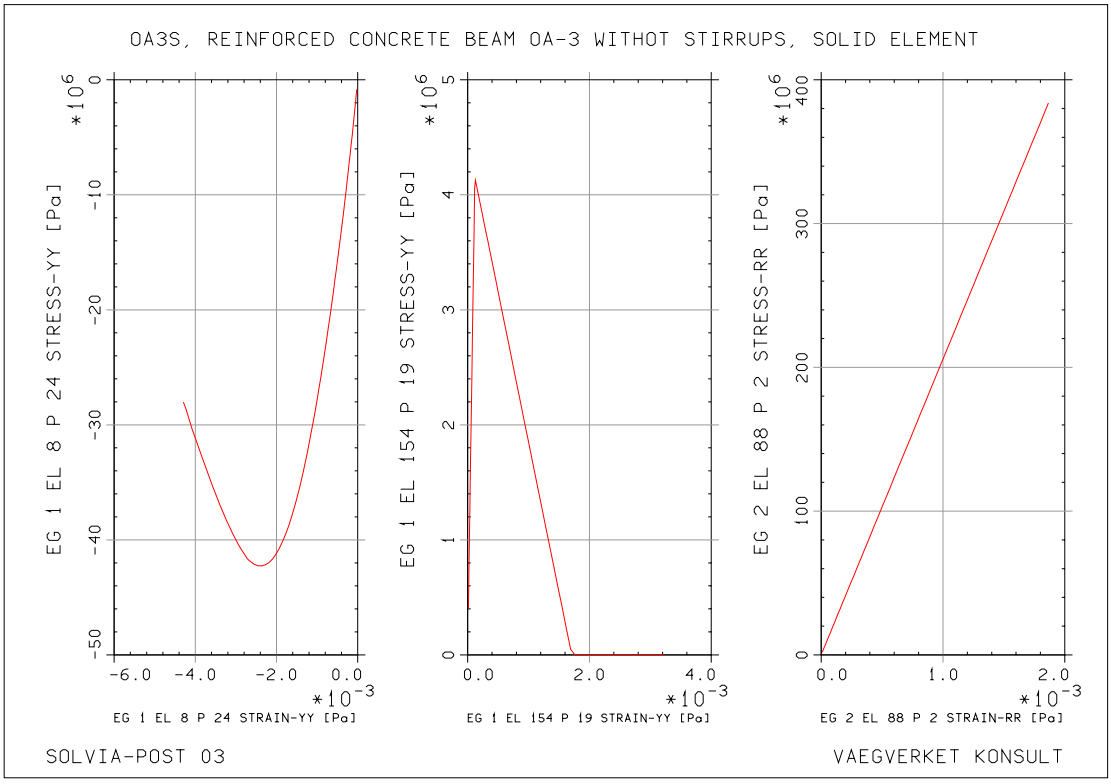

Figure 7.31 Stress-strain relationships in the concrete and reinforcing steel calculated in each load step, for Model 4. The first and second diagrams from the left to the right represent tensile and compressive behavior of the concrete, while the diagram on the right shows the tensile behavior of reinforcing steel.

7.5 Model 5

Model 5 was created for beam B-14, using solid elements. In the FE-analysis for this model, the parameters β and κ were chosen to be 0.887 and 16 respectively. The force norm used in the FE-analysis was equal to 80 *kN*.

7.5.1 Load-displacement relationship

According to the FE-model the maximum load and the mid-span deflection reached in the last load step are: 110.30 *kN* and 17.95 *mm* respectively, see Figure 7.32.

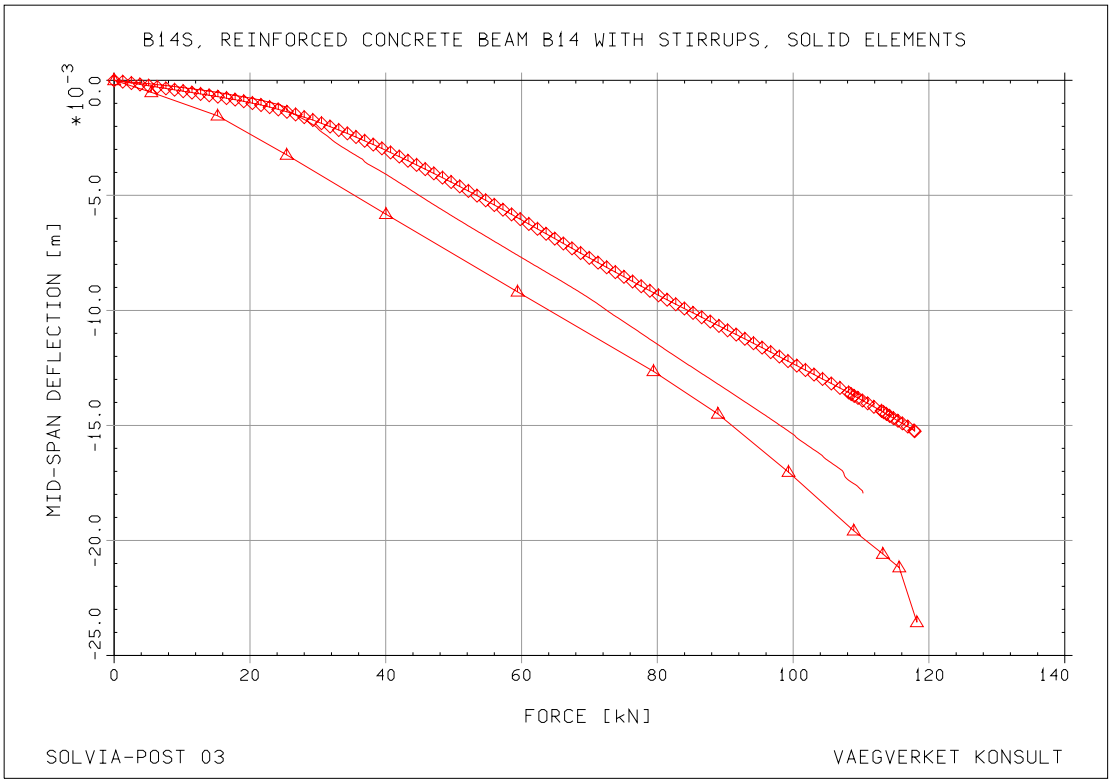

Figure 7.32 Load-deflection relationships for beam B-14, obtained in the last load step. The line with triangular symbols is according to the experimental results. The lines with rectangular and without symbols are according to FE-analysis for beam B-14 performed in 2D and in 3D, respectively.

The vertical displacement for model 5 as a contour plot and the same displacement for all the nodes in the model, shown as vector and calculated in the last load step are presented in Figure 7.33.

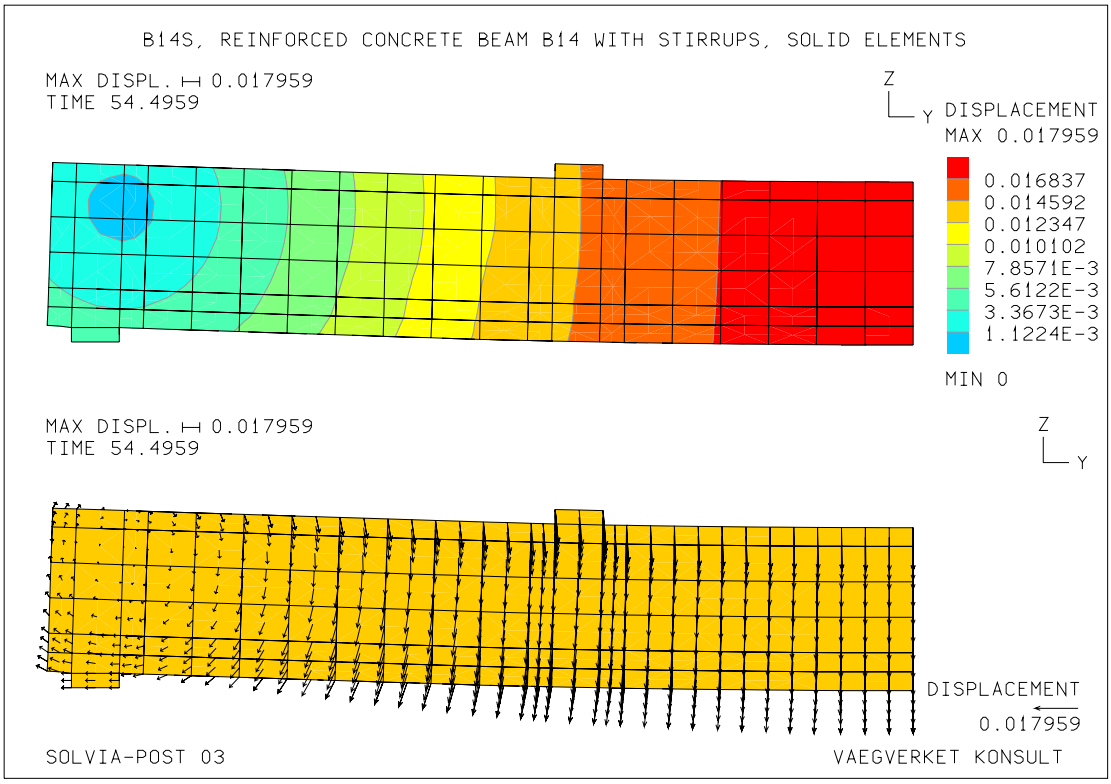

Figure 7.33 Contour and vectors plot of the displacements in the last load step for Model 5.

7.5.2 Crack pattern

The crushing zone at the loading plate for model 5, created with solid elements in 3D, reached in the last load step can be seen in Figure 7.34. The size of the crushing zone is almost the same for the two dimensional and three dimensional models created for beam B-14.

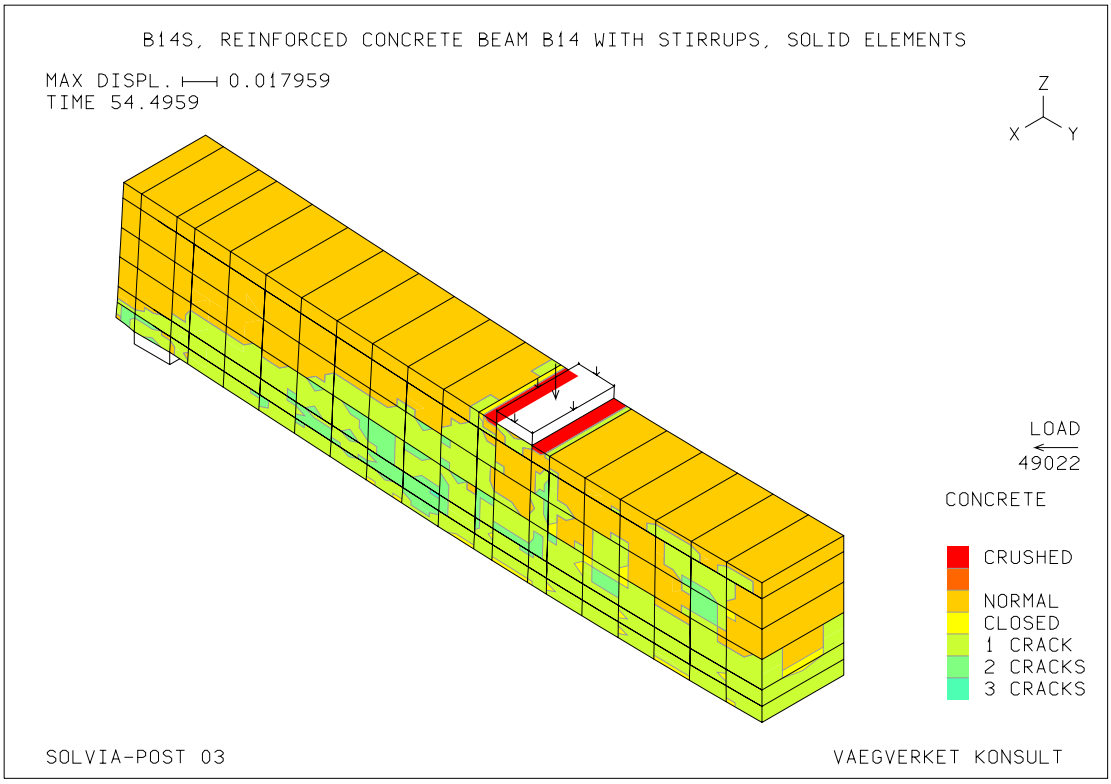

Figure 7.34 The contour plot of the crushing and cracking zone in 3D for Model 5.

Figure 7.35 shows the plot of the crushing zone and vector plot of crack-normal in y-z plane, obtained in the last load step.

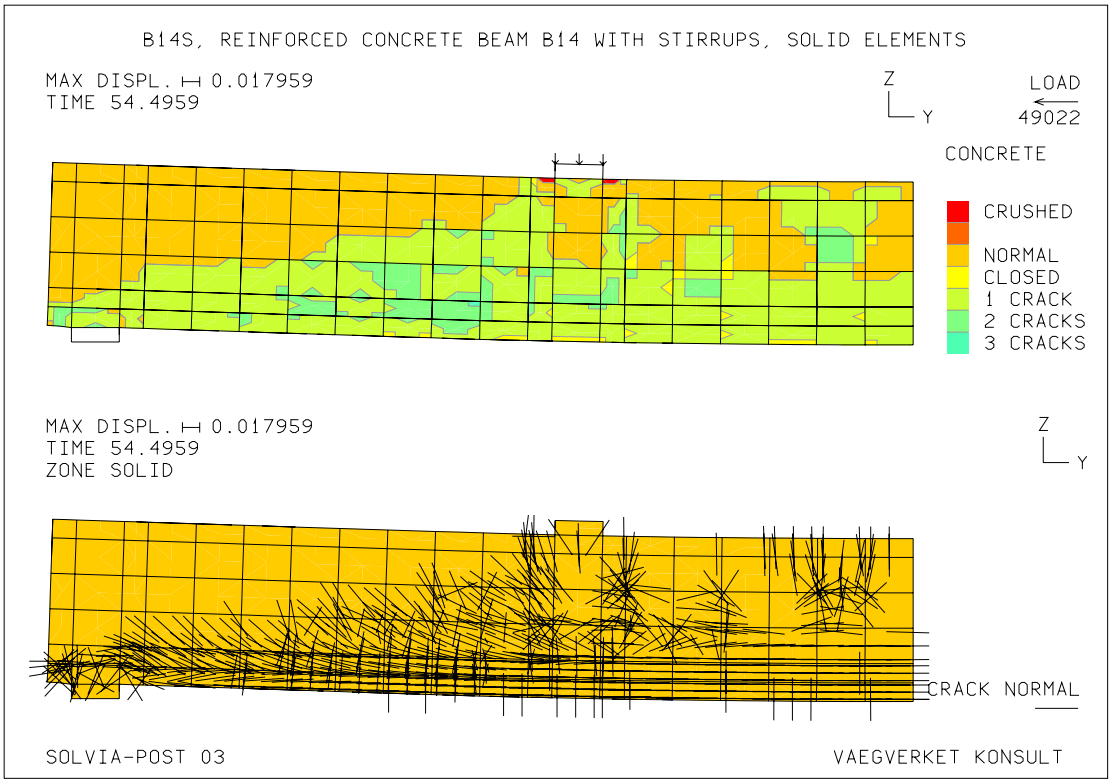

Figure 7.35 Contour plot of the state of concrete including the values of the maximum ultimate load, (upper plot) together with the plot of vector crack- normal, for Model 5. The plots were obtained in the last load step.

The crack pattern for model 5 is similar to crack pattern for model 1. The only difference is the 'critical diagonal tension crack' which can be seen more pronounced in model 5, see Figure 7.36. The crack trajectories in this figure represent the interpretation of the vector plot of crack normals.

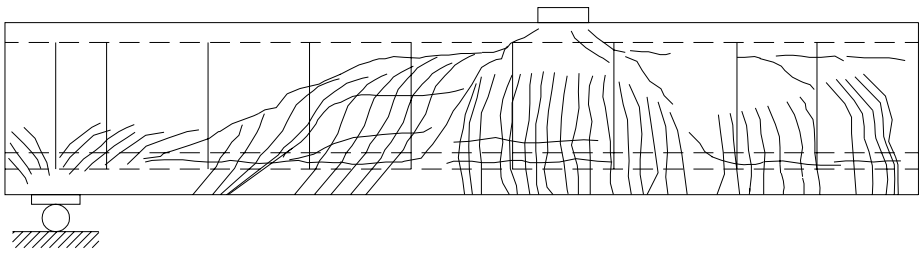

Figure 7.36 Crack trajectories according to the vector plot of crack normal in Figure 7.35, for Model 5.

The real crack pattern for beam OA-3 according to the experimental results can be seen in Figure 7.37.

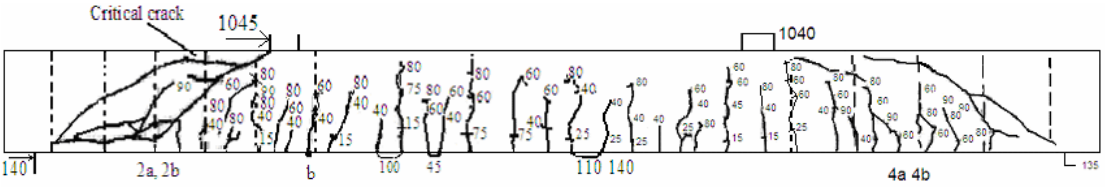

Figure 7.37 Crack pattern for beam B-14, according to the experimental results.

7.5.3 Stresses and strains in the concrete and reinforcement

Stress and strain variations over the selected cross-section and along the length of the outer reinforcement layer calculated in each integration (load) step are shown in Figure 7.38.

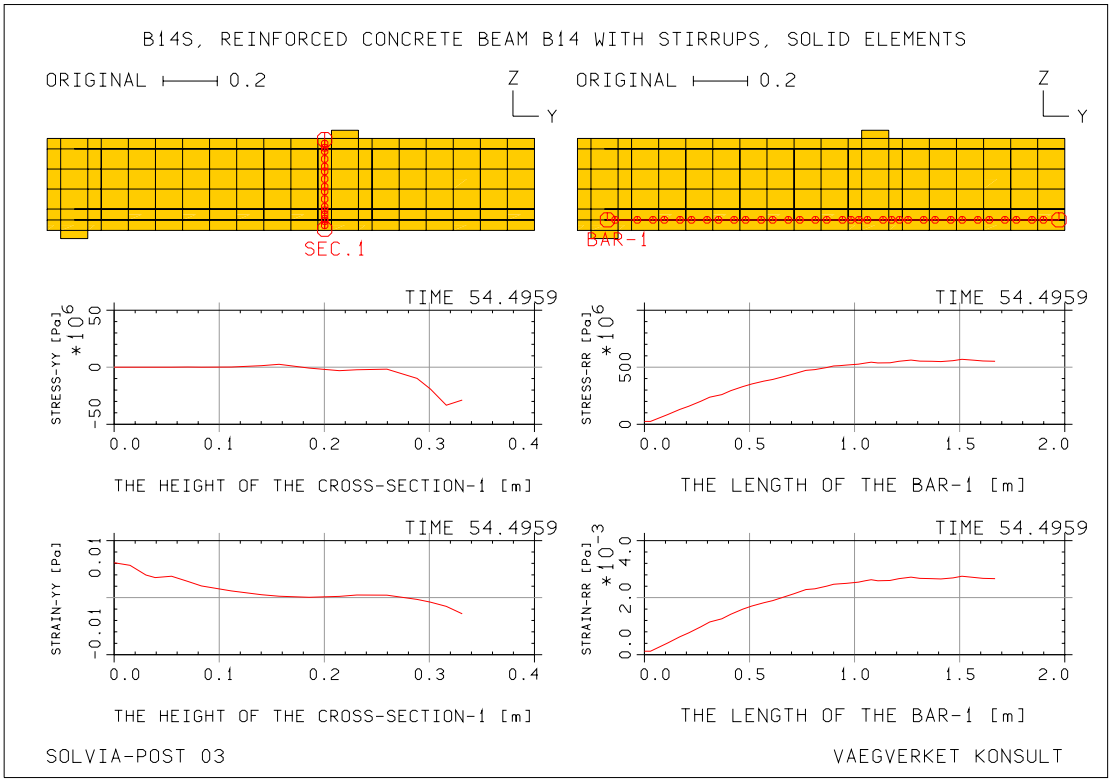

Figure 7.38 Stress and strain variation over selected cross section and along the longitudinal reinforcement for Model 5, calculated in each load step.

The stress-strain relationships for concrete and steel elements in selected points obtained in each load step can be found in Figure 7.39.

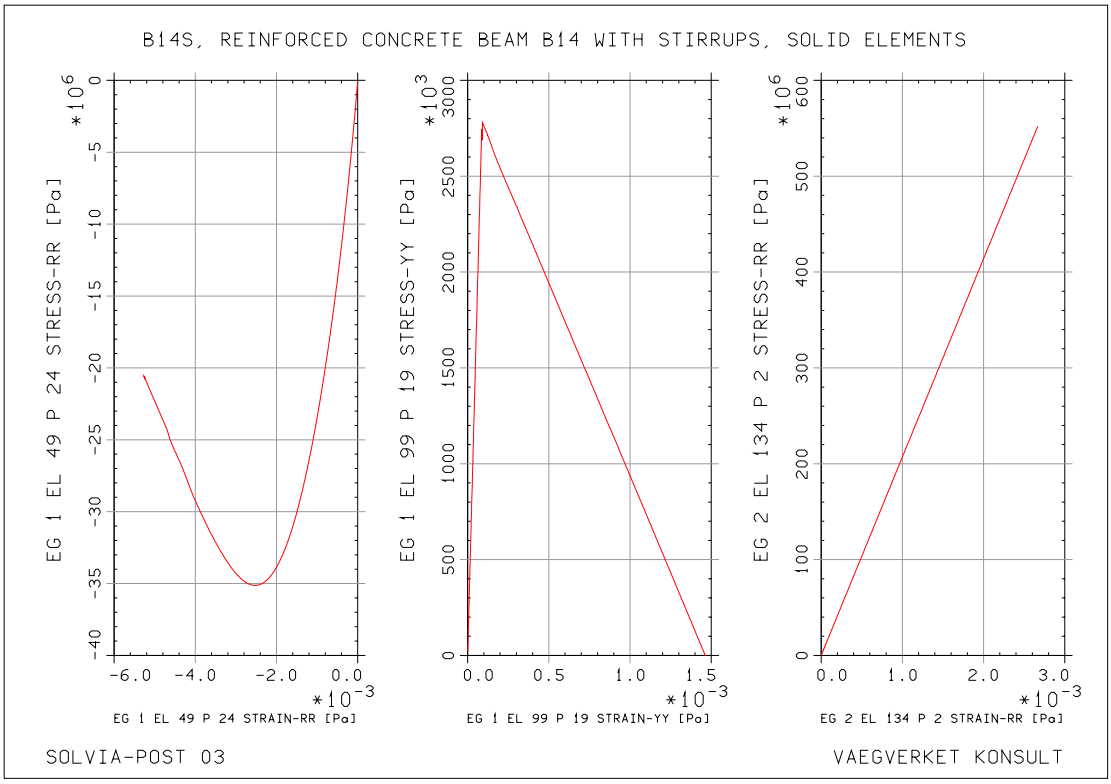

Figure 7.39 Stress-strain relationships in the concrete and reinforcing steel calculated in each load step, for Model 5. The first and second diagrams from the left to the right represent tensile and compressive behavior of the concrete, while the diagram on the right shows the tensile behavior of reinforcing steel.

7.6 Evaluation of the FE results

In the experimental studies, load-deflection relationships and shear types of failures for the beams were examined. These results were compared with the same results obtained from the FE analysis to evaluate the quality and accuracy of the numerical predictions. The comparison between the experimental and the FE-results is summarized below:

- Regarding load-deflection relationship, it was found that the maximum loads obtained from the FE-analyses, for the chosen combination of parameters β and κ, given in table 6.1 where 1%-9% less than the collapse loads obtained during the experiments. The only exception was model 3. In this case the ultimate load for the FE-model was 2.3% greater than the same load obtained in the experiments. The deflection according to FE-calculation is 13%-47% less than deflection in experimentally tested beams.

- Concerning the shear type of failure, in all FE models very similar crack trajectories as in the experimental studies where obtained. In the crack-pattern according to the FE-analysis, the flexural cracks initiated at the bottom and the 'critical diagonal tension cracks' which cause the failure of

the structures can be observed. The similar behavior of the beam can be observed in the experimental studies.

- The stress-strain relationships in the critical points of the beam, for both concrete and reinforcing steel, were very similar to those shown in the theoretical studies. The stress and strain variations over the critical concrete-sections and along the reinforcing bars have similar trends as the ones in the theoretical studies.

Based on the comparison between the FE results and the experimental results, it was concluded that all the models gave reasonably good numerical predictions and similar results (within a reasonable range) to the results according to experimental and theoretical investigations. The non-linear three dimensional FE-analyses gave better prediction of the deflection than the same analysis performed in 2D, although due to the boundary conditions, the model was slightly stiffer.

In FE-analysis for model 1 and model 3-4, the measured average values of modulus of rupture $f_{t,fl}$, were used as the tensile strength . In order to see the difference in the ultimate loads and deflections using the modulus of rapture compared to the splitting tensile strength of concrete $f_{t,sp,}$ a new FE-analysis was performed for model 1. It was observed, that the ultimate load obtained in the analysis, using splitting tensile strength of concrete was 13% less than the same load using modulus of rapture. The difference between deflections was 11%.

A detailed calculation of the ultimate load for the tested beams can be found in APPENDIX B.

A calculation of the fracture energy of concrete G_f, and parameters κ, calculated from the fracture energy can be seen in APPENDIX C.

8 Parametric investigations

In order to evaluate how the certain combination of the concrete parameters such as shear retention factor, β (defined as 'shefac' in the SOLVIA code), and the parameter which defines the ultimate crack strain, κ (called 'kappa' in the SOLVIA code), affects the ultimate load, beam-deflection and stresses in stirrups, a parametric study was carried out.

A summary of the variation of β and κ is presented in tables 8.1-8.5. For each of the models, three main combinations were performed and presented. The first combination includes large values for both β and κ. The second and third are: large κ with small β and large β with small κ. The load according to the FE-analysis corresponds to the half of the load obtained in the experiments for Model 1 and Model 3-4, because of the symmetrical boundary and loading conditions. In table 8.1-8.5, the ultimate load P_u, and the maximum deflection δ_{max} reached in the experiments can be also found.

In order to increase the number of the load steps, restart files were used for some of the cases in the parametric studies, where 'R' in the tables of the parametric investigations denotes restart files. In some of the analysis, the number of iterations was not possible to increase, while in the some of the models the restart files increased the number of the load steps and improve slightly FE analysis.

Table 8.1 Parametric investigation for Model 1, where 'R' denotes restart files

P_u=378.57 kN ; δ_{max}=27.94 mm Large κ and β								
κ	β	P_a [kN]	$2 \cdot \frac{P_a}{P_u}$	δ_a [mm]	δ_a / δ_{max}	Time	Step	
30	0.90	177.45	0.937	21.038	0.753	101.4	102	
45	0.95	179.59	0.948	20.922	0.749	102.62	105	
58	0.98	180.55	0.953	20.950	0.750	103.17	106	
65	1.00	180.64	0.954	20.877	0.747	103.22	105	
Large κ and small β								
40	0.10	93.362	0.493	9.943	0.356	53.35	78	R
40	0.10	102.11	0.539	11.467	0.410	58.35	80	
45	0.09	94.430	0.498	10.001	0.358	53.96	82	R
45	0.09	103.08	0.545	11.261	0.403	58.90	83	
35	0.10	98.116	0.518	11.641	0.417	56.07	131	R
30	0.3	138.42	0.731	18.325	0.656	79.10	81	R
35	0.35	143.5	0.758	18.133	0.649	82	82	R
Small κ and large β								
10	0.95	149.1	0.788	17.95	0.642	85.198	87	R
10	1	149.45	0.789	17.987	0.644	85.40	86	R
5	1	176.7	0.934	23.886	0.855	100.97	147	

Table 8.2 Parametric investigation for Model 2, where 'R' denotes restart files

P_u=118.22 *kN* ; δ_{max}=23.56 *mm*						Large κ and β				
κ	β	P_a [*kN*]	P_a / P_u	δ_a [mm]	δ_a / δ_{max}	stirrup-force [kN]		Time	Step	
						max	min			
30	0.90	117.45	0.99	14.180	0.602	-0.9312	6.2052	92.30	93	
45	0.90	118.72	1.004	13.849	0.588	-0.6348	3.5002	93.30	95	
40	1.00	122.42	1.036	14.442	0.613	-1.0052	2.3264	96.21	100	
45	1.00	122.42	1.036	14.309	0.607	-0.995	2.5265	96.20	107	
Large κ and small β										
35	0.20	77.02	0.651	10.211	0.433	-0.7168	15.104	60.26	86	R
35	0.20	87.65	0.741	12.009	0.510	-0.7201	22.178	68.88	90	
40	0.20	79.493	0.672	9.850	0.418	-1.125	7.8633	62.47	74	R
30	0.30	86.110	0.728	11.191	0.475	-1.3929	10.955	67.67	77	R
35	0.35	86.897	0.735	11.172	0.474	-1.2976	11.077	68.29	89	R
Small κ and large β										
10	1.00	103.48	0.875	12.853	0.546	-1.0874	4.4955	81.32	91	
7	1.00	97.843	0.828	12.197	0.518	-0.5778	1.9745	76.89	138	
7	0.95	118.2	1	15.654	0.664	-0.4479	9.0276	92.89	195	
10	0.95	118.85	1.005	15.522	0.659	-0.3138	9.7627	93.40	128	
6	1	73.156	0.619	8.7125	0.370	-0.664	2.0492	57.49	167	R
6	1	85.727	0.725	10.556	0.448	-0.5448	1.912	67.36	180	

Table 8.3 Parametric investigation for Model 3, where 'R' denotes restart files

P_u=467.25 kN ; δ_{max}=14.22 mm					Large κ and β					
κ	β	P_a [kN]	$2 \cdot \frac{P_a}{P_u}$	δ_a [mm]	δ_a / δ_{max}	stirrup-force [kN]		Time	Step	
						min	max			
45	0.90	190.58	0.816	5.012	0.352	-1.3255	1.1491	95.29	204	
30	1.00	198.55	0.850	5.263	0.370	-1.3787	1.2334	99.28	235	
40	1.00	202.37	0.866	5.326	0.375	-1.4054	1.2857	101.19	216	
40	0.90	225.11	0.964	7.235	0.509	-1.563	3.274	112.56	265	
Large κ and small β										
30	0.10	119.52	0.512	2.9761	0.209	-0.8279	0.6325	59.76	129	R
30	0.10	122.46	0.524	3.2395	0.228	-0.8482	0.8922	61.29	183	
35	0.20	129.62	0.555	3.2344	0.227	-0.8981	0.7177	64.81	135	R
35	0.20	134.6	0.576	3.5829	0.252	-0.9326	1.3672	67.30	138	
35	0.10	125.48	0.537	3.4348	0.242	-0.9373	1.3261	62.74	132	
30	0.30	135.75	0.581	3.8044	0.268	-0.9405	1.5682	67.87	143	R
30	0.30	160.29	0.686	5.2358	0.368	-1.1105	4.5857	80.14	155	
35	0.35	166.78	0.714	5.6293	0.396	-1.1548	4.6777	83.39	179	
Small κ and large β										
5	1.00	97.901	0.419	2.1441	0.151	-1.0024	0.48	48.95	163	R
5	1.00	181.62	0.777	5.8611	0.412	-1.9464	1.7862	90.81	349	
10	1.00	194.61	0.833	5.9941	0.422	-1.9592	3.2411	97.31	220	

Table 8.4 Parametric investigation for Model 4, where 'R' denotes restart files.

P_u=378.57 *kN* ; δ_{max}=27.94 *mm* Large κ and β								
κ	β	P_a [kN]	$2 \cdot \frac{P_a}{P_u}$	δ_a [mm]	δ_a / δ_{max}	Time	Step	
30	0.90	191.11	1.010	23.458	0.840	65	66	
45	0.90	191.09	1.009	22.947	0.821	65	65	
30	1	193.91	1.024	23.693	0.848	65.95	70	
45	1	194.92	1.029	23.323	0.835	66.13	70	
Large κ and small β								
35	0.20	111.32	0.588	14.171	0.507	37.87	49	R
35	0.20	115.92	0.612	14.972	0.536	39.43	51	
35	0.10	96.399	0.509	10.857	0.389	32.79	48	R
30	0.10	64.119	0.339	5.1843	0.186	21.81	26	R
30	0.30	144.35	0.763	19.475	0.697	49.10	52	R
35	0.35	141.11	0.745	17.281	0.619	48	48	R
35	0.35	153.11	0.809	20.259	0.725	52	52	
Small κ and large β								
5	1	137.23	0.725	17.343	0.621	46.67	149	R
10	1	190.04	1.004	25.433	0.910	64.64	82	
10	0.9	186.24	0.984	25.1	0.898	63.35	68	

Table 8.5 Parametric investigation for Model 5, where 'R' denotes restart files.

P_u=118.22 *kN* ; δ_{max}=23.56 *mm*					Large κ and β					
κ	β	P_a [*kN*]	P_a / P_u	δ_a [mm]	δ_a / δ_{max}	stirrup-force [kN]		Time	Step	
						min	max			
30	0.90	76.907	0.651	10.606	0.450	-0.2644	1.8781	37.99	380	R
30	0.90	103.66	0.877	15.872	0.674	-1.1073	6.3549	51.22	529	
35	1	70.492	0.596	8.2514	0.350	-0.4510	0.7697	34.83	349	R
40	1	72.142	0.610	8.3911	0.356	-0.5599	0.8815	35.63	361	R
45	1	74.475	0.630	8.6279	0.366	-0.6187	0.9197	36.80	373	R
Large κ and small β										
40	0.20	26.993	0.228	1.7340	0.074	-0.118	0.1704	13.37	135	
40	0.20	27.276	0.235	2.2982	0.098	-0.1170	0.6048	13.47	140	
30	0.10	24.446	0.207	1.0680	0.045	-0.1126	0.0995	12.013	124	R
30	0.30	25.990	0.220	1.7481	0.074	-0.1164	0.2165	12.85	133	R
35	0.35	27.063	0.229	2.1054	0.089	-0.1160	0.5129	13.37	143	
35	0.35	31.420	0.266	2.6661	0.113	-0.1318	0.9662	15.52	148	
Small κ and large β										
10	1.00	22.653	0.192	0.9602	0.040	-0.1114	0.0984	11.252	116	R
5	1.00	20.250	0.171	0.8396	0.035	-0.0928	0.0818	10	100	R

9 Conclusions

In this master thesis project, the capability and limitations of the SOLVIA FE-system for limit state design of reinforced concrete structures were investigated. The study was on shear failure for beam type members, focusing on the following parameters in the concrete material model:

1. The shear retention factors, β (defined as 'shefac' in the SOLVIA code).

2. The parameter κ, which defines the ultimate crack strain in tension (defined as 'kappa' in the SOLVIA code).

3. The type of elements used.

The concrete material in the beams was modeled with plane-stress elements in two dimensions (2D) and with solid elements in three dimensions (3D). It was found that the prediction of the ultimate load as well as the crack patterns for FE analysis with both plane-stress elements and solid elements, were very similar and close to the analyses obtained in the experiments. The deflections obtained in the FE-analysis were less than the deflection of the tested beams, but still within a reasonable range. The FE-analysis performed with solid elements gave better prediction of the deflection.

The stress-strain relationships, the stress and strain variations along the critical sections and reinforcing bars, obtained in the FE-analysis were very similar to those assumed in theoretical studies.

After a parametric investigation, related to variation of the concrete parameters β and κ, the following conclusions can be drawn:

- The combination with large values of β and κ gave very stable analyses in most of the cases. For some of the FE models (Model 2 and Model 4) the ultimate load was greater than the load according to the experiments, which makes the prediction unsafe. These combinations have to be avoided. The deflections were in all cases less than the deflections obtained from the experiments. The crack patterns for some of the models for certain combinations of κ and β were very similar to the real crack patterns, where the initiation and formation of a critical diagonal tension cracks with flexural cracks in the tension zone were observed.

- The combination with small κ and large β gave both stable and unstable analysis depending on the FE-model. The ultimate loads and deflections from the FE analysis were much smaller than in the experiments for all the models, except for model 3, which gave a good prediction of the ultimate load. Stresses and strains in the stirrups and in the longitudinal reinforcement were greater or lower, (depending on the model and the chosen values for κ and β) than the values obtained in combinations with large κ and β. The initiation of the diagonal tension cracks, with flexural cracks formed in the tension zone were also observed from the crack patterns.

- The last combinations in the parametric studies, with large κ and small β gave very unstable analyses, very low ultimate loads and small deflections. Stresses and strains in stirrups and in the longitudinal reinforcement decreased greatly for some of the models, compared with the values obtained for the combinations of κ and β mentioned above. In the crack patterns, only flexural cracks in the tension zone in the mid span could be seen, without initiation of a critical diagonal tension cracks.

In order to get a stable FE-analysis, with good predictions of the results, certain combinations of concrete parameters β and κ were selected for each model. It was found that parameter β had to be chosen between 0.85 and 0.9. To estimate parameter κ from the fracture energy of concrete a good starting point is to calculate it. However, for the analysis of reinforced concrete (with no bond slip between the reinforcement and the concrete), this value of κ must be increased because of the tension stiffening effect. In model 1-2 and model 4 it was found that the parameter κ had to be multiplied with a factor within range 1.5-3.5. In the FE-analysis for model 3 and model 5, the same parameter had to be multiplied with factors 4.3 and 3.2, respectively.

In general, it was shown that non-linear FE analyses performed in SOLVIA FE-system can be used for limit state analyses of simply supported reinforced concrete beams analyzed for shear type of failure.

10 References

Allen, D.E (1982): *Limit States Design*. National Research Council Canada. Institute for Research in Construction. Digest CBD-221, Rexdale, Ontario, Canada, 1981. (downloadable at http://irc.nrc-cnrc.gc.ca/cbd/cbd221e.html)

Basu, B (2003): *Structural Design 3A2*, course literature, Department of Civil, Structural and Environmental Engineering, Trinity College Dublin, Dublin, Ireland, 2003. pp 3 downloadable at: http://www.tcd.ie/Civil_engineering/staff/b_basu/3A2LEC13.pdf

Bathe, Klaus-Jürgen. (1996): *Finite Element Procedures*. Prentice Hall, Englewood Cliffs, New Jersey, pp 759-761.

BBK 94 (1994): *Boverkets handbok om betongkonstruktioner*: BBK 94 Band 1: Konstruktion. AB Svensk byggtjänst. Stockholm, Sverige, 1994 pp – 34,118,119.

Betong-Handbok (1990): *Betong-Handbok*. Utgåva 2: Konstruktion. AB Svensk byggtjänst. Örebro, Sverige, 1990 pp – 66.

Comité euro-international du béton (1990): *CEB-FIP model code 1990 design code.* London : T. Telford, 1993

Bresler and Scordelis (1961): *Shear strength of reinforced concrete beams.* Institute of Engineering Research. Series 100, issue 13. University of California, Berkeley, California, USA, June 1961, pp 14-16, 30, 32-33, 35-40, 42-43, 49-52, 55-56, 65, 68-69.

Buyukozturk, Oral (2004): *1.054/1.541 Mechanics and Design of Concrete Structures*. Lecture notes. Department of Civil and Environmental Engineering. Massachusetts Institute of Technology. Massachusetts, Boston, U.S.A, pp 1, 3-4 downloadable at: http://aka-ocw.mit.edu/NR/rdonlyres/Civil-and-Environmental-Engineering/1-054Spring2004/76D87641-71B5-4432-88B6-5194DD14312E/0/o_07_shr_f_st_sd.pdf

Eervenka, J., Jendele, L. (2001): *On the choice between discrete or smeared approach in practical structural FE analyses of concrete structures*. Fourth International Conference on Analysis of Discontinuous Deformation in Glasgow, Scotland, UK, June 2001, pp 10. Internet page: http://www.cervenka.cz/Web/printarticle.asp?id=56

Heidkamp, Holger (2000): *Solution of non-linear equilibrium equations in FE-analysis of concrete structures*. Master thesis. Department of Structural Mechanics, Chalmers University of Technology, Gothenburg, Sweden, 2000. pp 24-25, 28. (downloadable at www.inf.bauwesen.tu-uenchen.de/personen/holger/sol_nonl_fe.pdf)

Hirschhausen, Helge von (1999): *Crack control of restrained concrete structures*. Master thesis. Department of Structural Engineering, Chalmers University of Technology, Gothenburg, Sweden, 1999. pp 78,84

Jirásek, Milan and Zimmermann, Thomas (1998): *Rotating crack model with transition to scalar damagel*. Journal of Engineering Mechanics ASCE, Vol. 124 No. 3, March, 1998, pp 277-284. Internet page: http://dgcwww.epfl.ch/WWWLSC/jirasek.page/jem97b.html.

Johnson R.P.(2004): *Composite Structures of Steel and Concrete* (third edition). Blackwell Publishing, Oxford, UK (2004), pp 56-59.

Kotsovos, M.D and Pavlovic, M.N.(1995): *Structural concrete : finite-element analysis for limit-state design*. Thomas Telford, Heron Quay, London : 1995. pp 158, 164, 173-175, 179-180, 182-185, 248-250.

Larsson, Gunnar (1995): *The concrete material model in Solvia*. SOLVIA ENGINEERING AB, Västerås, Sweden, august, 1995, pp 1-3, 5-9.

MacGregor, James G. (1997): *Reinforced concrete mechanics and design*. Prentice Hall, New Jersey, United States, 1997, pp 190-195.

Mosley, W.H. (1999): *Reinforced concrete design*. Basingstoke : Macmillan, 1999, pp 15-16.

Nadim Hassoun, M (2002): *Structural concrete : theory and design*. Prentice Hall, New Jersey, United States, 2002, pp 38-42, 209.

Nawy, Edward G. (2003): *Reinforced concrete : a fundamental approach*. Prentice Hall, New Jersey, United States, 2002, pp 149,156.

Oehlers, Deric J. (1995): *Composite steel and concrete structural members fundamental behaviour*. Oxford, U.K. : Pergamon, 1995. pp 42.

Piyasena, Ratnamudigedara (2002): *Crack spacing, crack width and tension stiffening effect in reinforced concrete beams and one-way slabs*. Doctoral thesis. Griffith University Gold Coast Campus. Faculty of Engineering. Queensland, Austrialia, November, 2002, pp 2-28, 2-29, 2-31, 2-32. downloadable at: http://www4.gu.edu.au:8080/adt-root/uploads/approved/adtQGU20030606.165418/public/02Chapter1-4.pdf

Plos, Mario (1996): *Finite element analyses of reinforced concrete structures*. Concrete structures compendium 96:14. Göteborg, Sweden, 1996, pp 6, 32, 44-46.

Plos, Mario (2002): *Finite element analyses of reinforced concrete structures*. Lecture notes. Göteborg, Sweden, 2002, pp 2.

Reda Taha, Mahmoud (2003): *A novel fuzzy-based approach for quantifying tension stiffening of reinforced concrete structures*. ACI Structural Journal, Vol. 100, No.1, February 2003, pp 7-8.(downloadable at www.reda-taha.com/Publications/CI-Fuzzy-Cracking.pdf)

Reda Taha, Mahmoud and. Shrive, N.G (2001): *Fracture Mechanics of Concrete*. Fracture of Civil Engineering Materials ENCI-617. University of New Mexico,

Albuquerque, New Mexico, 2001, pp 1-3. (downloadable at www.unm.edu/~mrtaha/Publications/ENCI-617-Notes.PDF).

SOLVIA Finite Elment System (1999): *Solvia PRE for stress analysis.* Users manual. Report SE 99-1. SOLVIA ENGINEERING AB. Västerås, Sweden, 1999, pp 1.2, 6.41, 6.46, 6.52, 9.25-9.26.

APPENDIX

A- Mesh of the reinforcement for the models created in 3D

A-1 Model 4

A-2 Model 5

B- Calculation of the ultimate load

B-1 Beam OA-3

B-2 Beam B-14

B-3 Beam A-1

C- Calculation of the fracture energy of the concrete for tested beams

A- Mesh of the reinforcement for the models created in 3D

A-1 Model 4

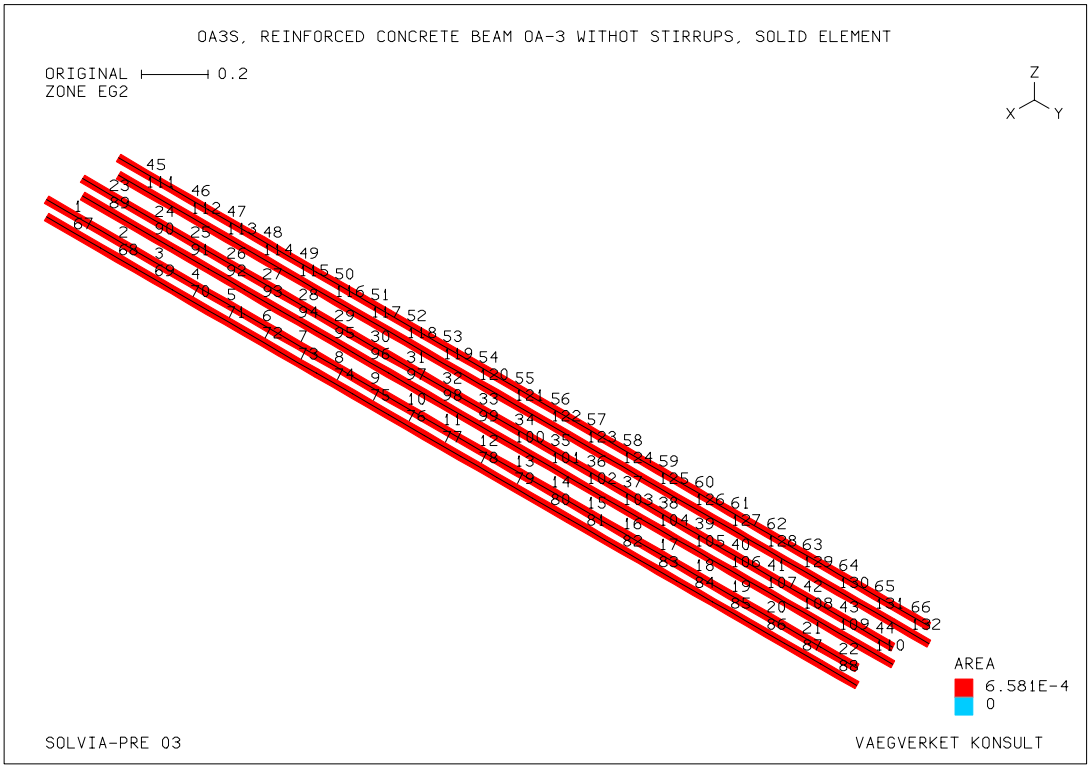

Figure A.1 Mesh of the steel reinforcement for Model 4.

A-2 Model 5

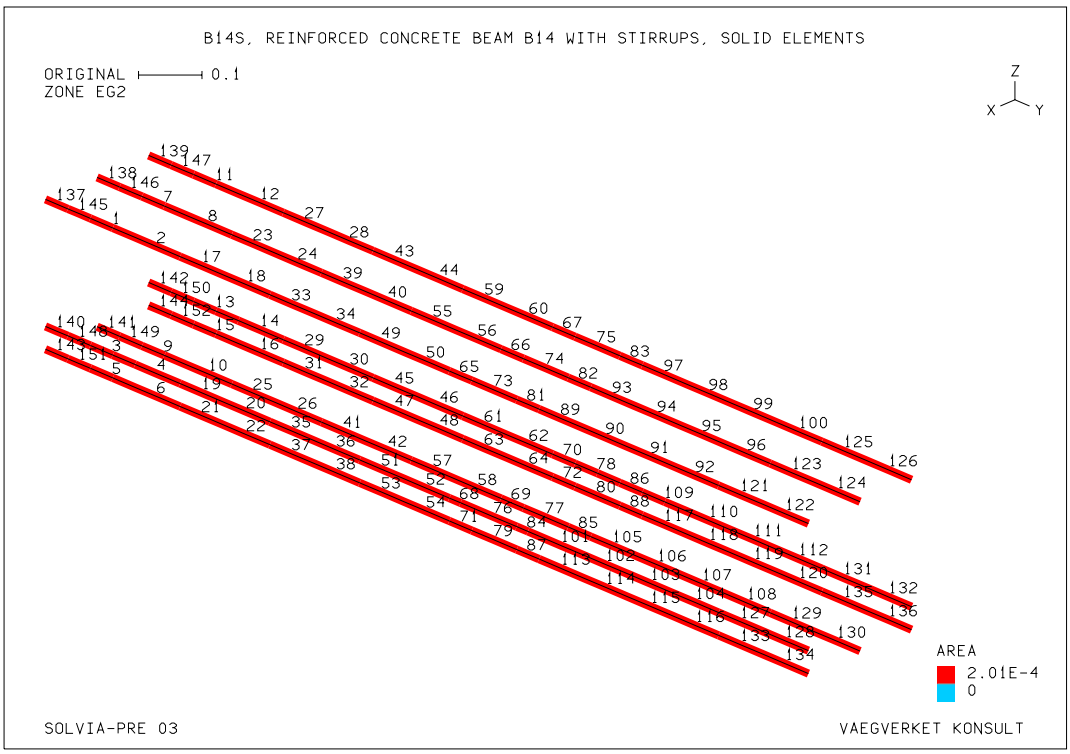

Figure A.2 Mesh of the longitudinal steel reinforcement for Model 5.

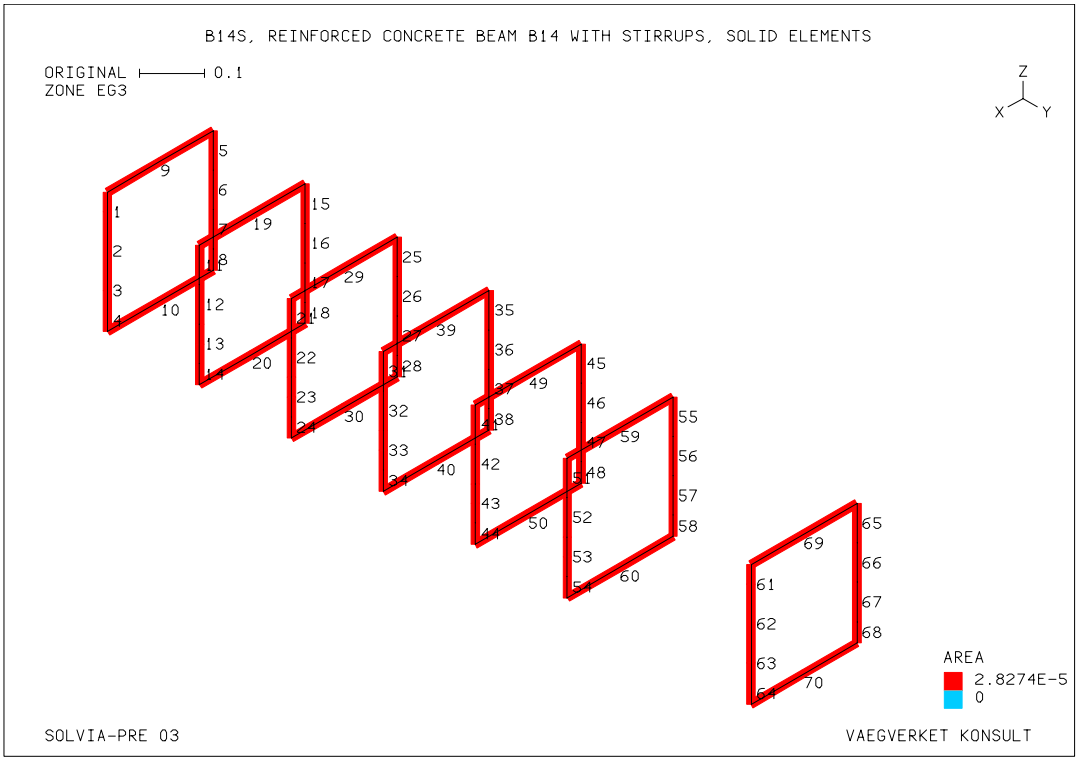

Figure A.3 Mesh of the shear reinforcement for Model 5.

B Calculation of the ultimate load

B-1 Beam OA-3

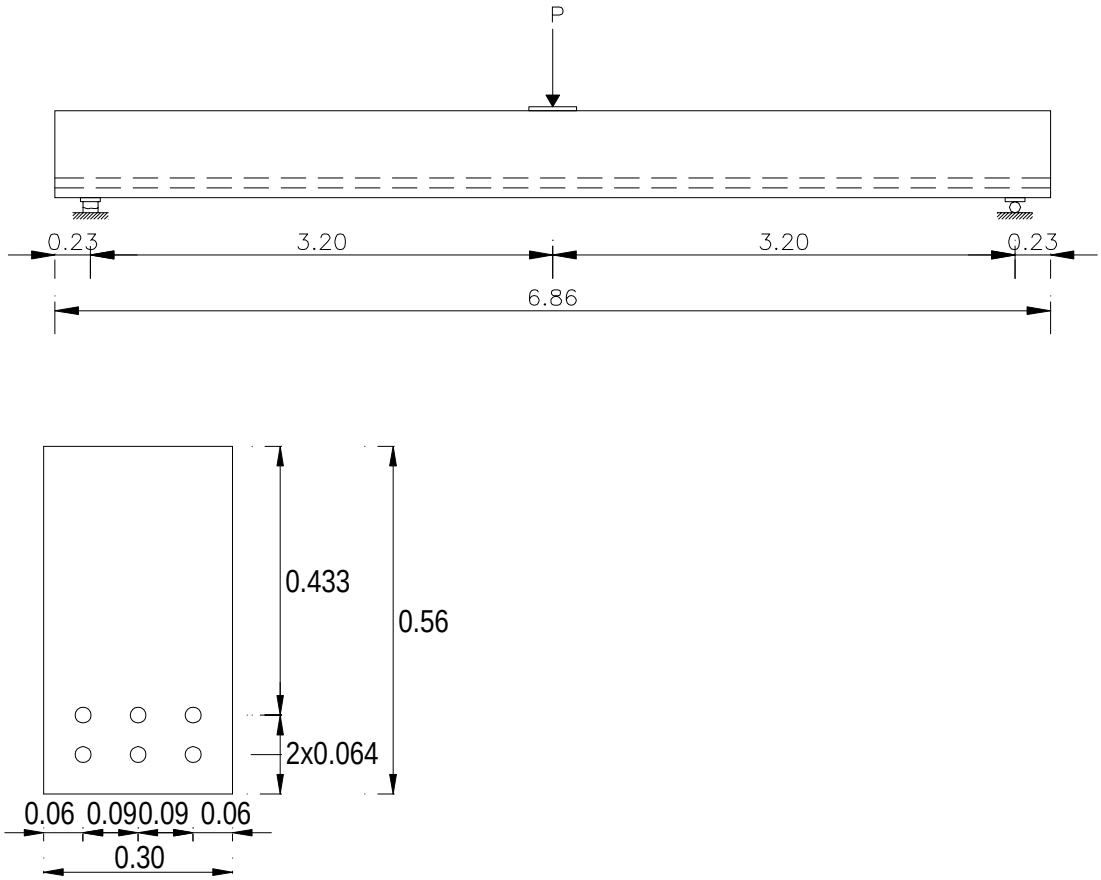

Figure B.1 Geometry, loading and cross section for beam OA-3.

Dimensions

$b_w = 0.305\ m$ $h = 0.56\ m$ $L = 6.40\ m$

$d = 0.465$ m

Materials

Concrete $f_c = 37.62\ MPa$ $f_t^{1} = 4.14\,MPa$

Reinforcing steel $f_y = 552.96\ MPa$ $A_s = 3847.81 \cdot 10^{-6}\ m^2$

$E_s = 205.72\ GPa$

The ultimate load due to flexural capacity

Flexural capacity of the section

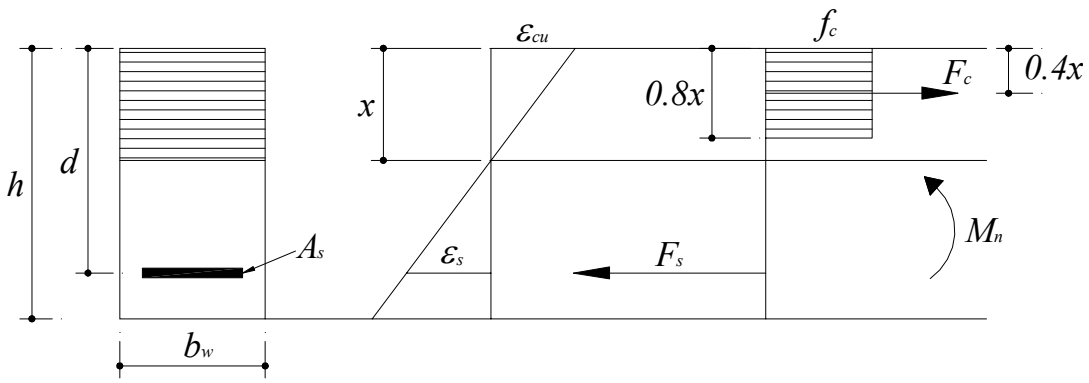

Figure B.2 Equilibrium and strain compatibility approach in the analysis of the flexural capacity of reinforced concrete beams.

Horizontal equilibrium

$$F_c = F_s \tag{B.1}$$

Force in the concrete

$$F_c = 0.8 f_c b_w x \tag{B.2}$$

Force in the steel reinforcement

$$F_s = \sigma_s \cdot A_s \tag{B.3}$$

[1] This corresponds to the average value of the modulus of rupture of concrete given in the experimental tests of Bresler Scordelis.

Strain in the steel reinforcement

$$\varepsilon_s = \frac{d - x}{x} \cdot \varepsilon_{cu} \tag{B.4}$$

Yield strain in the steel reinforcement

$$\varepsilon_y = \frac{f_y}{E_s} \tag{B.5}$$

Assumptions:

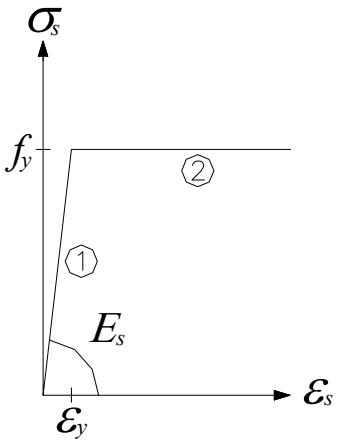

Figure B.3 Stress-strain relationship for reinforcing steel.

1) *Crushing of concrete*

$$\varepsilon_{cu} = 3.5 \cdot 10^{-3} \tag{B.6}$$

2) *Yielding of reinforcing steel*

$$\varepsilon_s \geq \varepsilon_y \tag{B.7}$$

$$\sigma_s = f_y \tag{B.8}$$

Substituting Equations (B.2), (B.3), (B.5) and (B.8) in Equation (B.1), the depth of the neutral axis is found:

$$0.8 \cdot 37.62 \cdot 10^6 \cdot 0.305x = 552.96 \cdot 10^6 \cdot 3847.81 \cdot 10^{-6}$$

$$x = 0.232 \; m$$

Check of assumptions

The strain at the level of the tensile reinforcement is found with Equation (B.4):

$$\varepsilon_s = \frac{0.465 - 0.232}{0.232} \cdot 0.0035$$

$$\varepsilon_s = 0.00352$$

The yield strain in the steel reinforcement is found with Equation (B.5):

$$\varepsilon_y = \frac{552.96 \cdot 10^6}{205.72 \cdot 10^9}$$

$$\varepsilon_y = 0.0027$$

$\varepsilon_s > \varepsilon_y$ $\therefore$ The reinforcement yields. The assumption is correct.

Flexural capacity

$$M_n = F_c \cdot (d - 0.4x) \qquad \text{(B.9)}$$

With Equation (B.2) $F_c = 0.8 f_c b_w x$, d = 0.465 and x = 0.232

$$M_n = 0.8 \cdot 37.62 \cdot 10^6 \cdot 0.305 \cdot 0.232 \cdot (0.465 - 0.4 \cdot 0.232)$$

$$M_n = 792.10 \ \ kNm$$

Ultimate load due to flexural capacity

$$P_f = 4 \cdot \frac{M_n}{L} \qquad \text{(B.10)}$$

$$P_f = 4 \cdot \frac{792.10}{6.40}$$

$$P_f = 495.06 \ \ kN$$

The ultimate load due to shear capacity

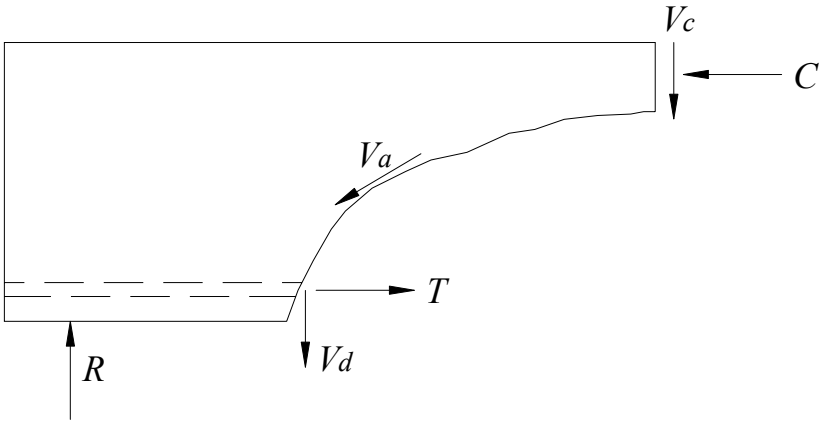

Figure B.4 Internal forces in the beam OA-3 failing in shear.

Shear resistance of the concrete without stirrups

$$V_c = b_w d f_v \tag{B.11}$$

Concrete basic shear strength

$$f_v = \xi \cdot (1 + 50 \cdot \rho_w) \cdot 0.30 f_t \tag{B.12}$$

Splitting tensile strength

For members subjected to bending and shear forces, the splitting tensile strength can be considered in calculations of the shear resistance as the tensile strength f_t. This parameter is defined as a function of the modulus of rupture according to *Betonghandbok* 11.11:6 with the Equation (B.13) as follows:

$$f_{t,fl} = \frac{5}{3} \cdot f_{t,sp} \tag{B.13}$$

$$f_{t,sp} = \frac{3}{5} \cdot f_{t,fl} = \frac{3}{5} \cdot 4.14 = 2.48$$

$$f_t = f_{t,sp} = 2.48 \text{ MPa}$$

Sectional constant relating to sectional depth and curtailment of reinforcement

$$\xi = 1.6 - d \text{ for } 0.2\ m < d \leq 0.50\ m \tag{B.14}$$

$$d = 0.465\ m$$

$$\xi = 1.6 - 0.465 = 1.135$$

Reinforcement ratio corresponding to A_{s0}

$$\rho_w = \frac{A_{s0}}{b_w d} \tag{B.15}$$

Ø=28,58 mm. 3 bars form 1 layer.

$$A_{s0} = 3 \cdot \frac{\pi(28.58)^2}{4} = 1923.91 \cdot 10^{-6}$$

$$\rho_w = \frac{1923.91 \cdot 10^{-6}}{0.305 \cdot 0.465} = 0.0136$$

Substituting the values obtained from Equations (B.13), (B.14) and the concrete tensile strength f_t in Equation (B.12):

$$f_v = 1.135 \cdot (1 + 50 \cdot 0.0136) \cdot 0.30 \cdot 2.48 \cdot 10^6$$

$$f_v = 1.419 \cdot MPa$$

With the value of f_v, the shear resistance V_c can be calculated with Equation (B.11):

$$V_c = 0.305 \cdot 0.465 \cdot 1.419 \cdot 10^6$$

$$V_c = 201.25 \ kN$$

V_c is the maximum shear force that acts in the beam and is equal to half of the concentrated load applied in the mid span.

Ultimate load due to shear resistance

$$P_v = 2 \cdot V_c \tag{B.16}$$

$$P_v = 2 \cdot 201.25$$

$$P_v = 402.50 \ kN$$

The ultimate load of the beam OA-3 is the lesser of the two calculated loads, and is due to shear.

$P^* = 402.50 \ kN$

B-2 Beam B-14

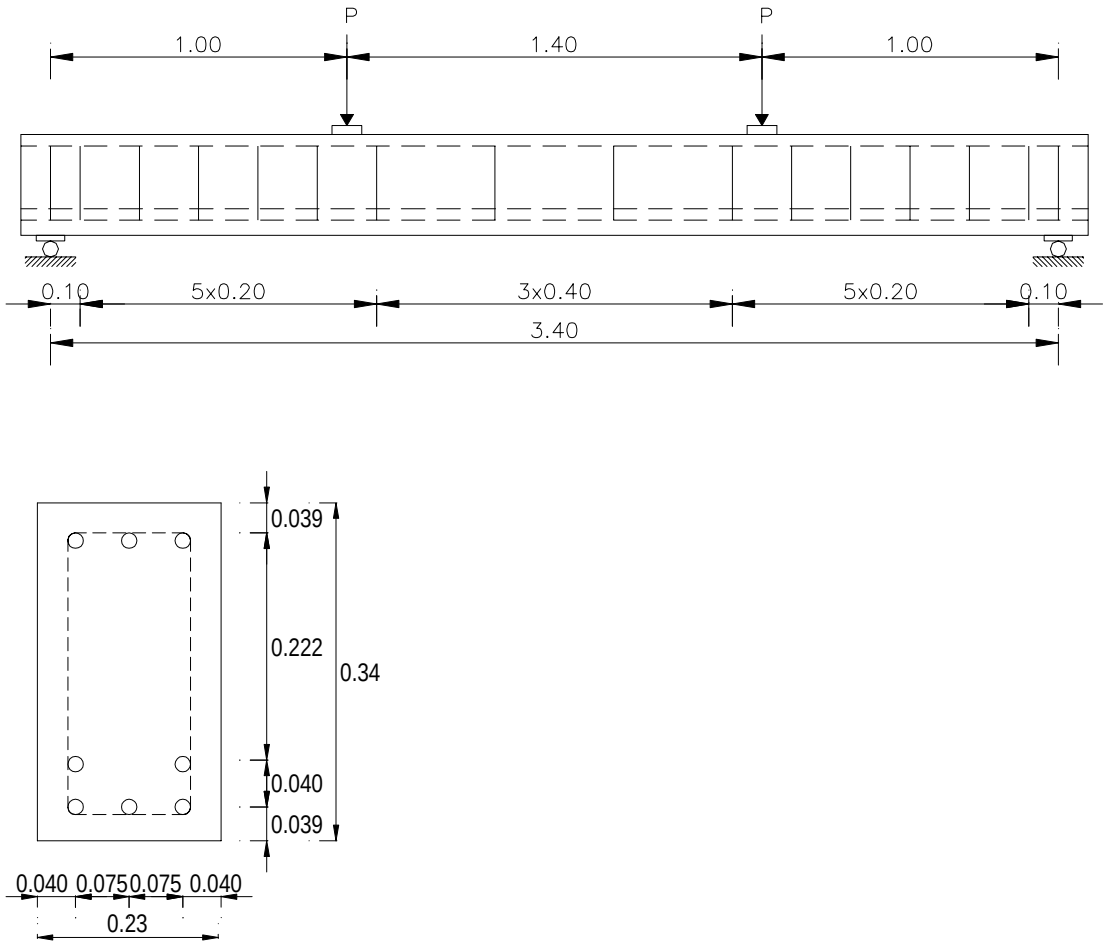

Figure B.5 Geometry, loading and cross section for beam B-14.

Dimensions

$b_w = 0.23\ m$ $h = 0.34\ m$ $L = 3.40\ m$

$d = 0.285\ m$ $d' = 0.039\ m$ $a = 1\ m$

Materials

Concrete $f_c = 29.20\ MPa$ $f_t = 2.78\ MPa$

Reinforcing steel $f_y = 628\ MPa$ $A_s = 1005.32 \cdot 10^{-6}\ m^2$

$A_s' = 603.19 \cdot 10^{-6}\ m^2$ $E_s = 207\ GPa$

Shear reinforcement $A_{sv} = 56.50 \cdot 10^{-6}\ m^2$ $f_{yv} = 532\ MPa$

$s = 0.20\ m$

The ultimate load due to flexural capacity

Flexural capacity of the section

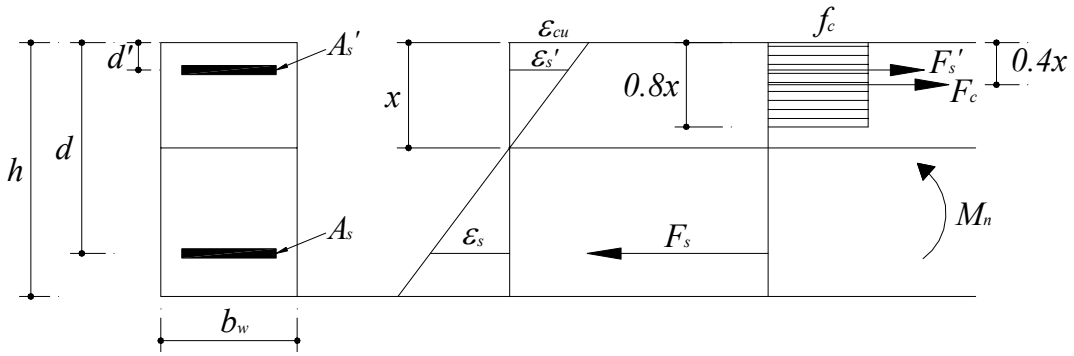

Figure B.6 Equilibrium and strain compatibility approach in the analysis of the flexural capacity of reinforced concrete beams.

Horizontal equilibrium

$$F_c + F_s' = F_s \tag{B.17}$$

Force in the concrete

$$F_c = 0.8 f_c b_w x \tag{B.18}$$

Force in the compressive reinforcement

$$F_s' = \sigma_s' \cdot A_s' \tag{B.19}$$

Force in the tensile reinforcement

$$F_s = \sigma_s \cdot A_s \tag{B.20}$$

Strain in the compressive reinforcement

$$\varepsilon_s' = \frac{x - d'}{x} \cdot \varepsilon_{cu} \tag{B.21}$$

Strain in the tensile reinforcement

$$\varepsilon_s = \frac{d - x}{x} \cdot \varepsilon_{cu} \tag{B.22}$$

Yield strain in the steel reinforcement

$$\varepsilon_y = \frac{f_y}{E_s} \tag{B.23}$$

Assumptions:

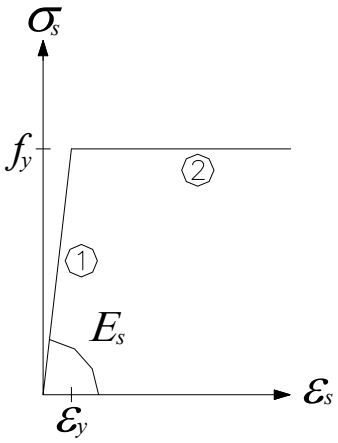

Figure B.7 Stress-strain relationship for reinforcing steel.

1) *Crushing of concrete*

$$\varepsilon_{cu} = 3.5 \cdot 10^{-3} \tag{B.24}$$

2) *The compressive steel behavior is described by part 1 in Figure B.7*

$$\varepsilon_s' < \varepsilon_y \tag{B.25}$$

$$\sigma_s' = \varepsilon_s' E_s \tag{B.26}$$

3) *The tensile steel behavior is described by part 2 in Figure B.7*

$$\varepsilon_s \geq \varepsilon_y \tag{B.27}$$

$$\sigma_s = f_y \tag{B.28}$$

Substituting Equations (B.2), (B.3), (B.4), (B.5), (B.10), (B.12) in Equation (B.1), the depth of the neutral axis is found

$$0.8 \cdot 29.20 \cdot 10^6 \cdot 0.23x + \frac{x - 0.039}{x} \cdot 0.0035 \cdot 207 \cdot 10^9 \cdot 603.19 \cdot 10^{-6} = 628 \cdot 10^6 \cdot 1005.32 \cdot 10^{-6}$$

$x = 0.077\ m$

Check of assumptions

The strain at the level of the compressive steel is found with Equation (B.5):

$$\varepsilon_s' = \frac{0.077 - 0.039}{0.077} \cdot 0.0035$$

$\varepsilon_s' = 0.0017$

The yield strain in the steel reinforcement is found with Equation (B.7):

$$\varepsilon_y = \frac{628 \cdot 10^6}{207 \cdot 10^9}$$

$\varepsilon_y = 0.0030$

$\varepsilon_s' < \varepsilon_y$ $\therefore$ The reinforcement does not yield. The assumption 2) is correct

The strain at the level of the tensile steel is found with Equation (B.6):

$$\varepsilon_s = \frac{0.285 - 0.077}{0.077} \cdot 0.035$$

$\varepsilon_s = 0.0094$

$\varepsilon_s > \varepsilon_y$ $\therefore$ The reinforcement yields. The assumption 3) is correct

Flexural capacity

$$M_n = F_c \cdot (d - 0.4x) + F_s'(d - d') \tag{B.29}$$

With $F_s' = \sigma_s' \cdot A_s'$ and $\sigma_s' = \varepsilon_s' E_s$

$$M_n = F_c \cdot (d - 0.4x) + \varepsilon_s' E_s A_s' (d - d')$$

With Equation (B.2), $d = 0.285$, $x = 0.077$, and $d' = 0.039$

$$M_n = 0.8 \cdot 29.20 \cdot 10^6 \cdot 0.23 \cdot 0.077 \cdot (0.285 - 0.4 \cdot 0.077) + 0.0017 \cdot 207 \cdot 10^9 \cdot 603.19 \cdot 10^{-6} (0.285 - 0.039)$$

$M_n = 158.67\ kNm$

Ultimate load due to flexural capacity

$$P_f = \frac{M_n}{a} \tag{B.30}$$

$$P_f = \frac{158.67}{1.00}$$

$$P_f = 158.67 \ \ kN$$

The ultimate load due to shear capacity

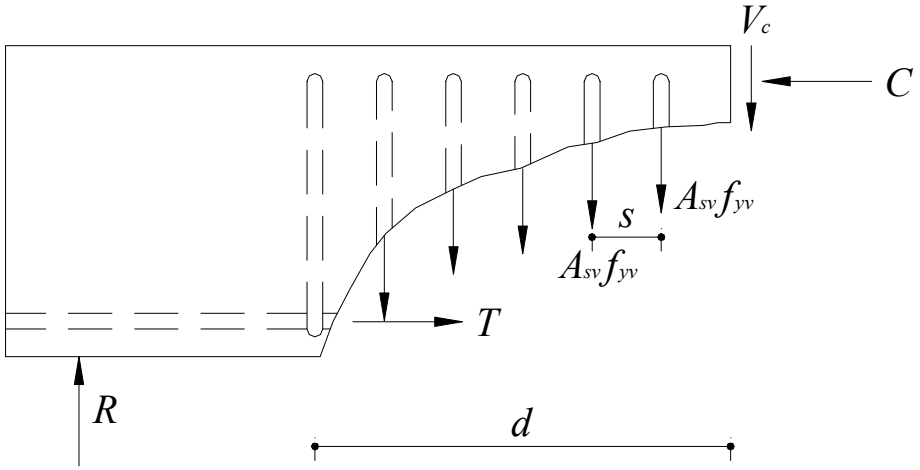

Figure B.8 Shear resisted by stirrups.

Shear resistance of concrete without stirrups

$$V_c = b_w d f_v \tag{B.31}$$

Concrete basic shear strength

$$f_v = \xi \cdot (1 + 50 \cdot \rho_w) \cdot 0.30 f_t \tag{B.32}$$

Sectional constant relating to sectional depth and curtailment of reinforcement

$$\xi = 1.6 - d \text{ for } 0.2\ m < d \leq 0.50\ m \tag{B.33}$$

$$d = 0.285\ m$$

$$\xi = 1.6 - 0.285 = 1.315\ m$$

Reinforcement ratio corresponding to A_{s0}

$$\rho_w = \frac{A_{s0}}{b_w d} \tag{B.34}$$

Ø=16 mm. 2 bars form 1 layer.

$$A_{s0} = 2 \cdot \frac{\pi (16)^2}{4} = 402.12 \cdot 10^{-6}$$

$$\rho_w = \frac{402.12 \cdot 10^{-6}}{0.23 \cdot 0.285} = 0.0061$$

Substituting the values obtained from Equations (B.17), (B.18) and the concrete tensile strength f_t in Equation (B.16).

According to BBK $f_t \leq 2.70\ MPa$

$$f_v = 1.315 \cdot (1 + 50 \cdot 0.0061) \cdot 0.30 \cdot 2.70 \cdot 10^6$$

$f_v = 1.39 \cdot MPa$

With the value of f_v, the shear resistance of concrete V_c can be calculated with Equation (B.15).

$$V_c = 0.23 \cdot 0.285 \cdot 1.39 \cdot 10^6$$

$$V_c = 91.11\,kN$$

Shear reinforcement contribution

$$V_s = A_{sv} f_{yv} \cdot \frac{0.9d}{s}(\sin\alpha + \cos\alpha) \qquad \text{(B.35)}$$

$\alpha = 0 \ \therefore$ No inclined reinforcement.

$$V_s = 56.50 \cdot 10^{-6} \cdot 532 \cdot 10^6 \cdot \frac{0.9 \cdot 0.285}{0.2}$$

$$V_s = 38.54\ kN$$

Shear capacity of the section with shear reinforcement

$$V_R = V_c + V_s \qquad \text{(B.36)}$$

$$V_R = 91.11 + 38.54$$

$$V_R = 129.65\,kN$$

Ultimate load due to shear resistance

V_R is the maximum shear force that acts in the beam, and therefore $P_v = V_R$

The ultimate load of the beam B-14 is the lesser of the two calculated loads, and is due to shear.

$P^* = 129.65\ kN$

B-3 Beam A-1

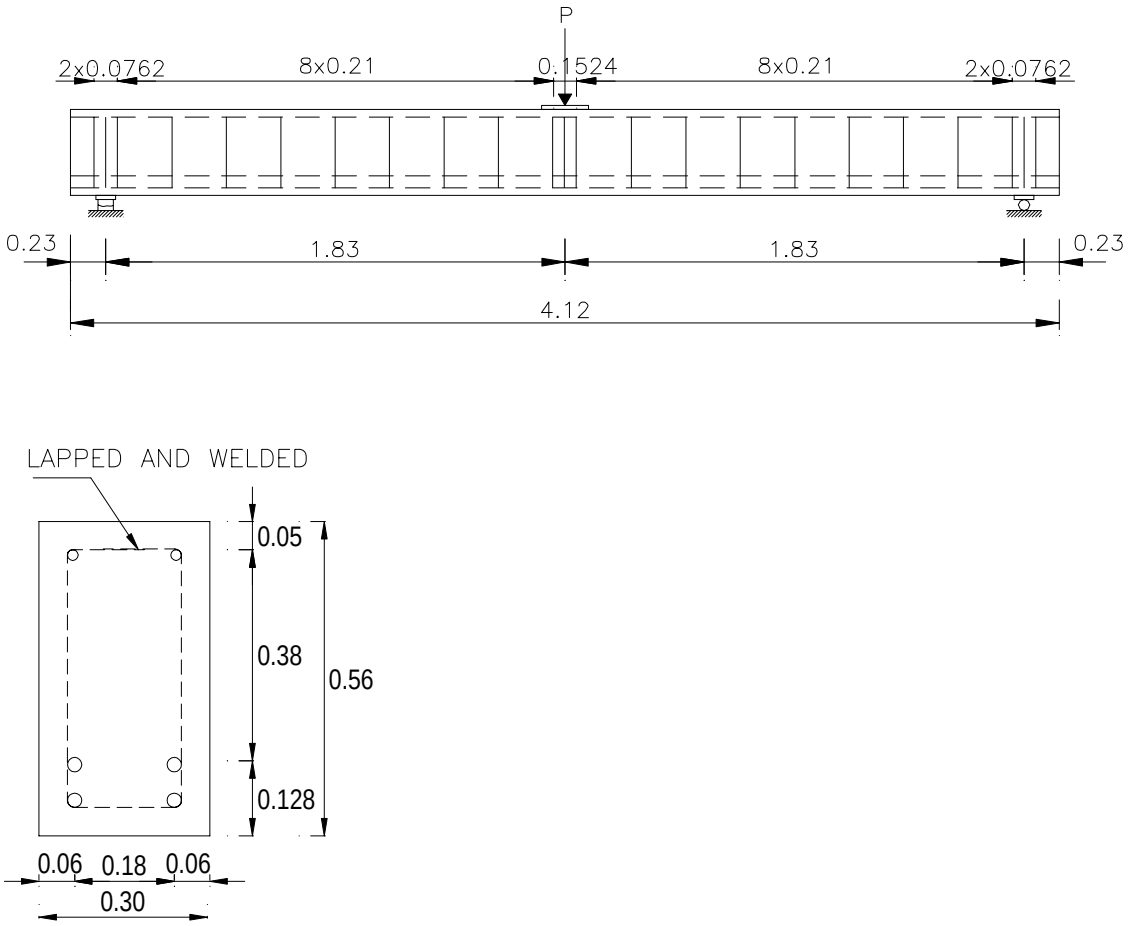

Figure B.9 Geometry, loading and cross section of the beam A-1.

Dimensions

$b_w = 0.305\ m$ $h = 0.56\ m$ $L = 3.66\ m$

$d = 0.465\ m$ $d' = 0.050\ m$

Materials

Concrete	$f_c = 24.09\ MPa$	$f_t^{1} = 3.86\,MPa$
Top reinforcing steel	$f_y' = 345.86\ MPa$	$A_s' = 253.35 \cdot 10^{-6}\ m^2$
	$E_s' = 201.576\ GPa$	
Bottom reinforcing steel	$f_y = 555.72\ MPa$	$A_s = 2565.21 \cdot 10^{-6}\ m^2$
	$E_s = 218.144\ GPa$	
Shear reinforcement	$A_{sv} = 63.34 \cdot 10^{-6}$ m²	$f_{yv} = 325.84\ MPa$
	$s = 0.21\ m$	

The ultimate load due to flexural capacity

Flexural capacity of the section

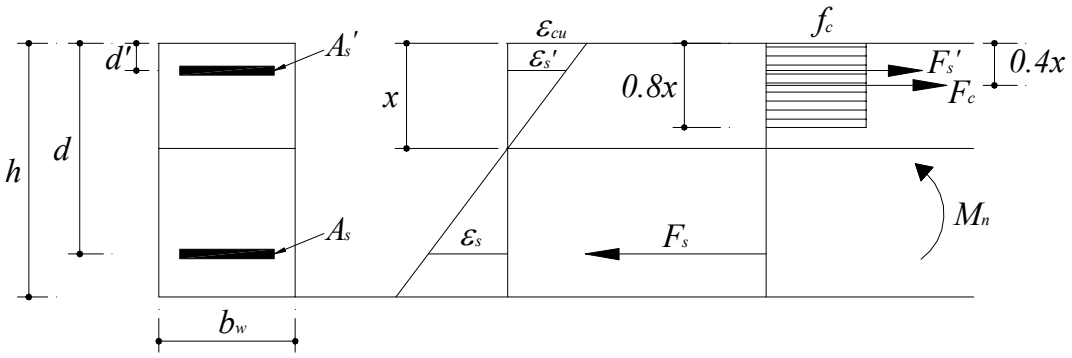

Figure B.10 Equilibrium and strain compatibility approach in the analysis of the flexural capacity of reinforced concrete beams.

Horizontal equilibrium

$$F_c + F_s' = F_s \tag{B.37}$$

Force in the concrete

$$F_c = 0.8 f_c b_w x \tag{B.38}$$

[1] This corresponds to the average value of the modulus of rupture of concrete given in the experimental tests of Bresler Scordelis.

Force in the compressive reinforcement

$$F_s' = \sigma_s' \cdot A_s' \tag{B.39}$$

Force in the tensile reinforcement

$$F_s = \sigma_s \cdot A_s \tag{B.40}$$

Strain in the compressive reinforcement

$$\varepsilon_s' = \frac{x - d'}{x} \cdot \varepsilon_{cu} \tag{B.41}$$

Strain in the tensile reinforcement

$$\varepsilon_s = \frac{d - x}{x} \cdot \varepsilon_{cu} \tag{B.42}$$

Yield strain in the compressive steel reinforcement

$$\varepsilon_y' = \frac{f_y'}{E_s'} \tag{B.43}$$

Yield strain in the tensile steel reinforcement

$$\varepsilon_y = \frac{f_y}{E_s} \tag{B.44}$$

Assumptions:

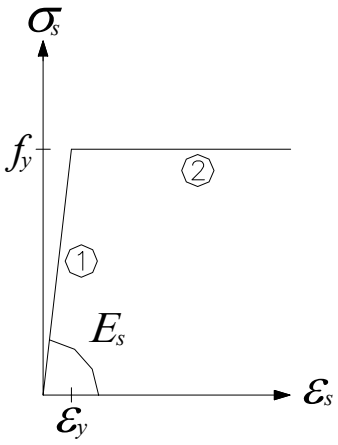

Figure B.11 Stress-strain relationship for reinforcing steel.

1) *Crushing of concrete*

$$\varepsilon_{cu} = 3.5 \cdot 10^{-3} \tag{B.45}$$

2) *The compressive steel behavior is described by part 2 in Figure B.11*

$$\varepsilon_s' \geq \varepsilon_y' \tag{B.46}$$

$$\sigma_s' = f_y' \tag{B.47}$$

3) *The tensile steel behavior is described by part 2 in Figure B.11*

$$\varepsilon_s \geq \varepsilon_y \tag{B.48}$$

$$\sigma_s = f_y \tag{B.49}$$

Substituting Equations (B.2), (B.3), (B.4), (B.11), (B.13) in Equation (B.1), the depth of the neutral axis is found:

$$0.8 \cdot 24.09 \cdot 10^6 \cdot 0.305x + 345.86 \cdot 10^6 \cdot 253.35 \cdot 10^{-6} = 555.72 \cdot 10^6 \cdot 2565.21 \cdot 10^{-6}$$

$x = 0.228\ m$

Check of assumptions

The strain at the level of the compressive steel is found with Equation (B.5):

$$\varepsilon_s' = \frac{0.228 - 0.05}{0.228} \cdot 0.0035$$

$\varepsilon_s' = 0.0027$

The yield strain in the compressive steel reinforcement is found with Equation (B.7):

$$\varepsilon_y' = \frac{345.86 \cdot 10^6}{201.576 \cdot 10^9}$$

$\varepsilon_y' = 0.00172$

$\varepsilon_s' > \varepsilon_y' \therefore$ The reinforcement yields. The assumption 2) is correct

The strain at the level of the tensile steel is found with Equation (B.6):

$$\varepsilon_s = \frac{0.465 - 0.228}{0.228} \cdot 0.035$$

$\varepsilon_s = 0.0037$

The yield strain in the tensile steel reinforcement is found with Equation (B.8):

$$\varepsilon_y = \frac{555.72 \cdot 10^6}{218.144 \cdot 10^9}$$

$\varepsilon_y = 0.0025$

$\varepsilon_s > \varepsilon_y \therefore$ The reinforcement yields. The assumption 3) is correct

Flexural capacity

$$M_n = F_c \cdot (d - 0.4x) + F_s'(d - d') \quad \text{(B.14)}$$

With $F_s' = \sigma_s' \cdot A_s'$, $\sigma_s' = f_y'$

$$M_n = F_c \cdot (d - 0.4x) + f_y' \cdot A_s'(d - d') \quad \text{(0.15)}$$

With Equation (B.2), $d = 0.465$, $x = 0.228$, and $d' = 0.050$

$$M_n = 0.8 \cdot 24.09 \cdot 10^6 \cdot 0.305 \cdot 0.228 \cdot (0.465 - 0.4 \cdot 0.228) + 345.86 \cdot 10^6 \cdot 253.35 \cdot 10^{-6}(0.465 - 0.05)$$
$$M_n = 536.68 \ kNm$$

Ultimate load due to flexural capacity

$$P_f = 4 \cdot \frac{M_n}{L}$$

$$P_f = 4 \cdot \frac{536.68}{3.66}$$

$$P_f = 586.54 \ kN$$

The ultimate load due to shear capacity

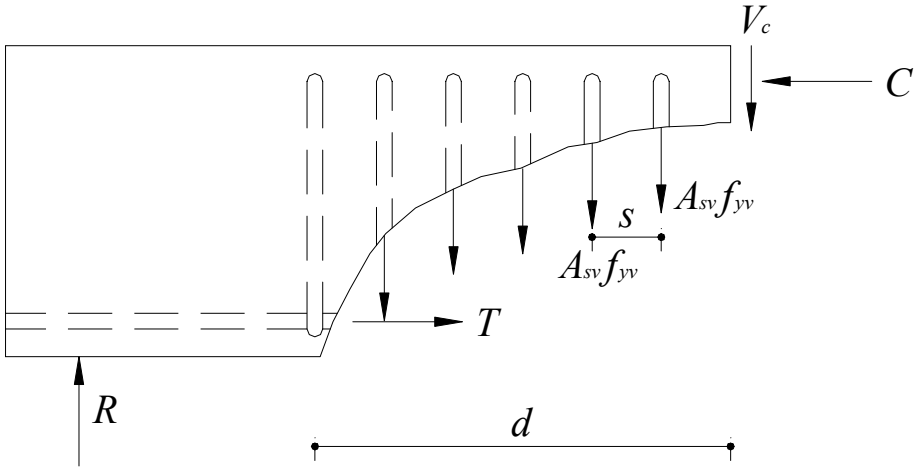

Figure B.12 Shear resisted by stirrups.

Shear resistance of concrete without stirrups

$$V_c = b_w d f_v \tag{B.16}$$

Concrete basic shear strength

$$f_v = \xi \cdot (1 + 50 \cdot \rho_w) \cdot 0.30 f_t \tag{B.17}$$

Splitting tensile strength

For members subjected to bending and shear forces, the splitting tensile strength can be considered in calculations of the shear resistance as the tensile strength f_t. This parameter is defined as a function of the modulus of rupture according to *Betonghandbok* 11.11:6 with the Equation (B.18) as follows:

$$f_{t,fl} = \frac{5}{3} \cdot f_{t,sp} \tag{B.18}$$

$$f_{t,sp} = \frac{3}{5} \cdot f_{t,fl} = \frac{3}{5} \cdot 3.86 = 2.32$$

$$f_t = f_{t,sp} = 2.32 \text{ MPa}$$

Sectional constant relating to sectional depth and curtailment of reinforcement

$$\xi = 1.6 - d \text{ for } 0.2\ m < d < 0.50\ m \tag{B.19}$$

$$d = 0.465\ m$$

$$\xi = 1.6 - 0.465 = 1.135\ m$$

Reinforcement ratio corresponding to A_{s0}

$$\rho_w = \frac{A_{s0}}{b_w d} \tag{B.20}$$

Ø=28.58 mm. 2 bars form 1 layer.

$$A_{s0} = 2 \cdot \frac{\pi(28.58)^2}{4} = 1282.60 \cdot 10^{-6}$$

$$\rho_w = \frac{1282.60 \cdot 10^{-6}}{0.305 \cdot 0.465} = 0.0090$$

Substituting the values obtained from Equations (B.18), (B.19) and the concrete tensile strength f_t in Equation (B.17):

$$f_v = 1.135 \cdot (1 + 50 \cdot 0.0090) \cdot 0.30 \cdot 2.32 \cdot 10^6$$

$f_v = 1.15\ MPa$

With the value of f_v, the shear resistance of concrete V_c can be calculated with Equation (B.16):

$$V_c = 0.305 \cdot 0.465 \cdot 1.15 \cdot 10^6$$

$$V_c = 162.22\ kN$$

Shear reinforcement contribution

$$V_s = A_{sv} f_{yv} \cdot \frac{0.9d}{s}(\sin\alpha + \cos\alpha) \tag{B.21}$$

$\alpha = 0 \ \therefore$ No inclined reinforcement.

$$V_s = 63.34 \cdot 10^{-6} \cdot 325.84 \cdot 10^6 \cdot \frac{0.9 \cdot 0.465}{0.21}$$

$$V_s = 41.13\ kN$$

Shear capacity of the section with shear reinforcement

$$V_R = V_c + V_s \tag{B.22}$$

$$V_R = 162.22 + 41.13$$

$$V_R = 203.35\ kN$$

V_R is the maximum shear force that acts in the beam and is equal to half of the concentrated load applied in the mid span.

Ultimate load due to shear resistance

$$P_v = 2 \cdot V_c \qquad \text{(B.23)}$$

$$P_v = 2 \cdot 203.35$$

$$P_v = 406.70 \ kN$$

The ultimate load of the beam A-1 is the lesser of the two calculated loads, and is due to shear.

$$P^* = 406.70 \ Kn$$

C Calculation of the fracture energy of the concrete for tested beams

According to the RILEM Draft Recommendation TC50-FMC contained in the CEB-FIP Model Code 90 the fracture energy G_f is determined on notched specimens loaded in flexure.

The fracture energy of concrete G_f, is the energy required to propagate a tensile crack of unit area.

Table C.1 Fracture energy G_f for different concrete grades and aggregate sizes.

Max. aggregate size d_{max} (mm)	G_f [Nm/m²]							
	C12	C20	C30	C40	C50	C60	C70	C80
8	40	50	65	70	85	95	105	115
16	50	60	75	90	105	115	125	135
32	60	80	95	115	130	145	160	175

The values of the fracture energy for the different beams in this thesis project were determined by interpolation of the values shown in Table C.1, and are shown in Table C.2.

Table C.2 Values of the fracture energy for tested beams.

Beam	d_{max} [mm]	f_c [MPa]	G_f [Nm/m²]
OA-3	19	37.62	90.89
B-14	19	29.20	77.55
A-1	19	24.09	69.89

The ultimate crack displacement w_u, for which the crack normal stress becomes zero, was calculated according to Hilleborg's Fictitious Crack Model, shown in Figure C.1. From this relationship, the fracture energy is approximated as the area under the curve, and w_u, could be found as:

$$w_u = \frac{2 \cdot G_f}{f_t} \tag{C.1}$$

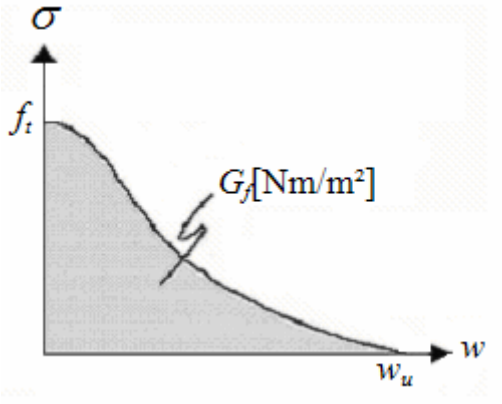

Figure C.1 Stress-crack opening relation for concrete after crack initiation.

The average crack spacing s_{rm}, was determined from the relation:

$$s_{rm} = 50 + x_1 + x_2 \frac{\phi}{\ell_r} \tag{C.2}$$

where

$x_1 = 0.8$ for high bond bars

$$x_2 = 0.25 - \frac{d_{ef}}{8(h - x)} \tag{C.3}$$

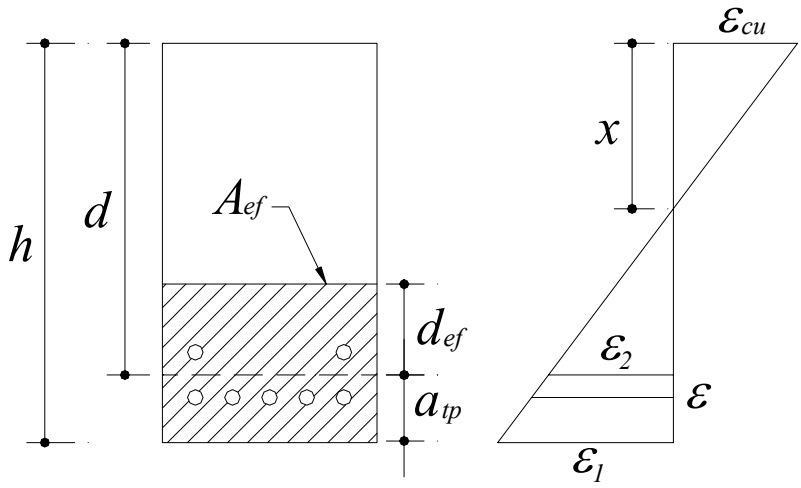

Figure C.2 Effective tension area

$$d_{ef} = 2c + \phi \tag{C.4}$$

$$a_{tp} = h - d \tag{C.5}$$

$$\ell_r = \frac{A_s}{A_{ef}} \tag{C.6}$$

The values of the average crack spacing are summarized in Table C.3 for the different beams based on the previous Equations.

Table C.3 Average crack spacing, S_{rm}, calculated for tested beams.

Beam	w_u[mm]	c[mm]	d_{ef}[mm]	h[mm]	x[mm]	$\emptyset$[mm]	A_s[mm²]
OA-3	0.0733	49.21	127	560	232	28.58	3847.81
B-14	0.0558	25	340	340	77	16	1005.31
A-1	0.0602	42.86	114.3	560	228	28.58	2566.10
Beam	d[mm]	a_{tp}[mm]	b_w[mm]	A_{ef}[mm²]		ℓ_r	S_{rm}[mm]
OA-3	465	95	305	67710		0.057	131.08
B-14	285	55	230	27830		0.036	127.47
A-1	465	95	305	63836.5		0.040	167.72

The ultimate crack strain ε_{tu} for smeared crack models in the case of perfect bond between the steel reinforcement and the surrounding concrete was calculated with Equation (C.7).

$$\varepsilon_{tu} = \frac{w_u}{s_{rm}} \tag{C.7}$$

The tensile crack strain ε_t for concrete was determined with Equation (C.8) according to Figure 4.2 in section 4.2.1 as:

$$\varepsilon_t = \frac{f_t}{E_o} \tag{C.8}$$

Finally the KAPPA values for the different beams were calculated with Equation (C.9) and are shown in Table C.4.

$$k = \frac{\varepsilon_{tu}}{\varepsilon_t} \tag{C.9}$$

Table C.4 Calculated values of parameter κ, for tested beams.

Beam	f_t[1][MPa]	E_o[MPa]	ε_{tu}	ε_t	κ
OA-3	2.48	33734.33	$5.59\text{x}10^{-4}$	$7.35\text{x}10^{-5}$	7.61
B-14	2.78	29720.36	$4.38\text{x}10^{-4}$	$9.35\text{x}10^{-5}$	4.67
A-1	2.32	26994.86	$3.59\text{x}10^{-4}$	$8.59\text{x}10^{-5}$	4.18

[1] The tensile strength of concrete f_t was considered as the value of the splitting tensile strength $f_{t,fl}$ calculated according to *Betong Handbok* 11.11:6 for the experimental tested beams of Bresler Scordelis.